Schweizerische Eidgenossenschaft
Confédération suisse
Confederazione Svizzera
Confederaziun svizra

Eidgenössisches Departement für
Umwelt, Verkehr, Energie und Kommunikation UVEK

Bundesamt für Energie BFE
Energieforschung

Schlussbericht

CON-COMP - Erforschung der Grundlagen der Phänomene und Auswirkungen von Kondensation in Kompressoren in Brennstoffzellenfahrzeugen

Datum: 14.11.2019

Ort: Volketswil

Auftraggeberin:
Bundesamt für Energie BFE
Forschungsprogramm Brennstoffzellen
CH-3003 Bern
www.bfe.admin.ch
energieforschung@bfe.admin.ch

Auftragnehmer/in:
Celeroton AG
Industriestrasse 22
CH-8604 Volketswil
www.celeroton.com

Autor/in:
Lukas Hediger, Celeroton AG, lukas.hediger@celeroton.com
Andreas Looser, Celeroton AG, andreas.looser@celeroton.com
Christof Zwyssig, Celeroton AG, christof.zwyssig@celeroton.com

BFE-Bereichsleitung: Stefan Oberholzer, stefan.oberholzer@bfe.admin.ch
BFE-Programmleitung: Stefan Oberholzer, stefan.oberholzer@bfe.admin.ch
BFE-Vertragsnummer: SI/501296-02

Zusammenfassung

Hochdrehende Turbo Kompressoren sind dank ihrer kompakten Bauweise und hohen Wirkungsgraden ideal geeignet für mobile Brennstoffzellensysteme, z.B. in Fahrzeugen, Drohnen oder als Notstromaggregate, und haben daher ein grosses Energieeinsparungspotential gegenüber Standardkompressoren. Brennstoffzellensysteme in mobilen Applikationen sind unterschiedlichen Klima- und Witterungsbedingungen ausgesetzt. Dabei können Temperaturwechsel, wie z.B. bei der Einfahrt in einen Strassentunnel oder die Ausfahrt aus einer klimatisierten Garage zu Kondensation führen. Dabei zeigt sich theoretisch wie auch experimentell, dass eine kritische Akkumulation von Kondensation auftreten kann, wenn das Kühlsystem des Kompressors träge, spezifisch mit einer Zeitkonstante von über einer Minute reagiert.

Inhaltsverzeichnis

1 Einleitung

Hochdrehende Turbo Kompressoren sind dank ihrer kompakten Bauweise und hohen Wirkungsgraden ideal geeignet für mobile Brennstoffzellensystem, z.B. in Fahrzeugen, Drohnen oder als Notstromaggregate, und haben daher ein grosses Energieeinsparungspotential gegenüber Standardkompressoren. Untersuchungen bezüglich Kondensation fehlen jedoch, daher werden in diesem Projekt Phänomene und Auswirkungen von Kondensation in Turbo Kompressoren erforscht.

2 Ausgangslage

2.1 Hintergrund / Stand der Technik

Brennstoffzellensysteme in mobilen Applikationen, zum Beispiel im Automobilbereich, sind unterschiedlichen Klima- und Witterungsbedingungen ausgesetzt, Abbildung 1. Dabei können Temperaturwechsel, wie sie z.B. bei der Einfahrt in einen Strassentunnel oder im Winter bei der Einfahrt in die Garage auftreten, zu Kondensation führen. Es gibt dabei grundsätzlich zwei Arten, wie Feuchtigkeit durch Kondensation auftreten kann:

1. Kumulierende Feuchtigkeit an einer oder mehreren Stellen im Kompressor, wenn über einen längeren Zeitraum Kondensation auftritt.
2. Kurzzeitige Kondensation durch transiente Vorgänge innerhalb des Kompressors oder des Brennstoffzellensystems

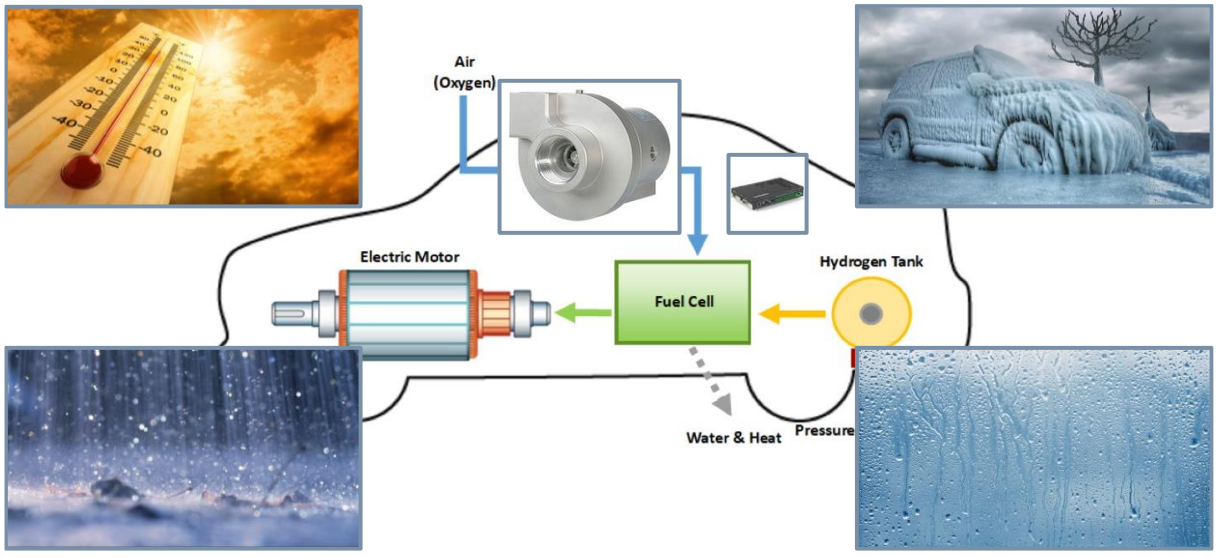

Abbildung 1: Umweltsituationen.

Beide Arten von Feuchtigkeit sind kritisch für den einwandfreien Betrieb des Kompressors. Dabei gibt es zwei Defektmechanismen, gezeigt in Abbildung 2:

- Etliche Materialien innerhalb des Kompressors vertragen keine anhaltende Feuchtigkeit und korrodieren. Die Materialwahl in einem hochdrehenden Turbo Kompressor ist dahingehend eingeschränkt, da neben der Resistenz gegen Feuchtigkeit zahlreiche andere Anforderungen bestehen, wie z.B. hohe mechanische und thermische Belastungsresistenz.
- Gewisse Subkomponenten des Kompressors vertragen auch keine kurzzeitige Feuchtigkeit,

z.B. wenn ein Gaslager verwendet wird, das bei Partikeln oder eben auch Feuchtigkeitstropfen instabil wird, touchiert und somit einen sofortigen Defekt erleidet. Ähnlich kann auch ein hochdrehender Impeller in Turbo Kompressoren je nach Auslegung der Schaufeln ab einer bestimmten Grösse von Feuchtigkeitstropfen bleibende Schäden erleiden.

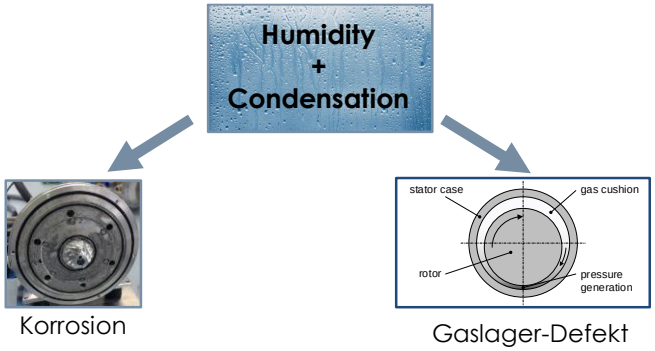

Abbildung 2: Auswirkungen von Kondensation: Turbo Kompressor mit Korrosion oder Gaslagerdefekt.

2.2 Motivation des Projektes

In einem Turbo Kompressor mit Gaslager treten unterschiedlichste Drücke und Temperaturen auf, sowohl im Bereich der Luftverdichtung als auch im Bereich der Lagerung. Daher sind Kondensationseffekte nicht trivial und erfordern eine vertiefte Betrachtung. Gemäss aktuellem Wissensstand von Celeroton findet sich in der Literatur keine allgemeingültige Auflistung von Entstehungsweisen und Auswirkungen von Kondensation in Kompressoren von Brennstoffzellensystemen, im Spezifischen von Turbo Kompressoren.

Die verschiedenen Entstehungsweisen und Auswirkungen, respektive Defektmechanismen können mit verschiedenen Gegenmassnahmen bekämpft werden. Jedoch gibt es Einschränkungen bezüglich Gegenmassnahmen – so ist z.B. eine starke Abtrocknung der Brennstoffzelle unerwünscht, da die Brennstoffzelle befeuchtete Luft benötigt. Gemäss aktuellem Wissensstand von Celeroton finden sich in der Literatur auch keine allgemeingültigen Aussagen zu Einschränkungen durch das Brennstoffzellensystem bezüglich Kondensations-Gegenmassnahmen.

3 Vorgehen und Methode

In einem ersten Schritt werden durch theoretische Betrachtungen kritische Situationen von mobilen Brennstoffzellensystemen bezüglich Kondensation bestimmt. Daraus wird abgeleitet, wie diese kritischen Situationen in einem Labortest nachzustellen sind.

In einem zweiten Schritt werden die kritischen Situationen im Labor reproduziert. Dabei werden die Kompressoren mittels Sensorik und Datalogging überwacht. Im Anschluss an die Tests werden die Kompressoren demontiert und inspiziert.

In einem dritten Schritt werden Randbedingungen definiert für Kondensations-Gegenmassnahmen, die in weiteren Projektschritten ausgearbeitet und umgesetzt werden. Dies sind Betriebsvorschriften für den Kompressor und das Brennstoffzellensystem sowie konstruktive Massnahmen im Kompressor zur Vermeidung von Kondensat.

Zur Erreichung der oben beschriebenen Projektziele wird folgendes Vorgehen gewählt:

I. Theoretische Bestimmung von kritischen Situationen von mobilen Brennstoffzellensystemen bezüglich Kondensation und daraus abgeleitete Testprozeduren zur Reproduktion (Kapitel 4.1)
II. Konzeption und Aufbau Testsetup zur Reproduktion von kritischen Situationen (Kapitel 4.3)
III. Erforschung verschiedener Möglichkeiten zur Detektion von Kondensation (Kapitel 4.4)
IV. Durchführen von Tests (Reproduktion von kritischen Situationen) (Kapitel 4.5)
V. Auswertung Tests: Inspektion von Kompressoren, spezifisch Lokalisierung von Akkumulation von Wasser (Kapitel 4.5)
VI. Definition der Randbedingungen für Kondensations-Gegenmassnahmen in Kompressor und Brennstoffzellensystem in weiteren Schritten (Kapitel 4.6)

4 Resultate

4.1 Kritische Bereiche im luftgelagerten Turbo Kompressor für Kondensation

Kritische Bereiche im Turbokompressor bezüglich Kondensation sind alle Bereiche, die mit feuchter Luft aus dem Einlass des Kompressors durchströmt werden können. Dies ist der Pfad für den Hauptmassenstrom, der durch den Kompressor gefördert wird, sowie die Spülgaspfade für die Luftlagerung. Beide sind in Abbildung 3 dargestellt.

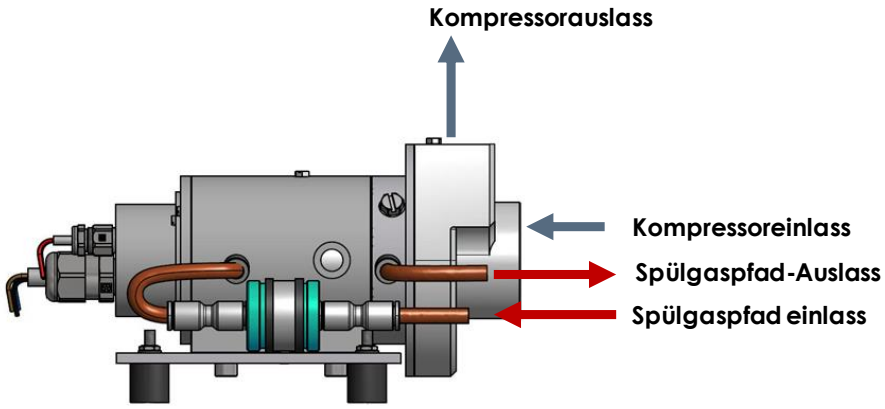

Abbildung 3: Anschlüsse des Kompressors für Hauptmassenstrom und Spülgaspfade.

4.2 Kritische Situationen von mobilen Brennstoffzellensystemen

Umweltsituationen und Betriebsbedingungen, welche bezüglich Kondensation innerhalb des Kompressors kritisch werden könnten, wurden analysiert und bewertet. Grundsätzlich können die Situationen in zwei Kategorien aufgeteilt werden:

- Kondensation von Restfeuchtigkeit aus abgeschlossenen oder nicht durchströmten Luftvolumen im Kompressor bei Abkühlvorgängen im Stillstand
- Akkumulation von Kondensat an kalten (d.h. unterhalb Taupunkt) Kompressorteilen durch anhaltende Zuführung von feuchter Luft im Betrieb

4.2.1 Kondensation von Restfeuchtigkeit

Ein Beispiel für Kondensation von Restfeuchtigkeit ist das Parkieren eines Brennstoffzellenfahrzeugs über Nacht im Freien, wobei sich die im Kompressor gefangene Luft im Verlauf der Nacht abkühlt und sich die ausfallende Feuchtigkeit an Kompressorteilen innerhalb des Kompressors niederschlägt. Die auf das Luftvolumen bezogene Menge an auskondensierbarem Wasser steigt mit zunehmender Temperatur und lässt sich gemäss Abbildung 4 in Abhängigkeit der Temperatur bestimmen. Als Worst-Case Annahme kann 100% gesättigte Luft bei 50°C angenommen werden, wobei die komplette Feuchtigkeit auskondensiert. Diese Menge an auskondensiertem Wasser füllt 1/10000 des Volumens aus. Betrachtet man das Volumen des Luftspaltes im Gaslager und würde sich das Wasser in einer homogenen Schicht auf der Lagerfläche ablagern, entspräche dies einer Schichtdicke von weniger als einem Nanometer. Diese Berechnung zeigt, dass die zu erwartenden Mengen an Kondensat aus Restfeuchtigkeit sehr gering sind. Daher stellt Kondensation von Restfeuchtigkeit kein zu untersuchendes Problem dar.

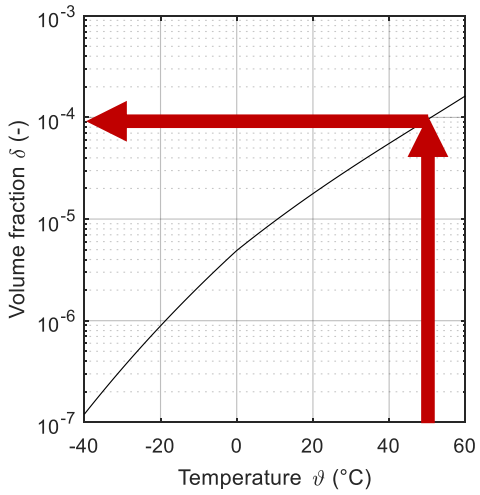

Abbildung 4: Volumenanteil von kondensierbarem Wasser ausgehend von gesättigter Luft in Abhängigkeit der Temperatur [1].

4.2.2 Akkumulation von Kondensat

Durch Akkumulation von Kondensat können sich je nach Dauer des Zustandes kritische Mengen an Kondensat bilden, welche über die im Kompressor geführten Spülgaspfade der Luftlagerung unter ungünstigen Umständen (z.B. durch Lageänderung oder Vibration) direkt in den Lagerspalt gelangen können. Die Funktionsfähigkeit der Luftlager wäre in einem solchen Fall nicht mehr gewährleistet.

Eine dauerhafte Taupunktunterschreitung wäre besonders gravierend. Eine solche kann aber im Fall von Kompressoren für Brennstoffzellenfahrzeuge nicht auftreten, da zur Kühlung von Systemkomponenten ausschliesslich Wärmetauscher zur Umgebungsluft und keine Kältemaschinen zum Einsatz kommen. Somit beschränkt sich mögliche Akkumulation von Kondensat auf eine vorübergehende Taupunktunterschreitung, d.h. auf Situationen mit transienten Vorgängen, wo der Kompressor zu Beginn kalt ist (z.B. geparkt, im Stillstand) und sich unmittelbar nach dem Start in eine warme und feuchte Umgebung begibt. Sobald sich der Kompressor dann aufgrund der im Betrieb anfallenden Verlustwärme genügend aufgeheizt hat, tritt keine Kondensation mehr auf. Kondensat, welches sich auf Kompressorteilen niedergeschlagen hat, kann dann wieder an die Umgebung

abgegeben werden. Beispiele von transienten Situationen mit möglicher Akkumulation von Kondensat sind:

- Einfahrt in langen Tunnel (welcher in der Tunnelmitte feucht und warm ist aufgrund der Erdwärme)
- Einfahrt in warme Garage bei tiefen Aussentemperaturen (Winter)
- Parken in (klimatisierter) Tiefgarage mit anschliessender Ausfahrt in warme und feuchte Umgebung (Sommer, Tropen)

Zur Definition von Testbedingungen werden die maximalen Taupunkttemperaturen in unterschiedlichen klimatischen Zonen untersucht. Dazu werden Daten aus [2] auf stündlicher Basis aus den Jahren 2000-2009 ausgewertet. Taupunkttemperaturen sind in tropischen Regionen auf Meereshöhe maximal und liegen bei rund 30°C. Zum Vergleich liegt die maximal aufgetretene Taupunkttemperatur in Zürich bei 20°C. Als weitere Referenz für im Strassennetz maximal auftretende Taupunkte kann der Gotthardtunnel betrachtet werden. Aufgrund der Erdwärme kann die Temperatur im Tunnelinnern auch im Winter auf 30°C steigen [4], siehe Abbildung 5.

Es kann angenommen werden, dass die Luftfeuchtigkeit dabei nahezu 100% erreicht. Mit einer Fahrzeug-Geschwindigkeit von 70 km/h ergibt sich ein Temperaturanstieg von mehr als 5°C/min, gemäss Standards kann dieser sogar 10°C/min betragen [3], d.h. die 30°C bei 100% Luftfeuchtigkeit werden innerhalb von einigen Minuten erreicht. Darüber hinaus ist bei der Einfahrt in den Gotthardtunnel ein Start bei Minustemperaturen möglich. Für die Ausfahrt aus der klimatisierten Tiefgarage in tropischen Gebieten ergibt sich sogar innerhalb Minutendauer ein maximaler Temperatursprung von ca. 18°C auf 30°C bei 100% Luftfeuchtigkeit.

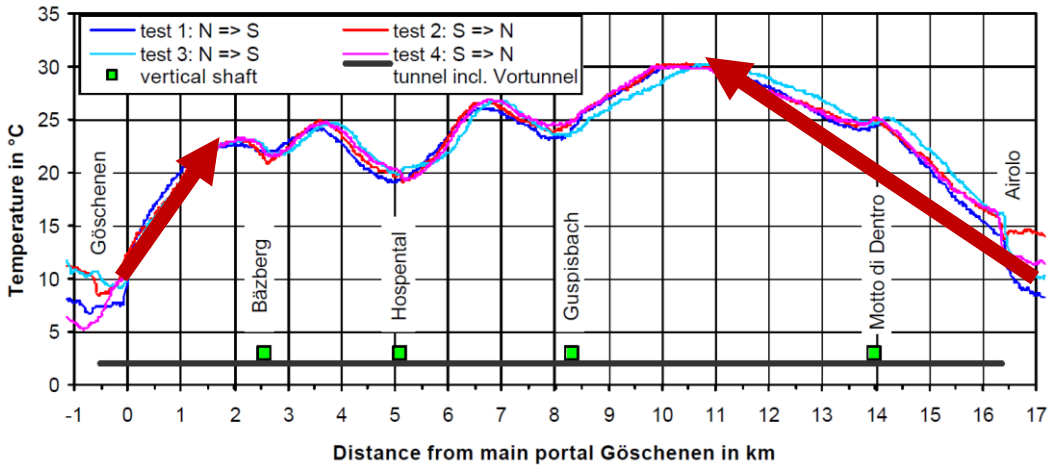

Abbildung 5: Temperaturprofil im Gotthardtunnel gemäss [4].

Um abzuschätzen, ob ein solcher Temperaturanstieg der Eintrittsluft für den Kompressor kritisch ist, wurde die Zeitdauer berechnet, welche benötigt wird, um bei einer Gehäusetemperatur von 10°C 1% des Volumens des Sperrgaspfades zu füllen, wenn laufend neu einströmende, gesättigte Sperrgasluft zugeführt wird. Das Resultat ist in Abbildung 6 in Abhängigkeit der Eintrittstemperatur gezeigt. Demnach beträgt die Dauer bei gesättigter Eintrittsluft von 30°C lediglich 1.3 Minuten. Dies ist kritisch, da die Zeitkonstanten der Kühlsysteme der Brennstoffzellen, aber auch des Kompressors selber, grösser als eine Minute sind.

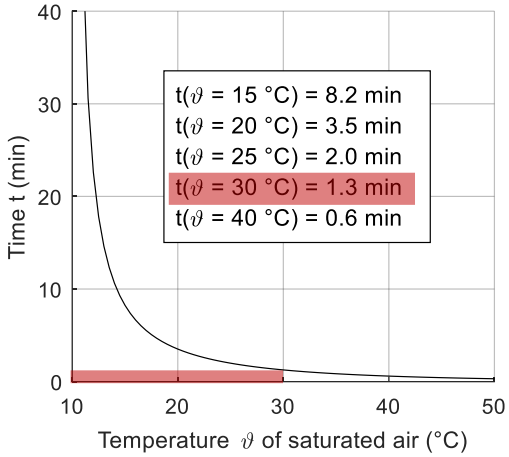

Abbildung 6: Zeit bis 1% des Spülgaspfades des CT-17-700.GB mit Kondensat gefüllt ist [4].

Für die Tests wird daher eine Zieltemperatur von 35°C bei 95% rel. Luftfeuchtigkeit (entspricht einer Taupunkttemperatur von 34°C) definiert, was eine Sicherheitsmarge gegenüber den 30°C beinhaltet. Bei Testbeginn ist der Kompressor im Stillstand auf 0°C gekühlt. Der Anstieg auf Zieltemperatur soll möglichst schnell erfolgen (< 1 Minute). Ausschlaggebend für einen einwandfreien Betrieb des Kompressors ist, wie oben gezeigt, auch die Dauer der Taupunktunterschreitung der einzelnen Kompressorteile, respektive die Dauer der Aufwärmphase sowie die Betriebsdauer danach. Hier spielt die Trägheit des gesamten Kühlkreislaufs eine entscheidende Rolle, welche aber massgeblich durch den Anwender bestimmt wird und daher nicht bekannt ist. Deshalb werden zwei Tests definiert, welche sich in der Kühlungsart und der Testdauer unterscheiden:

Test I

- Fortlaufende Kühlmittelzufuhr mit 0°C während einer Testdauer von 30 min.
- Der Test repräsentiert sehr träge Kühlkreisläufe.

Test II

- Unterbrechung der Kühlmittelzufuhr unmittelbar bei Testbeginn.
- Aufwärmen des Kompressors durch eigene Abwärme.
- Testdauer abhängig von gemessenen Gehäusetemperaturen, d.h. Testende sobald alle Temperaturen oberhalb von Taupunkttemperatur am Einlass (34°C).

4.3 Prüfstandsaufbau

Zur Untersuchung der Akkumulation von Kondensat im Kompressor wird ein Prüfstand konzipiert, welcher es ermöglicht, die Temperatur und Luftfeuchtigkeit der Eintrittsluft in den Kompressor transient zu regeln und damit Umweltsituationen im Labor nachzustellen. Der Prüfstand ist in Abbildung 7 schematisch gezeigt. Abbildung 8 zeigt den realisierten Prüfstand.
Da die festgelegten Zieltemperaturen und Taupunkttemperaturen über den Temperaturen im Labor liegen, kann die Luft direkt vom Labor (ohne Kühler und Entfeuchter) angesaugt werden und muss lediglich kontrolliert erwärmt und befeuchtet werden. Der Luftzustand wird an unterschiedlichen Stellen im Prüfstand mittels Druck-, Temperatur-, Feuchte- und Massenstromsensoren erfasst und kann entsprechend geregelt werden. Im Verbindungsrohr zwischen dem Befeuchter und dem Prüfling verhindert eine Temperierung des Rohrs auf eine Temperatur knapp oberhalb der angestrebten Taupunkttemperatur eine Auskondensierung der feuchten Luft bereits im Rohr. Mittels eines ausgangsseitig montierten Ventils lässt sich der Arbeitspunkt des Kompressors einstellen. Da es sich

um relativ kurzeitige Tests und keine Dauerversuche handelt, wird die befeuchtete Luft nicht zirkuliert, sondern schlussendlich ins Freie geblasen, was einen sehr einfachen Prüfstandsaufbau erlaubt. Zur Kühlung des Kompressors wird ein Chiller eingesetzt. Die Spülgasversorgung der Gaslager ist an den Kompressoreingang angeschlossen. Dies ist notwendig, da der Kompressoreingang in der Realität den Umgebungsbedingungen entspricht. In den Tests jedoch birgt es die Gefahr, dass sich schon in den Zuleitungen Kondensat bilden könnte. Es hat sich aber gezeigt, dass die verwendeten Kunststoffschläuche genügend isolierend wirken und Kondensation daher an diesen Stellen nicht messbar auftritt.

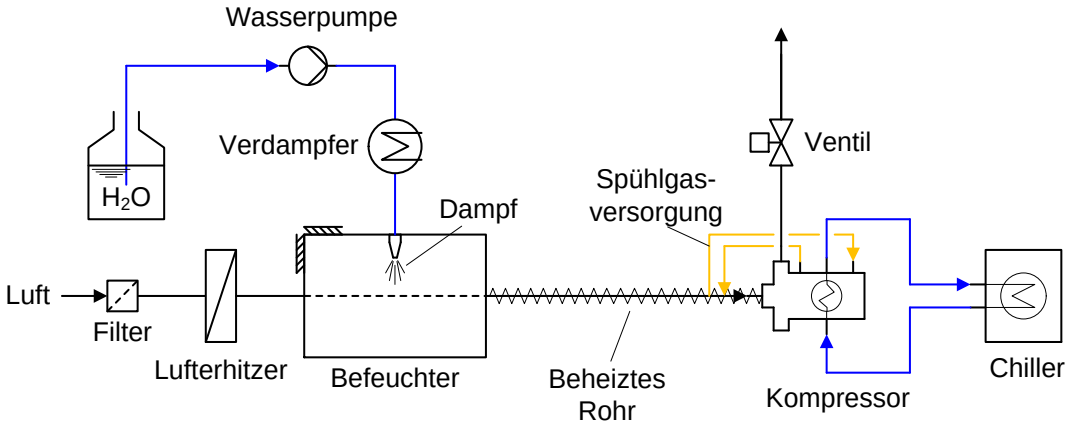

Abbildung 7: Blockdiagramm des Prüfstands zur Untersuchung von Akkumulation von Kondensat im Kompressor.

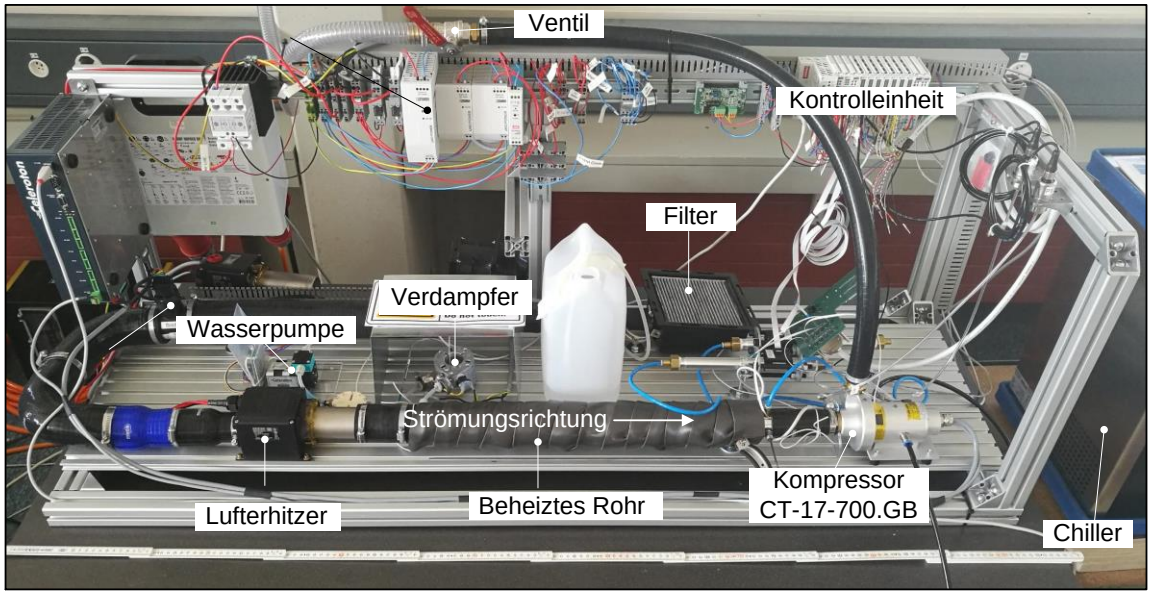

Abbildung 8: Realisierter Prüfstand mit CT-17-700.GB Kompressor.

Die Funktionalität des Prüfstandes wurde überprüft mit einem Testlauf, wobei die Temperatur und die relative Feuchtigkeit für 2 verschiedene Massenströme auf 35°C und 95% Luftfeuchtigkeit eingeregelt wurden. Die erreichten Werte gemäss Abbildung 9 haben leichte Regelabweichungen, aber sind

genügend genau für die Tests.

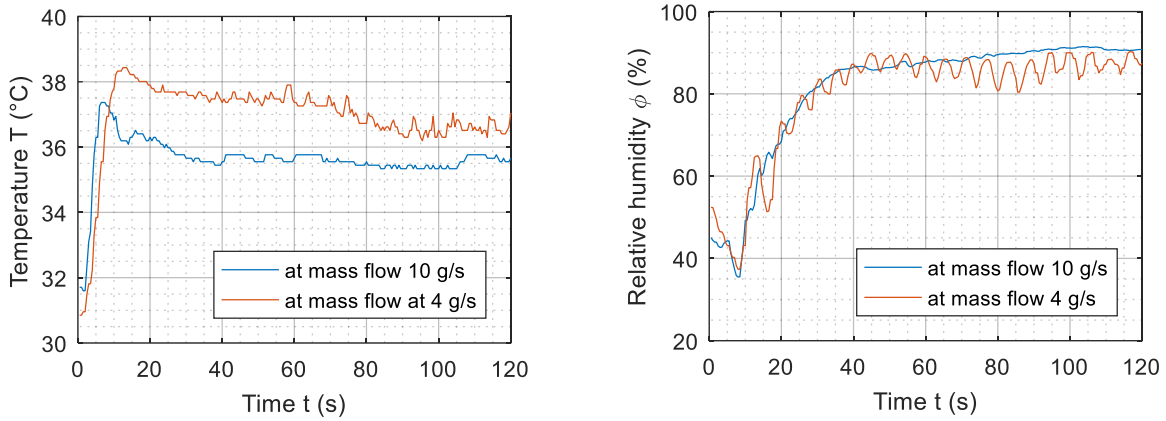

Abbildung 9: Funktionstests des Prüfstandes mittels Einregeln auf eine Kompressor-Eintrittstemperatur von 35°C und 95% relative Feuchtigkeit für 2 verschiedene Massenströme.

4.4 Detektion von Kondensation

Die Überprüfung von Kondensat im Kompressor kann durch visuelle Inspektion erfolgen. Bei sichtbar anfallenden Mengen an Kondensat erfordert dies ein Öffnen des Kompressors und einfachen Zugang zu den kritischen Stellen.

Da der Zugang zur Luftlagerung für eine visuelle Inspektion innert kurzer Zeit nur schwer möglich ist (d.h. ohne dass das Kondensat während der Inspektion wieder verdampft), wurde eine weitere Möglichkeit untersucht, um festzustellen, ob sich Kondensat im Lagerspalt befindet. Es ist zu erwarten, dass aufgrund der höheren Viskosität von Wasser gegenüber Luft ein höheres Reibungsmoment im Lager auftritt. Mit einem Auslaufversuch unter Aufzeichnung der Drehfrequenz Ω über die Zeit t lässt sich das Reibungsmoment

$$M = J\frac{d\Omega}{dt}$$

bestimmen. Dabei bezeichnet J das Massenträgheitsmoment des Rotors um die Rotationsachse. In Vorversuchen wurde das Reibungsmoment bei 15'000 U/min mit trockenem Lager, leicht befeuchtetem Lager und nassem Lager bestimmt. Bei leicht befeuchtetem Lager stieg das Reibungsmoment auf 150% des Wertes bei trockenem Lager, bei nassem Lager waren es rund 300%. Der Auslaufversuch reagiert also sehr empfindlich auf Kondensat im Lagerspalt und stellt daher ein einfaches Mittel zur Detektion von Kondensat im Lagerspalt dar.

4.5 Versuchsdurchführung und Auswertung

Auf dem Prüfstand wurde die Eintrittsluft in den Kompressor ausgehend von den Bedingungen im Labor auf eine Temperatur von 35° bei einer Luftfeuchtigkeit von 95% unter weniger als 30 s eingeregelt. Die Tests werden mit einem Celeroton Turbokompressor CT-17-700.GB durchgeführt, welcher mit zusätzlichen Temperatursensoren bestückt ist. Die Tests werden bei unterschiedlichen Drehzahlen des Kompressors durchgeführt, da die Drehzahl einen entscheidenden Einfluss auf die Erwärmung des Kompressors hat. Der Arbeitspunkt des Kompressors wird jeweils so gewählt, dass der Kompressor im Bereich des optimalen Wirkungsgrads betrieben wird. Nach den Versuchen wird jeweils ein Auslaufversuch zur Detektion von Kondensat im Lagerspalt sowie eine visuelle Inspektion durchgeführt (beides gemäss Kapitel 4.4).

4.5.1 Testserie I: Fortlaufende Kühlmittelzufuhr

Die Testserie I mit fortlaufender Kühlmittelzufuhr und den sich damit einstellenden Temperaturen gemäss Abbildung 10 verursacht bei allen Drehzahlen Kondensat im Bereich des Eintritts der Luftlager-Spülgasversorgung, welche sich an einem thermisch ungünstig angebundenen Ort, d.h. weit entfernt von Wärmequellen befindet. Die Temperatur liegt in diesem Bereich dauerhaft unterhalb des Taupunktes und neue feuchte Luft wird hier während dem Test laufend zugeführt. Kritisch ist, dass das Kondensat von hier aus unter ungünstigen Bedingungen (Vibration / Beschleunigung / Lagewechsel) in den Lagerspalt gelangen könnte. Die nach den Tests durchgeführten Auslaufversuche (Abbildung 11) deuten nicht auf Kondensat im Lager hin. In anderen Bereichen des Kompressors, wie z.B. im Bereich des Hauptströmungspfads des Kompressors ist keine Bildung von Kondensat feststellbar.

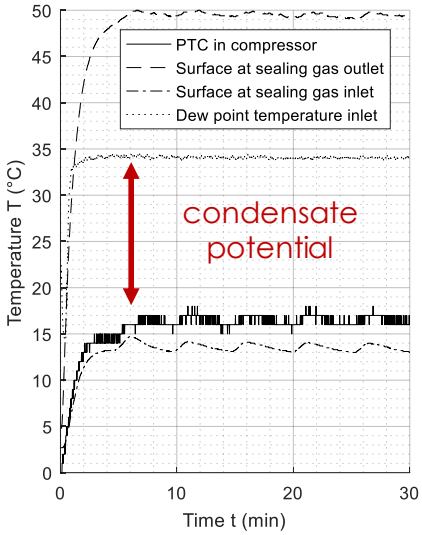

Abbildung 10: Temperaturunterschiede im Kompressor bei fortlaufender Kühlmittelzufuhr bei Kompressoreintrittstemperatur von 35 °C.

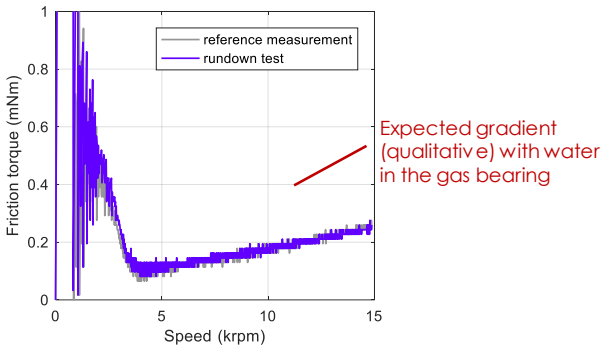

Abbildung 11: Auslaufversuch nach Abschluss der Testserie I.

4.5.2 Testserie II: Unterbrochene Kühlmittelzufuhr

Bei unterbrochener Kühlmittelzufuhr wird die Taupunkttemperatur an den kritischen Kompressorteilen bei der Nenndrehzahl von 280'000 U/min schon nach 2.5 min erreicht, bei einer Drehzahl von 120'000 U/min dauert dies rund 10 min (Abbildung 12). Zu beachten ist, dass bei tieferen Drehzahlen aufgrund

des tieferen Massenstroms des Kompressors auch die Menge der zugeführten Feuchtigkeit geringer ist. Es lässt sich daher schwer einschätzen, ob die hohen oder die tiefen Drehzahlen für den Kompressor kritischer sind. In den Tests bildeten sich aufgrund der Erwärmung des Kompressors und der dadurch reduzierten Testdauer keine feststellbaren Mengen an Kondensat. Ebenso zeigen die Auslaufversuche (Abbildung 13) kein Kondensat im Lager.

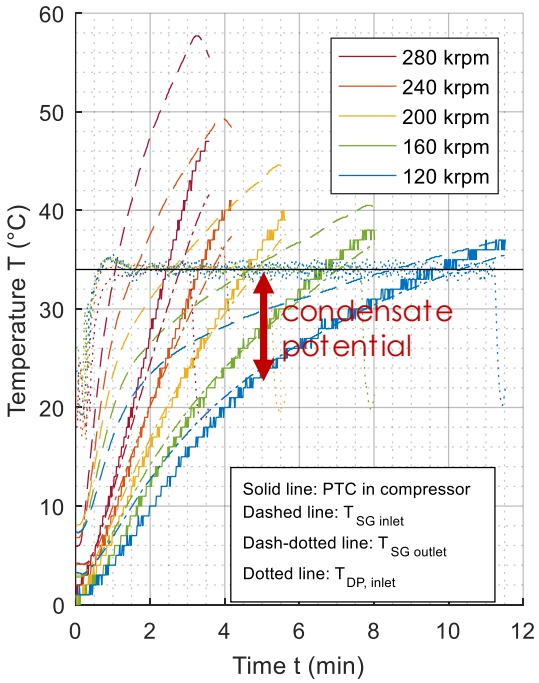

Abbildung 12: Eigenerwärmung des Kompressors bei unterbrochener Kühlmittelzufuhr bei verschiedenen Drehzahlen bei Kompressoreintrittstemperatur von 35 °C.

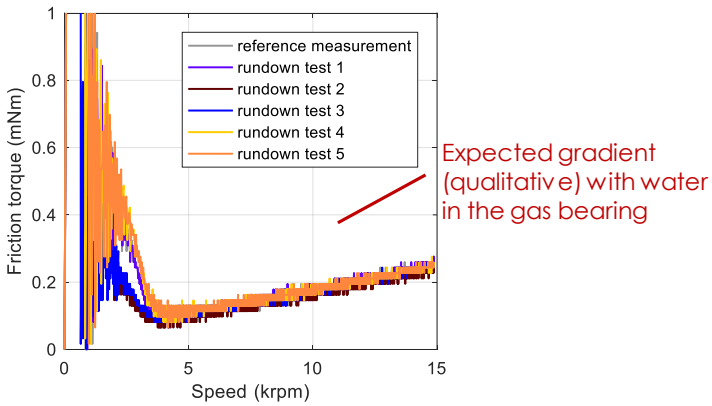

Abbildung 13: Auslaufversuch nach Abschluss der Testserie II.

4.6 Kondensations-Gegenmassnahmen

Wie mit den Tests gezeigt wird, ist die Dauer einer möglichen Taupunktunterschreitung für einen einwandfreien Betrieb des Kompressors massgebend. Die Trägheit des Kühlsystems spielt daher eine

entscheidende Rolle und muss bei der Systemintegration des Brennstoffzellensystems berücksichtigt werden. Der CT-17-700.GB erfordert eine kurze Aufwärmdauer des Kühlwasserkreislaufs von 2.5 min bei nomineller Drehzahl von 280'000 U/min auf eine Temperatur über dem Taupunkt. Die Dauer der Aufwärmphase darf bei tieferen Drehzahlen zunehmen, d.h. bei 120'000 U/min soll die Dauer weniger als 10 min betragen. Wenn eine Aufwärmdauer des Kühlkreislaufs von 2.5 eingehalten werden kann, ist ein einwandfreier Betrieb mit dem getesteten Kompressor ohne weitere Modifikationen oder Vorgaben bezüglich Drehzahl möglich.

Eine zusätzliche Massnahme ist die Reduktion der Aufwärmphase des Kompressors, nicht des gesamten Kühlkreislaufes. Dies könnte beispielsweise durch den Systemintegrator mittels eines Thermostats, welcher den Kühlkreislauf während der Aufwärmphase unterbricht, erfolgen. Der Thermostat könnte die Kühlung des Kompressors einschalten, sobald der Kompressor die Taupunkttemperatur oder alternativ eine feste Temperatur (z.B. 35°C) überschreitet.

5 Schlussfolgerungen und Ausblick

5.1 Schlussfolgerungen

Theoretische Berechnungen zeigen, dass das Auskondensieren von Restfeuchtigkeit kein Problem darstellt für Turbo Kompressoren in mobilen Brennstoffzellensystemen, aber eine kritische Akkumulation von Kondensat auftreten kann, wenn das Kühlsystem des Kompressors träge, im spezifischen Fall des untersuchten Kompressors mit einer Zeitkonstante von über einer Minute, reagiert.

Mögliche Gegenmassnahmen beinhalten Vorgaben für die Auslegung des Kühlsystems des Kompressors, Aufheiz- und Anfahrvorgänge im Kompressor und/oder Brennstoffzellensytem sowie konstruktive Anpassungen und Vorgaben für die Kompressoren selber.

Die in diesem Projekt erarbeiteten und dokumentierten theoretischen Grundlagen ermöglichen die Abschätzung der Risiken mit weiteren Kompressoren, Eintrittstemperaturen und Kompressor-Kühlbedingungen. Der Prüfstandsaufbau ermöglicht die experimentelle Untersuchung von weiteren Kompressoren in ähnlicher Baugrösse, oder mittels einer Erweiterung auch von Kompressoren grösserer Baugrösse.

5.2 Ausblick

In nachfolgenden, internen Projekten werden die konstruktiven Gegenmassnahmen im Kompressor umgesetzt in einer Weiterentwicklung des CT-17-700.GB und mit den Tests und dem Prüfstand entwickelt, im vorliegenden Projekt verifiziert. Die Neuentwicklungen (Celeroton Brennstoffzellenkompressoren und kundenspezifische Kompressoren) werden die Erkenntnisse dieses Projektes beinhalten.

Zudem werden die Bedienungsanleitungen zu den Kompressoren ergänzt mit den Erkenntnissen dieses Projekts, spezifisch den Anforderungen an den Kühlwasserkreislauf.

6 Publikationen

Im Zuge dieses Projektes sind folgende Publikationen entstanden:

- Lukas Hediger, Analysis of Robustness of Air Lubricated Turbo Compressors with Regard to Humidity and Condensation, Masterarbeit an der Hochschule Luzern – Technik & Architektur, 2019.

7 Referenzen

[1] ISO 16750-4: Damp heat cycle up to 55 °C (further referenced to: IEC 60068-2-30 (1980-01))

[2] Meteonorm, Meteotest AG, https://meteonorm.com/

[3] Standard: MIL-STD-810G: Environmental engineering considerations and laboratory tests

[4] U. Steinemann und F. Zumsteg, *Measurements of Air Flow, Temperature Differences and Pressure Differences in Road Tunnels*, Graz, Austria: International Conference „Tunnel Safety and Ventilation“ , 2004.

Lucerne University of
Applied Sciences and Arts

HOCHSCHULE
LUZERN

Technik & Architektur

MSE | MASTER OF SCIENCE IN ENGINEERING

Master Thesis | 2018/2019

MSE – Energy and Environment

Analysis of Robustness of Air Lubricated Turbo Compressors with Regard to Humidity and Condensation

Confidential

Author: **Lukas Hediger**

Supervisor: Prof. Dr. Mirko Kleingries
Lucerne University of Applied Sciences and Arts, Technikumstrasse 21, 6048 Horw

Expert: Dr. Gianfranco Guidati
ETH Zurich, SCCER-SoE, Sonneggstrasse 5, 8092 Zurich

Industrial partner: Dr. sc. ETH Andreas Looser
Celeroton AG, Industriestrasse 22, 8604 Volketswil

Submission date: June 21, 2019

Acknowledgment

I am grateful to my company (industrial partner) and especially to Dr. Andreas Looser whose experience, understanding and support made it possible for me to work on a topic that was of great interest to me. I really appreciated the generous time he spent for the valuable discussions. It was a pleasure working with him.

I would like to say a big thank to Prof. Dr. Mirko Kleingries for supervising me and always having a good advice.

Last but not least, I would like to take this opportunity to thank all the other people who have been involved in this project in any manner and who have always supported me in making this project possible.

Horw, June 2019
Lukas Hediger

Independency Declaration

I hereby declare that the present report is my own independent work without the use of aids than those indicated. All used text excerpts, quotations or contents of other authors were explicitly marked us such.

Place, Date: Signature:

Lukas Hediger

Content

Appendix

Analysis of Robustness of Air Lubricated Turbo Compressors with Regard to Humidity and Condensation

Lukas Hediger

Lucerne University of Applied Sciences and Arts

CC Thermal Energy Systems and Process Engineering

Technikumstrasse 21, CH-6048 Horw, Switzerland

lukas.hediger@gmail.ch

Submission date: June 21, 2019

Abstract. High-speed air lubricated turbo compressors like the CT-17-700.GB from the company Celeroton are thanks to their high efficiency, compactness and oil-freedom ideally suited for the application in automotive fuel cell systems. In the automotive sector, the environmental conditions cannot be controlled and raises the question of the effects of partial condensation of water vapor on the functionality and reliability of the gas bearing and other parts of the turbo compressor. A theoretical analysis of partial condensation processes reveals that in environmental and operating situations, where condensate can accumulate within the turbo compressor, are considered most critical. In order to identify critical spots in the turbo compressor and experimentally investigate critical condensation processes under real situations a test rig is developed, constructed and commissioned, which provides temperature and humidity controlled air to a compressor. Based on findings from the experimental investigations measures are proposed.

Keywords. air lubricated turbo compressor, gas bearing, partial condensation, humid air, simulation, experimental investigation

1 Introduction

1.1 Motivation

High-speed turbo compressors with gas bearing (also known as air lubricated turbo compressors when used with air) from the company Celeroton are thanks to their compact design and high efficiency ideally suited for mobile fuel cell (FC) systems. Mobile FC systems are e.g. used in vehicles, UAVs (Unmanned Aerial Vehicles) or as emergency power generators. In a FC system, the compressor transports the necessary air to the fuel cell so that the chemical reaction of oxygen and hydrogen can be used to generate electricity. FC systems in mobile applications experience different climatic and weather conditions. In particular, gas bearing turbo compressors of Proton Exchange Membrane (PEM) fuel cells [1] for automotive applications are subject to a large range of ambient temperatures and relative humidities. A change of air state (temperature and humidity) can lead to partial condensation of water vapor from air in the sealing gas path of the turbo compressor. Partial condensation is conceivable at many locations within the compressor and critical for the proper operation. Particularly critical with regard to condensations are the components of the gas bearings, where even small quantities of liquid can lead to a failure. In addition, if the exposure to humidity and condensate is prolonged the components without appropriate corrosion protection corrode or a short circuit can occur on electrical parts. Thus, the knowledge of the effect of ambient humidity and partial condensation of water vapor on the performance of the gas bearing and other parts of the compressor are necessary to ensure a reliable functionality.

1.2 State of the Art and Research

Air lubricated turbo compressors from the company Celeroton are designed in such a way that they can be operated with pure and humid air. However, they have not been designed for pure water vapor or as hybrid bearings consisting of water droplets and air and they cannot operate in liquid or mixed phase. Preventive heating of the bearing parts to avoid liquid in the bearing clearance is not a solution either. A gas bearing design for air and pure water vapor combined is generally not feasible as the dynamic viscosity of air and water vapor differ too much to avoid self-excited instability in both cases. Moreover, condensed water may freeze and destroy the bearing parts by expansion of the ice in the bearing clearance. Condensed water in other parts of the compressor represent also a risk as the water could reach the gas bearing through ventilation channels. Therefore, condensed water in compressors with gas bearings have to be avoided.

So far, the air lubricated turbo compressors have not been tested experimentally under high temperatures in combination with high humidity.

The effects of humid air on aerodynamic journal bearings was theoretically investigated and studied first in [2]. The investigations are limited to residual humidity and do not address effects of condensate accumulations. However, the author found out, that high levels of ambient temperature increase the sensitivity of load capacity and stability to humid-air effects, as the mass concentration of water in air increases. Further the author claims, that in realistic situations, the presence of liquid droplets in the bearing clearance is unlikely to be a threat to the integrity of the system due to the very small volume fraction (volume of liquid divided by the total volume) calculated in worst-case scenarios.

1.3 Objectives

The present work investigates the humid air and condensation effects on the performance and reliability of air lubricated turbo compressors from the company Celeroton. The investigations are exemplary performed with the turbo compressor CT-17-700.GB. Two sealing gas concepts of the turbo compressor exists. Both sealing gas concepts are compared with each other.

The main objectives are to: (1) identify and theoretically analyze critical environmental and operating situations with partial condensation processes, (2) design and construct a test rig which allows the experimental investigation of the critical situations, (3) carry out a system identification of the thermal behavior of the compressor and (4) based on the findings and observations, work out measures against condensation and devise design guidelines to improve the robustness of the turbo compressor.

1.4 Master Thesis Outline

After the motivation and the objectives of this work are known, the functionality and the design of the air lubricated turbo compressor and its applications in a fuel cell system are presented in chapter 2. Chapter 3 is devoted to the development of the theoretical fundamentals of humid air, where thermal state properties of humid air are presented and then the changes in air state are discussed. Many subsequent investigations regarding partial condensation of water vapor from humid air are based on these fundamentals. In chapter 4 critical environmental and operating conditions of the turbo compressor with risks for condensation are theoretically analyzed. The most critical situations are investigated experimentally. Therefore, a test grid is developed, constructed and commissioned, which is described in chapter 5. Additionally, standards are analyzed for finding appropriate test scenarios and for defining the requirements of the test rid. Moreover, a feedback control strategy is developed to control the test rid. In chapter 6, the experimental investigations are documented. Finally, in chapter 7 the work is summarized and future work are presented. Concepts of the test rig, data sheets, photos and additional information are attached in the appendix.

2 Air Lubricated Turbo Compressor and its Application in a Fuel Cell

Air lubricated turbo compressors like the CT-17-700.GB [3] and the CT-17-1000.GB [4] from the company Celeroton work as a centrifugal compressor and are equipped with gas bearings. The unique gas bearing technology benefits from high lifetime and oil-freedom, uses these advantages to stand out from conventional ball bearing systems and makes new application fields accessible. A preferred application of these turbo compressors is in mobile fuel cell systems. This chapter gives an overview of the turbo compressor, the gas bearing technology and describes the integration of the turbo compressor in a fuel cell system for mobile applications.

2.1 Overview of the Air Lubricated Turbo Compressor

An overview of the turbo compressor CT-17-700.GB is shown in Figure 2-1. The turbo compressor is equipped with several connectors for the main working fluid (air inlet and outlet), cooling water and the sealing gas.

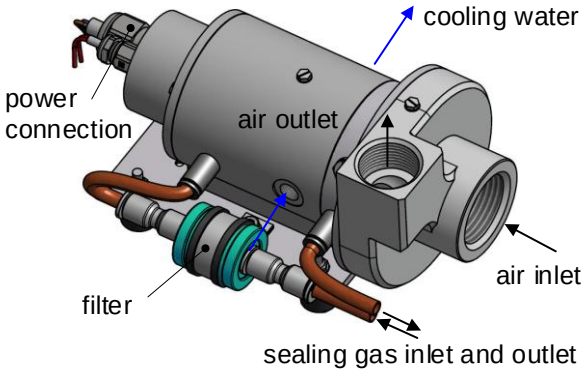

Figure 2-1: Overview of CT-17-700.GB

In Figure 2-2 a sectional view of the compressor is depicted showing the rotor, impeller and further parts.

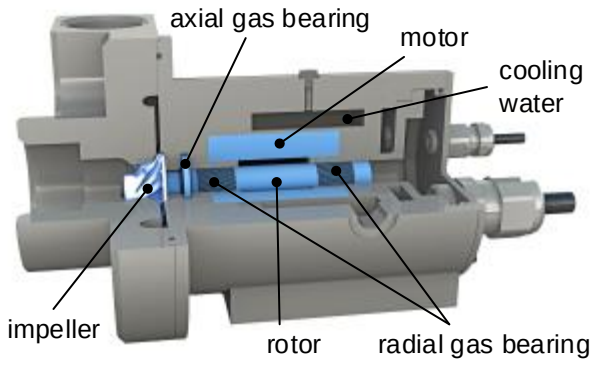

Figure 2-2: Sectional view of the CT-17-700.GB

The functionality and the design of the gas bearing turbo compressor will be described in more detail in the next subchapters.

2.1.1 Working Principle of Turbo Compressors

Compressors can be divided into two categories according to their compression principle: positive displacement compression and dynamic compression. The first one includes, for example, reciprocating (piston) compressors and orbital (scroll) compressors. In **positive displacement compression**, the air is drawn into one or more compression chamber, which are then closed from the inlet. Gradually, the volume of the chambers decreases. As a result, the pressure increases, and the air is compressed. Upon reaching the design built-in pressure ratio, a port or valve is opened, and the air is discharged through the outlet due to continued reduction of the chamber volume.

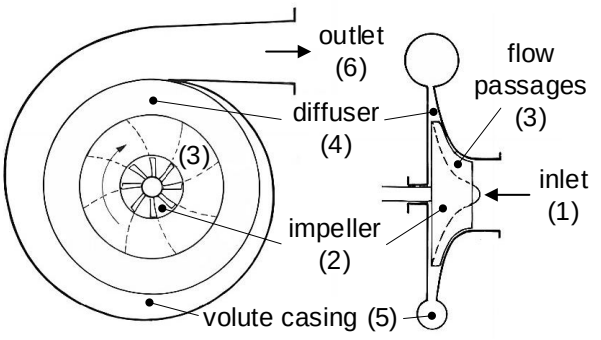

Figure 2-3: Centrifugal (radial) compressor schematic diagram

In **dynamic compression**, the air is drawn between blades on a rapidly rotating impeller and accelerated to a high velocity. The pressure built-up is then realized partially in the rotating impeller and when the air is discharged through a stationary diffusor, where the kinetic energy is converted into pressure. Most dynamic compressors are turbo compressors with either an axial, radial or mixed flow pattern. Unlike positive displacement compressors, dynamic compressors can supply continues flow.

The turbo compressor CT-17-700.GB from Celeroton have a radial flow pattern as depicted in Figure 2-3. In radial turbo compressor, the air enters the compressor through the eye of the impeller (1). The impeller (2) consists of several blades, which form flow passages (3) for the air. From the eye, the air enters the flow passages formed by the impeller blades, which rotate at very high speed. As the air flows through the blade passages towards the tip of the impeller, it gains simultaneously momentum and static pressure. At the tip of the impeller, approximately 60 % of the total pressure rise has already been converted. From the tip of the impeller, the air flows into an annular channel of increasing radius around the impeller, referred as the diffusor (4). In the diffuser, the air is decelerated and as a result the dynamic pressure drop (losses of kinetic energy) is converted to static pressure rise, thus increasing the static pressure further. The air from the diffuser enters the volute casing (5) where further conversion of velocity into static pressure takes place due to the divergent shape of the volute. Finally, the pressurized air leaves the compressor at the outlet form the volute casing (6). Between the tip of the impeller and the outlet of the compressor the residual 40 % of the pressure rise are converted.

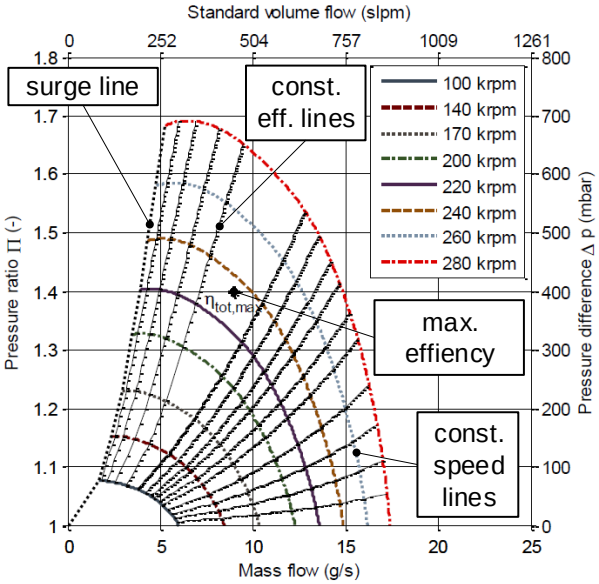

Figure 2-4: Centrifugal compressor map of CT-17-700.GB given for an inlet temperature of 20 °C and inlet pressure of 1 bar(a) [3]

A typical centrifugal compressor map (of the compressor CT-17-700.GB) is shown in Figure 2-4, which depicts the

relation of mass flow, pressure ratio and speed. The turbo compressor operating points are limited by the surge line and the maximum speed line which is the 280 krpm line.

2.1.2 Functionality of Gas Bearings

In a rotor-stator-system the gas bearing is formed from a thin gas cushion between the rotor and the stator case. The required lifting power is established through an overpressure built in the gas cushion, which increases with deflection. The gas exerts force against the deflection of the rotor and keeps it in the center of the stator case, and therefore ensures a contactless bearing of the rotor from the stator [5]. By means of non-contact operation mechanical wear can be completely avoided [6]. The main required technical characteristic of the gas cushion is having the correct stiffness and damping in order for the gas cushion to absorb disruptions such as unbalance and vibration.

Basically, there exist two methods on how the pressure in the gas cushion can be built-up. One option is the usage of externally pressurized gas bearings. Here, the pressure within the air gap is ensured by an external feed. The rotor can be kept in the center of the stator case; therefore, rotation can be realized from standstill without any stiction. The other option is the use of self-acting gas bearings that allows a more compact design of the overall system since no external pressure feed is necessary. In self-acting gas bearings, the pressure within the gas cushion is built-up by the rotation of the rotor relative to the stator case as depicted in Figure 2-5. However, this type of gas bearing has to be operated at a minimum rotational speed, the so-called lift-off speed. From this speed on, the pressure build-up in the gas cushion resulting in a lifting force is large enough to overcome gravity and lets the rotor hover. Besides the lifting force, the stiffness and damping are different to externally pressurized gas bearings and moreover strongly dependent on the rotational speed. Celeroton's turbo compressor employ self-acting gas bearings, in particular herringbone grooved journal bearings and spiral groove thrust bearings as they enable a more compact design without external pressure feed [5].

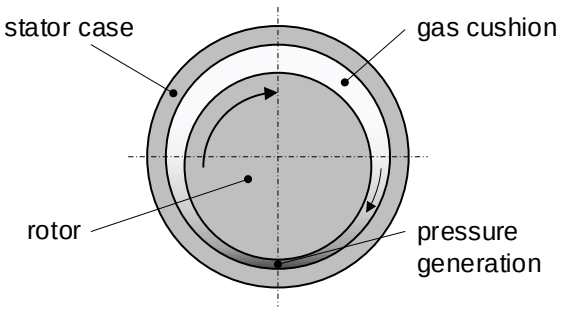

Figure 2-5: Self-acting gas bearing

2.1.3 Air Management in Turbo Compressor

Celeroton's turbo compressor CT-17-700.GB use a sealing gas to protect the gas bearings from impurities such as dust particles sucked in from the ambient air. If no sealing gas is used, dust particles could penetrate into the gas bearing by passing the small gap between the back side of the impeller and the volute casing. Once there, the dust particles could lead to abrasion in the gas bearing that ultimately leads to an accumulation of particles and finally to a system failure.

In order to prevent the impurities entering the gas bearings two different variants are implemented in the CT-17-700.GB providing the sealing gas flow:

- For the **impeller-propelled sealing gas** (IPSG) the sealing gas flow is maintained by

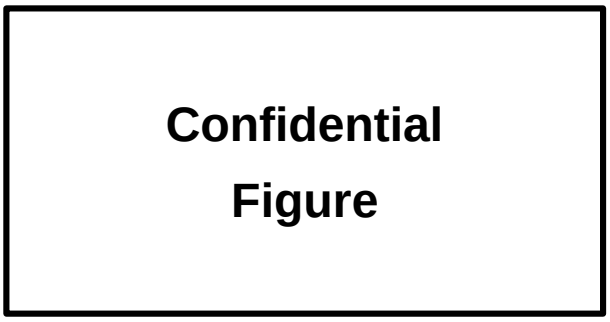

Figure 2-6: Flow direction of the impeller-propelled sealing gas

- For the **high-pressurized sealing gas** (HPSG) the sealing gas is

Figure 2-7: Flow direction of the high-pressurized sealing gas

In neither of these variants is a sealing gas flow through the radial gas bearing, as a result of a symmetric herringbone grooved bearing design.

2.1.4 Thermal Management in Turbo Compressor

Any kind of losses (mechanical, electrical, flow etc.) which occur during operation generate heat. Mainly, the following losses can be identified in a gas bearing turbo compressor: air friction losses in the axial and radial gas bearing, air gaps and at the impeller, electrical losses in the motor such as iron and winding losses, heat transfer from the compressed air to the volute which spreads the heat over the compressor housing.

The heat generated must be dissipated from the turbo compressor in order to guarantee high efficiency and long lifetime. For this reason, the cooling is realized with cooling water to protect the turbo compressor from superheating. According to the user manual of the turbo compressor CT-17-700.GB [7], the minimum cooling water inlet temperature has to be at least ambient temperature to avoid condensation of water vapor from air.

2.2 Turbo Compressor in a Fuel Cell System

A literature review in [8] indicates that the turbo compressor is most popular among all FC vehicles. The reasons for this are described in this chapter. Besides, the general requirements for a compressor in mobile fuel cell systems, various subsystems of the fuel cell system and the integration of the compressor are presented.

2.2.1 Compressor Requirements for Mobile Fuel Cell Systems

For automotive applications the following requirements need to be considered [9].

- **Oil free.** Oil which is pernicious for the fuel cell membrane is not allowed in the air supply of the fuel cell stack.
- **Pressure ratio.** The pressure ratio (ratio between the outlet and inlet pressure) should be around 1.5–3.0, depending on the fuel cell stack.
- **Small pressure ripple.** Large pressure ripples (greater than 100–200 mbar) may damage the thin polymer-membrane and produce voltage pulsation, which should be avoided.
- **Weight.** Weight should be as small as possible, since additional weight causes more power consumption.
- **Volume.** A compact compressor gives more space for other components.

The five requirements listed above have been used to compare nine different compressors. These are centrifugal, claw, lobe, membrane, piston, rotary, screw, scroll and side channel compressors. The most adapted compressor for FCs regarding the five characteristics is the centrifugal compressors [9]. Other requirements which were not included in the comparison but should be considered as well are efficiency, price and reliability.

Additional requirements are given in [1] and are as follows.

- **Low parasitic consumption (high efficiency).** The air compression system can consume up to 15 % of the fuel cell generated power. To keep the parasitic consumption as low as possible, highly efficient air compressors are needed.
- **Flexible flow operation.** Depending on the power demand of the fuel cell vehicle, the fuel cell has to act quickly to provide the needed power and work around an optimized operating range. Therefore, the compressor should be able to supply a flexible flow rate according to the situation.
- **Low noise.** Especially in vehicles, the noise emission is also a performance index. Generally, rotary compressors have lower noise than reciprocating compressors that open a port or valve to discharge the compressed air.

2.2.2 Proton Exchange Membrane Fuel Cell

In automotive applications, Proton Exchange Membrane Fuel Cells (PEMFCs) appear to be the most suitable because their working conditions at low temperatures (around 70 °C for low temperature PEMFC [1]) allow the system to start up faster than those technologies using high temperature FCs [9]. In addition, the solid state of their electrolyte prevents leakage and entails only low corrosion. Moreover, due to its merit of high power density, PEMFCs are preferably employed in mobile applications what makes them the perfect choice for transportation applications.

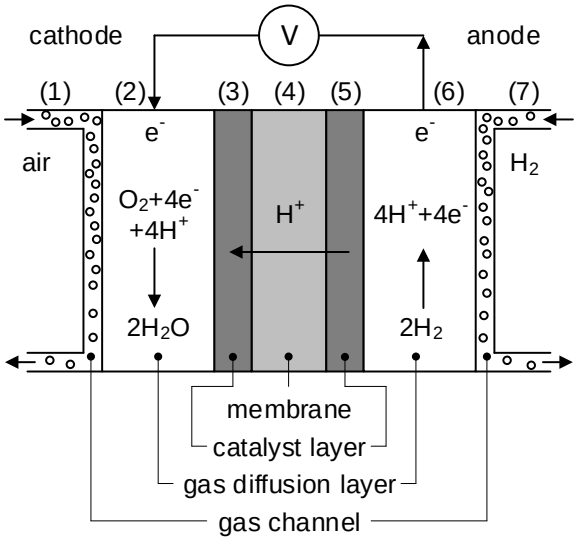

Figure 2-8: Proton exchange membrane fuel cell model

The PEMFCs use solid polymer electrolytes to exchange the ions between two porous electrodes, which is a conductor of protons and an insulator for electrons. In Figure 2-8, the basic working principle of a PEMFC is shown. A single cell consists of seven elementary layers as explained in [1]: The cathode gas channel (1) which is used to circulate the air, the cathode gas diffusion layer (2) where water and oxygen diffuse, the cathode catalyst layer (3) where the oxygen is consumed and the water is produced, the membrane (4) where allowing protons to pass through while blocking electrons, the anode catalyst layer (5) where hydrogen is consumed, the anode gas diffusion layer (6) where hydrogen and water diffuse, and the anode gas channel (7) which is used to circulate the hydrogen. A commercial FC consists of numerous single cells united into one or several stacks depending on the power capacity.

2.2.3 Subsystems of a PEMFC System

The PEMFC needs a great deal of auxiliary equipment, among which is the air turbo compressor (Figure 2-9). The turbo compressor is part of the **air management subsystem**, which is used to supply the compressed air to the fuel cell cathode, where the electro-chemical reaction takes place, producing the electricity with the water and heat as byproducts. The major tasks of the air management subsystem are as follows [10]:

- **Air supply.** The air management subsystem has to supply sufficient reactant flow to keep the required oxygen excess ratio over the full power range. The oxygen is taken from the environmental air, which is circulated by a compressor or blower.
- **Air cleaning.** Any particle or chemical substance, such as carbon monoxide, can be harmful for the catalyst and the membrane. Therefore, the air has to be filtered before entering the stack.
- **Air pressurization.** The air supplied to the PEMFC has generally a pressure from slightly above atmospheric pressure to 2.5 bar(a), depending on the stack design. Optimal pressure around 1.5–2.5 bar(a) is recommended [11]. According to [9] pressurizing the air to the FC implies a high efficiency and gives better water balance characteristics that improves the water management. Moreover, higher air pressure implies a more compact stack (i.e. less weight and consequently less expensive) and higher power density. As a drawback, compared with low pressure FCs, more parasitic power losses are produced by the turbo compressor.
- **Air humidification.** The polymer membrane has to be maintained in a fully hydrated state to have optimal working conditions. To fulfill this target, the air management has consequently to balance water usage, consumption and the amount of water injected.

Besides the air management subsystem, the PEMFC system consists of further subsystems. These are the fuel supply, humidification, cooling and power management subsystems [1]. During the operation of a FC, the task of the **fuel supply subsystem** is to continuously provide the anode side with hydrogen (Figure 2-9). Basically, there are two kinds of fuel supply methods. On the one hand, pure and pressurized hydrogen, that is stored in a tank, is directly transported to the fuel cell stack. On the other hand, available fuels such as methanol, gasoline, natural gas and other hydrocarbons are reformed to produce hydrogen on site, and then supply it to the FC. For most mobile applications and especially in the automotive sector, the first method is adopted because of its high purity and reliability.

The target of the **humidification subsystem** is to maintain proper membrane humidity. This is one of the key requirements for the FC to reach its optimum performance. The intention of humidification of gases entering the FC is to maintain proton conductivity of the electrolyte in the

membrane. Without humidification, the membrane becomes too dry and impedes the proton transport. Therefore, this leads to poor fuel cell function or even failure. The humidification subsystem is integrated into the air management subsystem.

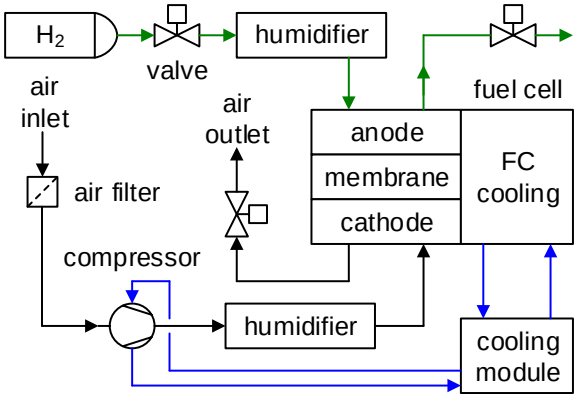

Figure 2-9: Subsystems in a PEMFC system

During the operation of PEMFCs, large amount of heat is generated which should be effectively removed to avoid overheating of the membrane and other components. This is where the **cooling subsystem** comes in (Figure 2-9), which ensures the optimum working temperature between the narrow range of 60 °C to 80 °C. A high temperature can significantly exacerbate the degradation of the membrane and the catalyst, and reduce the stack performance, while a lower temperature is not favorable for the reaction kinetics [12]. Among several cooling methods, such as using highly thermal conductive material as heat spreaders, air flow cooling, liquid cooling etc., the liquid cooling method is widely employed in automotive applications because of its strong cooling capability.

For hybrid vehicles, where the FC operates in combination with energy storage devices, such as batteries and ultracapacitors to output energy, **power management** strategy affects the vehicle performance considerably. The energy flow which is determined by the power management method is controlled by DC/DC converters. In situations, where peak loads are needed, the FC alone might not satisfy the load demand because of its slow response. Energy storage devices such as batteries and ultracapacitors complement the primary energy source to provide quick burst of power and thus to absorb fast transient power changes [13].

3 Fundamentals of Humid Air

This chapter is devoted to the development of the theoretical fundamentals of humid air, where the thermal state properties of humid air are presented and the changes in air state are discussed. Furthermore, the circumstances under which condensation occurs are explained. The equations (mainly summarized from the literature [14]) serve as a basis for all subsequent calculations and simulations performed in this work.

3.1 Thermal State Properties of Humid Air

Humid air implies a condensable gas mixture of water vapor (condensable) and air, considered as incondensable. The mixture is treated as a two-component mixture and the fact that air itself is already a mixture is not taken into account.

Air can be described in the states occurring in the natural environment by the ideal gas equation if the total pressure is less than ten bar [15]. The exact characterization of an air state requires the specification of at least three of the following thermal state properties: pressure, mass loading, relative humidity and enthalpy.

3.1.1 Partial and Total Pressures of Gas Mixtures

The total pressure p exerted by a gas mixture is equal to the sum of the partial pressures p_i of the individual gases i if they would occupy a container alone at the same temperature. This empirical law related to the ideal gas law is known as the Dalton's law and formulated as follows [16]:

$$p = \sum_{i=1}^{n} p_i \tag{3-1}$$

For humid air the total pressure p is composed of the air partial pressure p_A and water vapor partial pressure p_V:

$$p = p_A + p_V \tag{3-2}$$

Air (dry air) is treated as a gas mixture consisting of nitrogen, carbon dioxide and argon. There is no water vapor in dry air. If air is brought into contact with water, which is practically always the case in nature, the water "sees" an environment with a water vapor partial pressure of zero and begins to evaporate immediately. This evaporation can continue until the partial pressure of the water vapor reaches the saturation vapor pressure determined by the temperature of the air. Here the vapor in the air is in thermal equilibrium with the water. This means that vapor can only be absorbed in a gas until the partial pressure of the vapor corresponds to the saturation vapor pressure at the temperature of the mixture [14].

Figure 3-1 shows the vapor pressure curve of water vapor and explains that the partial pressure of water vapor p_V can reach at most the saturation vapor pressure $p_{VS}(\vartheta)$ at the temperature of humid air (1→2). If unsaturated humid air is cooled down, the water vapor content and the partial vapor pressure p_V remain constant until the dew point is reached

(1→3). In this state the humid air is saturated, and the partial pressure of the water vapor corresponds to the saturation vapor pressure of the dew point temperature.

The vapor pressure curve can be described with the Antoine equation

$$\log p_{VS} = A - \frac{B}{C + T} \tag{3-3}$$

with p_{VS} in (bar), T in (K), and the parameters

$$A = 4.6543; B = 1435.264; C = -64.848 \tag{3-4}$$

for the temperature range 255.9–373 K [17].

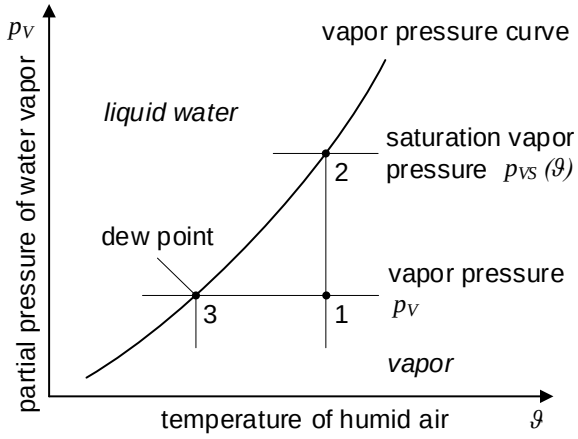

Figure 3-1: Vapor pressure curve of water

3.1.2 Mass Loading and Relative Humidity

In processes with humid air, the mass of dry air remains constant whereas only the mass of water vapor in the air can change due to humidification or dehumidification. Thus, the mass loading X can be expressed as the ratio between the water vapor m_V and the mass of dry air m_A:

$$X = \frac{m_V}{m_A} = \frac{\dot{m}_V}{\dot{m}_A} \tag{3-5}$$

For dry air X becomes zero and for pure water or water vapor X becomes infinity. Since the mass of humid air is composed of the mass of dry air and that of vapor, the mass of humid air can be calculated as follows:

$$m = m_A + m_V = (1 + X) \cdot m_A \tag{3-6}$$

The mass loading X can also be described with the partial pressures of water vapor p_V and air p_L and the molar masses $M_W = 18\ g/mol$ and $M_L = 29\ g/mol$. Here, the factor 0.622 only applies for air:

$$X = \frac{M_W}{M_A} \cdot \frac{p_V}{p_A} = 0.622 \cdot \frac{p_V}{p - p_V} \tag{3-7}$$

The state with maximum water loading is called the saturation state and is indicated with the index "S" for saturation. If a vessel contains liquid water in addition to the moist air, the air will absorb water until thermal equilibrium or saturation is reached. Unsaturated air states between the extreme values $0 < X < X_S$ can be described with the specification of the relative humidity. The relative humidity φ of humid air is the ratio of the water vapor pressure p_V to its saturation pressure $p_{VS}(\vartheta)$ which is determined by the temperature ϑ of the humid air:

$$\varphi = \frac{p_V}{p_{VS}(\vartheta)} = \frac{X}{X_S} \cdot \frac{p - p_V}{p - p_{VS}(\vartheta)} \tag{3-8}$$

Thus φ is in the range of $0 < \varphi < 1$.

Conversely, the mass loading can also be expressed as a function of the relative humidity:

$$X = 0.622 \cdot \frac{\varphi \cdot p_{VS}(\vartheta)}{p - \varphi \cdot p_{VS}(\vartheta)} \tag{3-9}$$

and for the saturated state ($X = X_S$) where φ becomes equal to 1:

$$X_S = 0.622 \cdot \frac{p_{VS}(\vartheta)}{p - p_{VS}(\vartheta)} \tag{3-10}$$

The degree of saturation ψ is the ratio of the mass loading X of humid air to the mass loading X_S of saturated humid air at the same temperature and pressure.

$$\psi = \frac{X}{X_S} \tag{3-11}$$

3.1.3 Specific Enthalpy of Humid Air

Unsaturated humid air is a gas mixture. Its specific enthalpy is related to the mass of dry air. The enthalpy of humid air is:

$$H_{1+X} = H_A + H_V = m_A \cdot h_A + m_V \cdot h_V \tag{3-12}$$

The specific enthalpy of humid air h_{1+X} related to the mass m_A of dry air with the specific heat capacity at constant pressure of air $c_{p,A}$ and the reference temperature ϑ is:

$$\begin{aligned} h_{1+X} &= \frac{H_{1+X}}{m_A} = h_A + \frac{m_V}{m_A} \cdot h_V \\ &= c_{p,A} \cdot \vartheta + X \cdot h_V \end{aligned} \tag{3-13}$$

The specific enthalpy of water vapor h_V contains superheat enthalpy ($c_{p,V} \cdot \vartheta$) in addition to evaporation enthalpy Δh_v at 0 °C:

$$h_V = \Delta h_v + c_{p,V} \cdot \vartheta \tag{3-14}$$

Thus, the specific enthalpy of the unsaturated humid ($X < X_S$) air applies:

$$h_{1+X} = c_{p,A} \cdot \vartheta + X \cdot (\Delta h_v + c_{p,V} \cdot \vartheta) \tag{3-15}$$

For temperatures below 100 °C, the following substance data according to Table 3-1 can be used:

Table 3-1: Substance data [14]

Thermal State Property		Value
Specific heat capacity of air	$c_{p,A}$	1.004 kJ/(kg K)
Evaporation enthalpy water	Δh_v	2501 kJ/kg
Specific heat capacity of water vapor	$c_{p,V}$	1.860 kJ/(kg K)

For temperatures above 100 °C, the mean values of the specific heat capacities and the enthalpy of steam shall be used.

If the mass of water vapor in humid air rises to such an extent that the mass loading becomes greater than the value X_S the humid air is supersaturated, and the excess humidity condenses out. Above the temperature of 0.01 °C, the humid air then contains water in the form of fine droplets. Such a mixture is called fog. At temperatures below 0.01 °C, the water precipitates as ice, snow or frost in solid form (freezing fog). Effects like fog and freezing fog are not treated within this work.

3.2 State Changes of Humid Air

In processes with humid air, the state changes of humid air can be diverse and complex. For example, in the air management subsystem of a FC the state of humid air changes continuously. In order to understand how the state changes work, it is advisable to break down an entire process into the respective subprocesses. By focusing on the subprocesses the equations for the calculation of a state change of humid air can be derived from detailed energy and mass balances. The derivation of the equations and the state changes are discussed by the example of the air management subsystem and laying in addition the basis for the further part of this work. The state changes are divided into isobaric processes such as heating, cooling, dehumidification and humidification and into non-isobaric processes like compression and expansion. On the one hand, the isobaric state changes are depicted in a *h,X*-diagram (enthalpy, mass loading-diagram first introduced by Richard Mollier in 1923), which is a practical tool for the graphical representation of isobaric processes. On the other hand, the non-isobaric state changes are explained in a *h,s*-diagram (enthalpy-entropy-diagram).

3.2.1 Pressure Dependence of Relative Humidity

The lines of constant relative humidity in a the *Mollier h,X*-diagram constructed for a given pressure apply only to this pressure (Figure 3-2). When using this diagram for a different pressure, conversion must be made. Equations (3-7) and (3-8) give:

$$\frac{\varphi \cdot p_{VS}(\vartheta)}{p} = \frac{X}{0.622 + X} \tag{3-16}$$

For humid air with given values of mass loading X, temperature ϑ and pressure p applies:

$$\varphi = \varphi_0(X, \vartheta) \cdot \frac{p}{p_0} \tag{3-17}$$

Here φ_0 is the relative humidity in the *h,X*-diagram and p_0 the pressure that applies to the diagram. This correlation enables the conversion of the *Mollier h,X*-diagram into a different total pressure.

3.2.2 Heating and Cooling

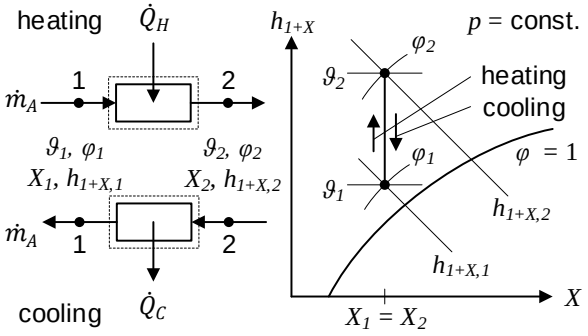

Figure 3-2: Air heating and cooling system and the corresponding state change in the *h,X*-diagram

Humid air is for example heated or cooled in a heat exchanger (HEX) or in a tube due to convective heat transfer. In such a process, if no humidification or dehumidification occur, the mass loading of water vapor X stays constant. If humid air is heated, the relative humidity decreases and increases, if humid air is cooled. The corresponding state changes are shown in Figure 3-2. The prevailing processes are assumed to be stationary. Thus, regarding the system boundary the following mass and energy balances are valid.

Mass balance for dry air

$$\dot{m}_{A,1} = \dot{m}_{A,2} = \dot{m}_A \tag{3-18}$$

and for water vapor / water

$$\begin{gathered}\dot{m}_{V,1} = \dot{m}_{V,2} = \dot{m}_V \\ \Rightarrow \dot{m}_{A,1} \cdot X_1 = \dot{m}_{A,2} \cdot X_2 = \dot{m}_A \cdot X\end{gathered} \tag{3-19}$$

Energy balance for heating case

$$\begin{gathered}\dot{H}_{1+X,1} + \dot{Q}_H = \dot{H}_{1+X,2} \\ \Rightarrow \dot{m}_A \cdot h_{1+X,1} + \dot{Q}_H = \dot{m}_A \cdot h_{1+X,2}\end{gathered} \tag{3-20}$$

and for cooling case

$$\begin{gathered}\dot{H}_{1+X,1} = \dot{H}_{1+X,2} + \dot{Q}_C \\ \Rightarrow \dot{m}_{A,1} \cdot h_{1+X,1} = \dot{m}_{A,2} \cdot h_{1+X,2} + \dot{Q}_C\end{gathered} \tag{3-21}$$

3.2.3 Dehumidification

When humid air is cooled, the relative humidity increases. This air state change takes place from 2 to 1 according to the previous Figure 3-2. In the limiting case, the relative humidity reaches the value 1 and the air is saturated. This state is indicated in Figure 3-3 as the dew point. If the humid air is cooled down further, either the humidity precipitates (condensates) at the cool surface or fog forms, depending on the cooling. The precipitation of water takes place with the state change from the dew point to the point 2. At temperatures above 0 °C the precipitation of humidity from air is known as dew formation and at temperatures below 0 °C frost formation.

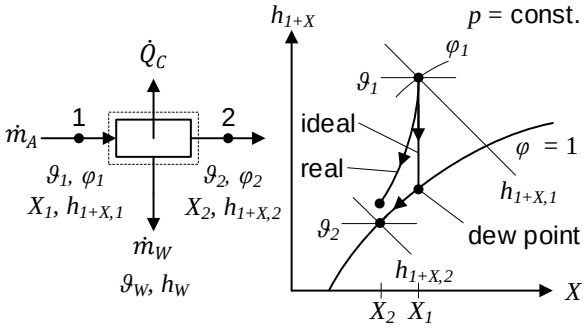

Figure 3-3: Air dehumidification with dew formation and corresponding state change in the *h,X*-diagram

In technical processes, the state change of humid air does not follow the ideal line but the real one. This fact is explained with a temperature profile perpendicular to the flow direction of the air. Near the wall, the air cools down to saturation, whereas in regions further away from the wall, the air remains unsaturated. If a mean value is formed for the temperature and the relative humidity of the air flow, the air at state point 2 is still unsaturated, but the mass loading decreases. With regard to the drawn system boundary in Figure 3-3 the following mass and energy balances apply.

Mass balance for dry air

$$\dot{m}_{A,1} = \dot{m}_{A,2} = \dot{m}_A \tag{3-22}$$

and for water vapor / water

$$\dot{m}_{V,1} - \dot{m}_{V,2} = \dot{m}_W = \dot{m}_A \cdot (X_1 - X_2) \tag{3-23}$$

Energy balance

$$\begin{gathered}\dot{H}_{1+X,1} = \dot{H}_{1+X,2} + \dot{H}_W + \dot{Q}_C \\ \Rightarrow \dot{m}_A \cdot h_{1+X,1} = \dot{m}_A \cdot h_{1+X,2} + \dot{m}_W \cdot h_W \\ + \dot{Q}_C\end{gathered} \tag{3-24}$$

3.2.4 Humidification with Water or Steam

When air is mixed with water or water vapor (steam), the mass loading increases. One possibility for introducing water is the direct injection of fine droplets, which evaporate in the air. So that the water can evaporate, the air cools down accordingly. The fact that the air cools down during the evaporation of water is due to the high evaporation enthalpy of water (Table 3-1). Another possibility for the humidification is mixing the air with steam. Here, the air temperature remains constant or rises slightly depending on whether the steam is added saturated or superheated.

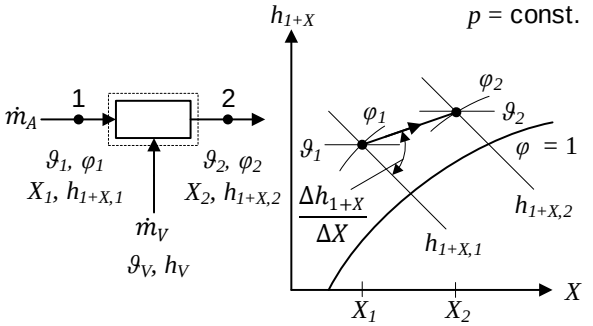

Figure 3-4: Air humidification with steam and corresponding state change in the *h,X*-diagram

The state of water or steam cannot be represented in the *h,X*-diagram because the mass loading of steam and water is infinite. However, the direction of the mixing can be represented. For this purpose, the enthalpy is derived according to the mass loading.

The mass and energy balances for the mixing process are as follows:

Mass balance for dry air

$$\dot{m}_{A,1} = \dot{m}_{A,2} = \dot{m}_A \tag{3-25}$$

and for water vapor / water

$$\begin{aligned} &\dot{m}_{V,1} + \dot{m}_V = \dot{m}_{V,2} \\ \Rightarrow\ &\dot{m}_A \cdot X_1 + \dot{m}_V = \dot{m}_A \cdot X_2 \end{aligned} \tag{3-26}$$

Energy balance

$$\begin{aligned} &\dot{H}_{1+X,1} + \dot{H}_V = \dot{H}_{1+X,2} \\ \Rightarrow\ &\dot{m}_A \cdot h_{1+X,1} + \dot{m}_V \cdot h_V = \dot{m}_A \cdot h_{1+X,2} \end{aligned} \tag{3-27}$$

By changing the energy balance (3-27) to h_V the following equation is obtained:

$$h_V = \frac{\dot{m}_A \cdot h_{1+X,2} - \dot{m}_A \cdot h_{1+X,1}}{\dot{m}_V} = \frac{\Delta h_{1+X}}{\Delta X} \tag{3-28}$$

Equation (3-28) shows that the slope of the mixing line (Figure 3-4) is the enthalpy of the steam h_V (or water h_W). The change in mass loading ΔX is the mass of water supplied divided by the mass of dry air.

3.2.5 Pressure Increase – Adiabatic Compression

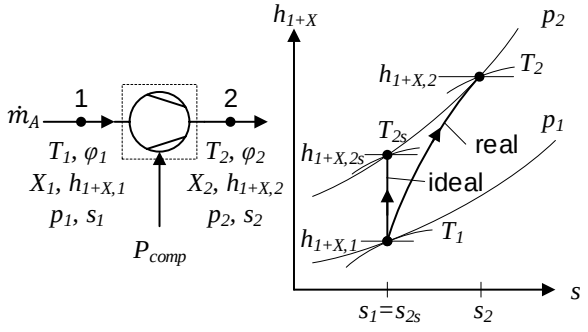

Figure 3-5: Adiabatic air compression and corresponding state change in the *h*,*s*-diagram

The pressure of humid air is for example increased in a turbo compressor. Figure 3-5 shows the compression of air in the *h*,*s*-diagram assuming an adiabatic state change (no heat transfer). In compression, the enthalpy change and thus the pressure change work with dissipation (real case) is greater than in the isentropic state change (ideal case). This is due to internal friction, which increases the temperature more than frictionless compression, so additional work is required for the real compression. Furthermore, when humid air is compressed the dew point pressure and temperature, which are linked, rise. This is due to an increase of the water vapor partial pressure in the same ratio as the total pressure as explained in chapter 3.1.1. The mass loading remains constant, whereas the relative humidity decreases as a result of the temperature rise.

For compression, the mass and energy balances are as follows:

Mass balance for dry air

$$\dot{m}_{A,1} = \dot{m}_{A,2} = \dot{m}_A \tag{3-29}$$

and for water vapor / water

$$\begin{aligned} &\dot{m}_{V,1} = \dot{m}_{V,2} = \dot{m}_V \\ \Rightarrow\ &\dot{m}_{A,1} \cdot X_1 = \dot{m}_{A,2} \cdot X_2 = \dot{m}_A \cdot X \end{aligned} \tag{3-30}$$

Energy balance

$$\begin{aligned} &\dot{H}_{1+X,1} + P_{comp} = \dot{H}_{1+X,2} \\ \Rightarrow\ &\dot{m}_A \cdot h_{1+X,1} + \dot{m}_A \cdot w_{comp} = \dot{m}_A \cdot h_{1+X,2} \end{aligned} \tag{3-31}$$

with P_{comp} as the compressor power and w_{comp} as the specific compressor work. The effective internal compressor power P_{comp} supplied to the air can be calculated with the isentropic compressor power $P_{comp,s}$ and the isentropic efficiency η_s. The isentropic efficiency is defined as

$$\eta_s = \frac{h_{1+X,2s} - h_{1+X,1}}{h_{1+X,2} - h_{1+X,1}} = \frac{P_{comp,s}}{P_{comp}} = \frac{w_{comp,s}}{w_{comp}} \tag{3-32}$$

and describes the ratio of the ideal to real compression. A typical specification used to describe the pressure change of air in a compressor is the pressure ratio Π.

$$\Pi = \frac{p_2}{p_1} \tag{3-33}$$

The pressure ratio is formed from the quotient of the high pressure p_2 to the lower pressure p_1.

3.2.6 Pressure Decrease – Isenthalpic Expansion

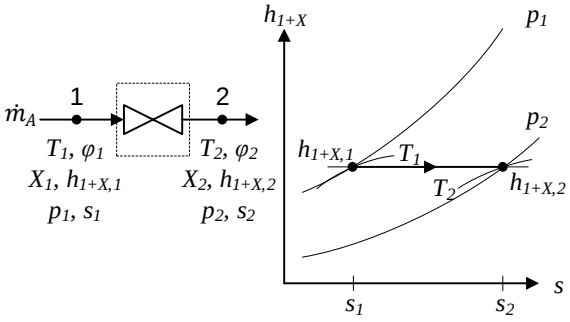

Figure 3-6: Isenthalpic air expansion and corresponding state change in the *h*,*s*-diagram

Isenthalpic state changes occur in adiabatic throttling processes when the changes in kinetic and potential energy are negligible. This is for example the case in a throttle or in a tube due to wall friction. For ideal gases, the isenthalpic change of state is the same as for the isothermal. With real fluids, the isenthalpic change in pressure is accompanied by a change in temperature. The state change can be demonstrated in the *h,s*-diagram of a real gas (Figure 3-6). For the isenthalpic process, the mass loading remains constant, whereas the relative humidity decreases as a result of the pressure loss. For expansion, the mass and energy balances are as follows:

Mass balance for dry air

$$\dot{m}_{A,1} = \dot{m}_{A,2} = \dot{m}_A \tag{3-34}$$

and for water vapor / water

$$\begin{aligned} \dot{m}_{V,1} &= \dot{m}_{V,2} = \dot{m}_V \\ \Rightarrow \dot{m}_{A,1} \cdot X_1 &= \dot{m}_{A,2} \cdot X_2 = \dot{m}_A \cdot X \end{aligned} \tag{3-35}$$

Energy balance

From the first law of thermodynamic

$$\begin{aligned} q + w = h_{X+1,2} - h_{X+1,1} + \frac{1}{2}(c_2^2 - c_1^2) \\ + g \cdot (z_2 - z_1) \end{aligned} \tag{3-36}$$

where q is the heat, w the work, c the velocity, z the height and g the gravitational constant, the isenthalpic state change of expansion can be derived. The following assumptions are made for this purpose: an adiabatic expansion, where heat transfer is negligible ($q = 0$), no work is performed ($w = 0$), change in kinetic energy is negligible small ($c_2 - c_1 \cong 0$) and the change in potential energy is zero ($z_2 - z_1 = 0$).

$$0 = h_{X+1,2} - h_{X+1,1} \Rightarrow h_{X+1,1} = h_{X+1,2} \tag{3-37}$$

4 Theoretical Analysis of Situations with Partial Condensation Processes

In the automotive sector, most components of a vehicle are exposed to all kinds of environmental conditions. For example, temperatures about 55 °C in the Death Valley (USA) or temperatures below -40 °C in the Arctic stress the components thermally [18]. Further stressors are rain and humid air. The latter one can lead to humidity within the components if water precipitates from air due to partial condensation. Especially in the context of this work, the focus lies on partial condensation within the turbo compressor, since in the turbo compressor different temperatures and pressures occur both influencing the tendency for condensation.

Air drawn from the environment flows both through the turbo compressor and, via sealing gas paths and ventilation ducts, through the gas bearings and parts of the electrical machine. Via these channels, air humidity can reach many components of the compressor and partial condensation that builds a liquid film is basically conceivable at many locations in the compressor with yet undetermined effects. For this reason, a risk analysis of possible critical environmental situations and operating conditions is carried out in order to select relevant situations for the further proceeding. Moreover, simple physical models are developed to estimate the possible impacts of a certain situation.

4.1 Risk Analysis and Assessment of Critical Situations

Table 4-1 shows a compilation of possible critical environmental situations and operating conditions of the turbo compressor, where partial condensation can appear. Each situation is illustrated with at least one example. To identify and analyze potential issues that could negatively impact the main functionality of the turbo compressor and to determine specific situations which needs a closer examination, a risk analysis is carried out. These situations are assessed according to their frequency (F) and consequence (C) from numbers one (improbable) to five (frequent) and one (negligible) to ten (catastrophic) respectively. The product of the frequency and consequence gives the risk (R), which is given in the risk matrix (Table 4-2). The number of the risk gives information about the severity of the risk and divides it into the three levels: low (acceptable), medium (undesirable), high (unacceptable).

In the first situation (defined as an unacceptable situation with R = 20) the turbo compressor is continuously operated with a cooling water temperature ϑ_{CW} below the dew point temperature of air ϑ_{DP}. In such a situation, the condensate is accumulated within the compressor and drying is impossible. It has to make clear, that although the cooling water temperature is lower than the dew point temperature partial condensation is not necessarily occurring. During operation the heat losses heat up the compressor housing. This can lead to cases where the surface temperature of the air ducts ϑ_{surf} is still higher than the dew point temperature and no condensate can accumulate although the cooling water temperature is lower than the dew point temperature. To be precise it must be $\vartheta_{CW} < \vartheta_{surf} < \vartheta_{DP}$ for condensation, but for simplification reasons it is assumed that in every case where $\vartheta_{CW} < \vartheta_{DP}$ the heat losses have less influence, so that there is still a production of condensate.

Since a continuous accumulation is undesirable (prohibited) and situation **one** concerns here an employment in FC boats it is not relevant for further investigations, because it is not an automotive application.

Table 4-1: Compilation of critical situations

No.	Situation	Example	Frequency	Consequence	Risk	Comments/Measures
1	Stationary operation of turbo compressor with cooling water temp. below dew point temp. of ambient air	Operation with low cooling water temp., FC boat with sea water cooling, FC car with active cooling (e. g. with refrigeration unit system)	2 Condensation occurs only at low cooling water temp.: $\vartheta_{CW} < \vartheta_{DP}$, active cooling is less common, not used in automotive application	10 Continuous condensation, accumulation of condensate, drying impossible during operation	20	To prevent this situation from occurring, ϑ_{CW} must be at least high enough, so that the wall temp. of the air ducts together with the waste heat from the motor does not fall below ϑ_{DP}. At partial load, ϑ_{CW} should be higher than at full load.
2*	Stationary operation with ϑ_{CW} below ϑ_{DP} of air state after compression	A small amount of compressed and hot air is removed and fed to the sealing gas path → air cools down in the compressor housing and condenses, as the ϑ_{DP} is low	3 Condensation occurs only if $\vartheta_{CW} < \vartheta_{DP}$ at outlet	10 Continuous condensation (accumulation), in such a case drying is impossible	30	The compression of humid air increases ϑ_{DP} (see vapor pressure curve of water); this means that ϑ_{CW} must be selected higher than in situation 1
3	Transient situation (I), change of inlet conditions: cold compressor goes into warm humid environment, operation with ϑ_{CW} and ϑ_{surf} temp. < ϑ_{DP}	Entrance in warm and humid tunnel/garage in winter, especially by cold start, driving from battery, driving down a mountain: on the peak cold and dry and in the valley warm and humid.	5 This situation can happen every day, when the car is driven into a warm and humid garage/tunnel	7 Condensation can only occur at the beginning till $\vartheta_{surf} \geq \vartheta_{DP}$, condensate can accumulate	35	If the compressor is already warm and $\vartheta_{CW} > \vartheta_{DP}$ then no condensation is possible. At partial load $\vartheta_{CW} < \vartheta_{DP}$ could remain. Measures: Shorten time until compressor is warm, increase losses, introduce reactive current at the winding, install heating; heating water instead of cooling water
4	Transient situation (II), change of cooling condition: temperature shock caused by external influences, sudden cool down of compressor during operation below the dew point	Thoroughfare through a cold river with FC-SUV and worst case got stuck	1 Such a situation can very rarely occur	7 Condensation if $\vartheta_{CW} < \vartheta_{DP}$, condensate can accumulate temporarily	7	Temporary situation, it will condensate compulsorily, in order to be able to operate such a system, it needs measures in such a situation: Switch off the cooling water, insulate it, mount it in the bonnet at the top.

No.	Situation	Example	Frequency	Consequence	Risk	Comments/Measures
5	Transient situation (III), environment heats up faster than the thermal mass of compressor and environment gains faster more humidity	Test: thawing in fridge, course of the day: cold compressor under the bonnet, where air may heat up faster and gain additional humidity	4 A lot of cars are parked outside	4 Not much condensate will accumulate, temporary situation	16	Temporary situation, where residual humidity can condensate within the compressor.
6	Cooling down in standstill	Operation during the day, park and cooling through night, condensation of water vapor in compressor → residual humidity	5 Once the car is turned off the compressor cools down and encapsulated residual humidity condensates	4 Only residual humidity that is already in the compressor can precipitate	20	Temporary situation, where residual humidity can condensate within the compressor.
7	Combination of radiation and high humidity (compressor not in operation)	Park on a meadow or wet street (no rain)	2 Less cars are parked on a meadow	4 Less humidity can enter the compressor (diffusion) and residual humidity condensates	8	Much more condensate can accumulate on the housing, because compressor cools from outside to the inside (temperature gradient).
8	Locations and land regions with high humidity or wetness	Days with relative humidity of 100 %, car wash, cloud burst, wet street, (burst pipe, irrigation) and with a constant low ϑ_{CW}	3 This can happen occasionally	7 Condensation if $\vartheta_{comp} < \vartheta_{DP}$	21	Temporary situation; can be investigated together with situation 2 because the maximum relative humidity of 100 % cannot be exceeded.
9	Repeated cooling and heating	Temperature cycles in the course of the day	5 (same as in situation 5)	4 Residual humidity can precipitate	20	-
10	Residual humidity in closed volumes when exposed to temperature cycles	Power converter housing, compressor: coil if encapsulated. Temperature cycles during operation and transport.	4 Once the humidity is encapsulated, it cannot leave the closed volume → repeated condensation and evaporation	4 This can lead to corrosion within the power converter, no accumulation of more condensate	16	Measure: transport in vacuum packaging. This situation was chosen, among other things, because of the electronics.

* implies only for the turbo compressor concept with the high-pressurized sealing gas (HPSG)

Table 4-2: Risk matrix

Risk Matrix (Risk = F x C)*							
			C - Consequence				
	Description		Negligible	Marginal	Serious	Critical	Catastrophic
		Weight	1	2	4	7	10
F - Frequency	Frequent	5	5	10	20	35	50
	Probable	4	4	8	16	28	40
	Occasional	3	3	6	12	21	30
	Remote	2	2	4	8	14	20
	Improbable	1	1	2	4	7	10

* Color explanation: risk (priority for investigation); acceptable (low), undesirable (medium), unacceptable (high)

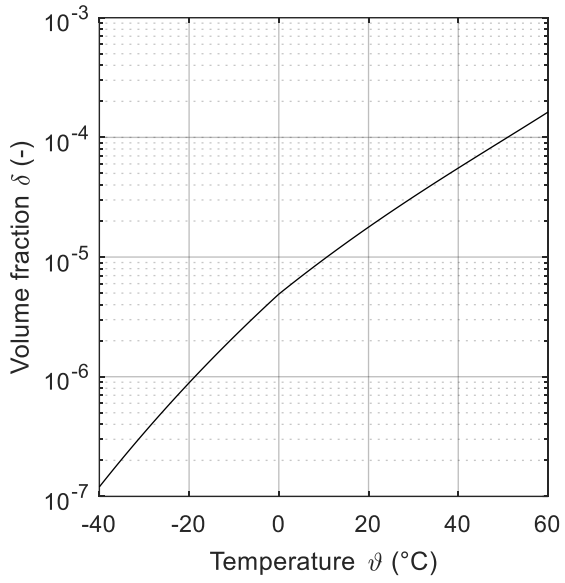

Figure 4-1: Volume fraction of water as a function of temperature in the limit case where all the water content condenses ($\varphi = 100$ % and $p = 1.0135$ bar(a))

The situation **four** and **seven** are low of risk and therefore currently not further of interest. However, the situations **five**, **six**, **nine** and **ten** show a medium risk. In these situations, residual humidity can precipitate as condensate from encapsulated air of the turbo compressor. By virtue of the significant difference of density (three orders of magnitude) between the gas and liquid phase, i.e. air and water as condensate, the liquid phase, might occupy an insignificant volume in the mixture. In order to analyze this, the volume fraction of water, defined as the volume of the liquid phase over the total two-phase volume, is used:

$$\delta = \frac{V_{liquid}}{V_{liquid} + V_{gas}} = \frac{V_{liquid}}{V} \tag{4-1}$$

Figure 4-1 shows the volume fraction of the mixture for different ambient temperatures and ($\varphi = 1$ and $p = 1.0135$ bar(a)) in the situation where all the water from the saturated mixture condenses, which is an overestimation of reality [2]. Under this assumption, the volume fraction gets the following expression, which is derived in appendix A1:

$$\delta = \frac{1}{1 + \frac{1}{X} \cdot \frac{\rho_{liquid}}{\rho_{gas}}} \tag{4-2}$$

The maximum value barely reaches 0.02 % for a temperature of 60 °C, which is suggested to be sufficiently small to discard any risk linked to the formation of a local liquid film in the bearing clearance [2]. The influence of liquid water droplets formed in the bearing clearance due to condensation can therefore be questioned. This can be illustrated by considering a bearing clearance in the magnitude of around 10 µm. For saturated air at 50 °C the volume fraction δ is equal to 10^{-4} and thus the condensate thickness becomes 1 nm. Furthermore, liquid films at other places within the turbo compressor seem to be insignificant, and especially at temperatures below 55 °C which are common in automotive applications and as will be illustrated later in section 4.2.

The risk analysis shows a high risk for situation **three**. In this situation the compressor is operated, and the environ-

mental conditions change suddenly i.e. cold compressor enters warm and humid environment for instance. This can happen frequently when the FC vehicle is driven into a warm and humid tunnel in the winter or out of a cold garage in the tropics. During the operation of the turbo compressor condensate can accumulate till the surface temperature becomes higher than the dew point temperature ($\vartheta_{surf} \geq \vartheta_{DP}$) due to heating of the compressor under operation.

The condensate, which can accumulate in situation **three**, will most probably not produce an evenly distributed water film on the surface of the sealing gas path due to the temperature gradient in the compressor. It is much more likely that a cold spot will cause the condensate to accumulate locally. Even a small accumulation of a few tenths of milliliter at a less dangerous location can be problematic if the water droplet separates from this local location and, for example, penetrates into the gas bearing or reaches the electrical components of the compressor.

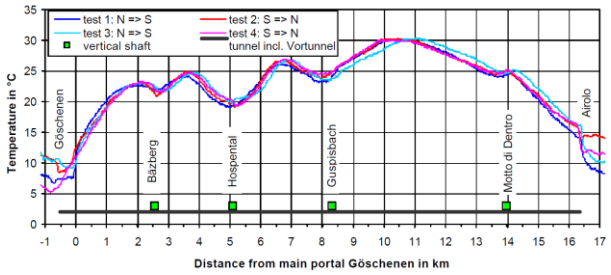

Figure 4-2: Temperature distribution in the Gotthard road tunnel on February 4, 2004 [19]

A concrete example should explain the situation two in more detail. For this purpose, it is investigated how much condensate can be accumulated in a certain time after a FC car is entering a warm and humid tunnel in winter. Figure 4-2 shows the temperature distribution in the Gotthard road tunnel (Switzerland) on February 4, 2004 [19]. According to a statement from one of the authors, Franz Zumsteg, it is possible that the relative humidity of the air in the road tunnel can easily reach 100 % when the street is wet and water droplets evaporate, which before were swirled up from the rotating tires of the cars. In addition, the air can remain trapped in one place for up to two hours, especially in a countercurrent tunnel which is a tunnel where the cars drive in both directions. For this example, it is assumed that the compressor is cooled with cooling water. The heat absorbed by the cooling water from the compressor is transferred to the environmental air via a heat exchanger (HEX). Depending on the HEX design, the temperature difference between the air and the cooling water will reach 5 K at its worst case regarding condensation. This means, that the cooling water has a temperature of 10 °C, when the FC car enters the Gotthard road tunnel from the direction of Göschenen. Furthermore, it is assumed that a condensate volume of 0.3 ml (0.3 cm^3), which corresponds to one percent of the sealing gas path volume, is already critical for a reliable functionality of the compressor. In order to estimate and calculate the time until 0.3 ml is filled with condensate, equation (4-1) is modified with:

$$V_{liquid} = \frac{\dot{m}_W \cdot t}{\rho_W} = \frac{\dot{m}_A \cdot \Delta X_S \cdot t}{\rho_W} \qquad (4\text{-}3)$$

Here, ΔX_S is the difference between the mass loading of saturated ambient air $X_S(\vartheta)$ at given temperature ϑ and the mass loading of saturated air $X_S(\vartheta_{CW})$ at the cooling water temperature $\vartheta_{CW} = 10\,°C$:

$$\Delta X_S = X_S(\vartheta) - X_S(\vartheta_{CW} = 10\,°C) \qquad (4\text{-}4)$$

By inserting equation (4-3) into (4-1) and solving the equation for time t yields:

$$t = \frac{\delta \cdot \Delta V \cdot \rho_W}{\dot{m}_A \cdot \Delta X_S} \qquad (4\text{-}5)$$

With the equation (4-5) and the summarized assumptions from Table 4-3 the accumulation time, until a condensate volume of one percent of the sealing gas path volume is generated (i.e. volume fraction δ is equal to 0.01), can be calculated for different saturated air states.

Table 4-3: Assumption for calculating the water accumulation time in the sealing gas path

Assumption	**Value**	**Note**
Sealing gas (air) mass flow $\dot{m}_A$:	0.2 g/s	Measurement
Saturated air / relative humidity φ:	100 %	Statement from [19]
Air pressure p:	1.0135 bar(a)	Assumption
Total volume V of sealing gas path:	30 ml	Calculated (CAD)
Compressor operated with cooling water temperature at:	10 °C	Assumption
Complete condensation of water vapor from saturated air until cooling water temperature	-	Assumption (worst case)

The results are shown in Figure 4-3 and represent an overestimation of reality, where all humidity of the saturated air condenses until the saturated air state at the cooling water temperature is reached (as described with equation (4-5)).

Saturated air at 20 °C and 30 °C lead to a condensate accumulation of 0.3 ml already after 3 minutes and 30 seconds and 1 minute and 20 seconds respectively. Since the time constant of the turbo compressor until reaching stationary thermal operating point is bigger than one minute, the water accumulation is critical. Moreover, an accumulation of 0.3 ml at the sensitive location can be critical for the compressor and therefore this situation needs to be examined more closely. Since this calculation is also a function of the air mass flow, a reduction of the seal gas mass flow could be considered as a possible measure to reduce condensation.

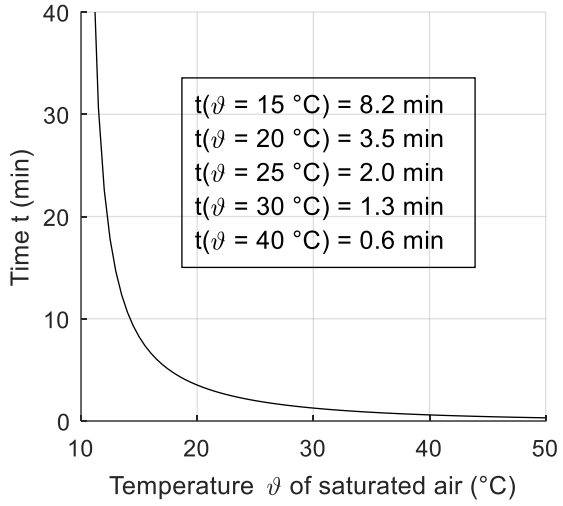

Figure 4-3: Condensate accumulation time until one percent of the total sealing gas volume is filled with condensate related to temperatures of different saturated ambient air states

Situation **eight** considers locations with high humidity (φ almost equals 100 %) and **two** is only valid for the compressor with the high-pressurized sealing gas. Both situations will be discussed later in section 4.2 and section 4.3 respectively.

4.2 Analysis of Dew Point Temperatures in different Land Regions on Earth

Road vehicles are owned and operated in nearly all land regions of the earth. Significant variation in environmental conditions owing to climatic environment, including diurnal and seasonal cycles, can therefore be expected. Regarding the condensation effects within the turbo compressor, the dew point temperature is an important indicator whether it comes to condensation of water vapor or not. Consequently, the information about the globally appearing dew point temperatures is a valuable knowledge, when it comes to discussions about the minimum allowable cooling water temperature, so that under no circumstances condensation can occur. The following analysis refers to situation **eight** from the previous section 4.1.

In order to analyze and cover the dew point temperature of the entire world a representative number of ten cities has been selected (Table 4-4). For the selection process, the world map of Köppen-Geiger climate classification served as the basis. Consideration has been given to worldwide ranges in temperature, humidity, precipitation and atmospheric conditions, including altitude.

The world map of Köppen-Geiger climate classification [20] provides data in a high resolution of 5 arc minutes (0.5° = 30 arc minutes). The Köppen-Geiger climate classification scheme divides climates into five main climate groups: A (tropical), B (dry), C (temperate), D (continental), and E (polar). Furthermore, the second letter indicates the seasonal precipitation type, while the third letter indicates the level of heat. Compared to the usually known climate zones (tropical, subtropical, temperate and cold) the main advantage of the Köppen-Geiger climate classification scheme is the high level of detail, that also takes the altitude into consideration. The world map of Köppen-Geiger climate classifications and all classification types inclusive its explanations are given in appendix A2.

In Table 4-4 the selected ten cities are listed which are classified into the specific climate groups (more information is given in appendix A3). The list includes regions from hot and humid cities like Singapore (Af = Equatorial rainforest, fully humid) down to cold and humid cities like Yakutsk (Dfc = Snow climate, fully humid, cold summer and cold winter). Moreover, an altitude difference of more than 4’000 meters is covered with Dubai and El Alto.

Table 4-4: Selection of cities and its climate classification according to Köppen-Geiger

City	Classification	Climate zone	Weather station (m a. s. l.)
Singapore (SGP)	Af	Tropical	30
Brasilia (BR)	Aw	Tropical	960
Dubai (UAE)	Bwh	Tropical	0
Lima (PE)	Bwh	Tropical	10
Madrid (E)	Bsk/Csa	Subtropical	662
Zurich (CH)	Cfb	Temperate	413
Bogota (CO)	Cfb	Tropical	2’560
El Alto (RB)	ET	Tropical	4’090
Moscow (RUS)	Dfb	Temperate	148
Yakutsk (RUS)	Dfc	Cold	106

The climate data to determine the dew point temperature for each city is provided by meteonorm [21]. Meteonorm is a global climate database generating accurate and representative typical years of any place on earth. The database consists of more than 8'000 weather stations, five geostationary satellites and a globally calibrated aerosol climatology. On this basis, sophisticated interpolation models, provide results with high accuracy worldwide.

The data used originates from the period 2000–2009 and is combined to a representative year. With the meteorological parameters such as temperature, relative humidity and pressure the dew point temperature can be calculated for each hour per representative year. The results are depicted in Figure 4-4 and show the frequency in hours against the dew point temperature over the period of one representative year.

The dew point temperature analysis shows highest dew point temperatures for Singapore. Here, the dew point temperature is within a small range of 18 to 30 °C compared to the other cities. In Singapore, for almost 1800 hours per year the dew point temperature is 25 °C. Both are indicators for a land region with high humidity. A similarly high maximum dew point temperature of 28 °C was measured in Dubai. But the dew point temperature distribution is within a higher range of 5 to 28 °C. Every other city, whether they are located in the high north, close to the equator, on an altitude of 4'090 m or almost on sea level, the maximum dew point temperature is approximately 20 °C.

Based on the analysis of the dew point temperature, the allowing minimum cooling water temperature for the compressor must be at least 30 °C in order to prevent condensation in all land regions on earth. Since the climate data from meteonorm summarizes the date to one representative year, maximum values of extreme years vanish. Thus, a safety margin of additional 5 to 10 °C should be considered.

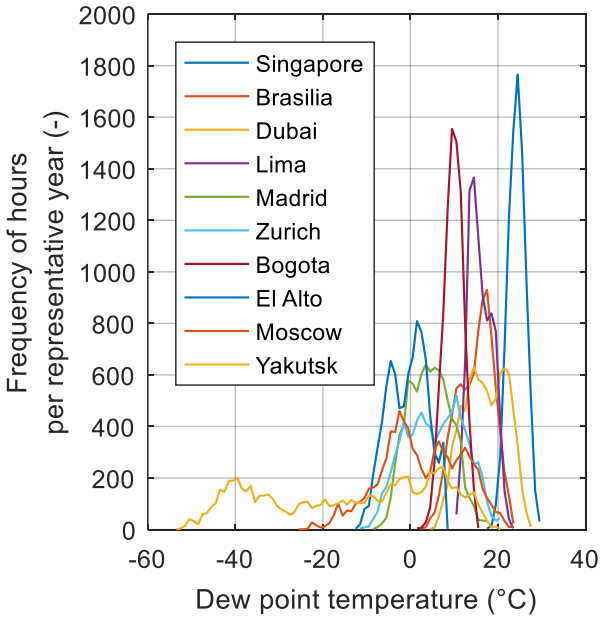

Figure 4-4: Frequency of hours per representative year

4.3 Comparison of the Sealing Gas Concepts Regarding the Dew Point Temperature

As in section 2.1.3 introduced there exists two different sealing gas concepts for the turbo compressor. In the impeller-propelled sealing gas (IPSG) the air is taken at the pressure level of the inlet. In contrast, in the high-pressurized sealing gas (HPSG) the air is removed at the pressure level of the outlet.

A change in air pressure impacts the water vapor partial pressure proportionally and therefore the dew point temperature. As a result, the dew point temperature of the two sealing gas concepts differs due to the different pressure levels of the sealing gas paths. A pressure increase therefore leads to a dew point temperature increase. This behavior is exemplary illustrated in Figure 4-5 and explained with the vapor pressure curve. For the drawn example with a partial water vapor pressure of 20 mbar, an air temperature of 30 °C at the inlet (state 1) and with a maximum pressure ratio of 1.7 for the turbo compressor the dew point temperature rises about 9 °C from 18 °C to 27 °C. Due to the exponentially course of the vapor pressure curve, the effect of pressure increase on the dew point temperature is bigger for lower partial water vapor pressures than for higher partial pressures for a constant pressure ratio.

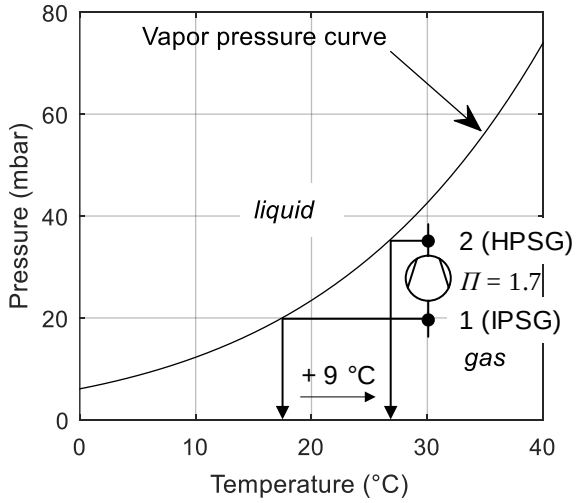

Figure 4-5: Influence of pressure increase on dew point temperature and comparison of sealing gas concepts

As analyzed in the previous section 4.1 and defined as the critical situation **two**, there can also exist situations where the cooling water temperature is lower than the dew point temperature at the outlet of the compressor but higher than the dew point temperature at the inlet. This means the concept with the HPSG therefore has a higher tendency for partial condensation than the concept with the IPSG, because of the higher dew point temperature. But the mass flow through the sealing gas path of the IPSG concept is therefore almost three times bigger than for the HPSG (Table 4-5). Therefore, it is not clear which sealing gas concept is more prone for an accumulation of condensate, because the accumulation time is unknown.

Table 4-5: Comparison of sealing gas concepts

Criteria	**IPSG**	**HPSG**
Dew point temperature	lower	higher
Max. mass flow	200 mg/s	60 mg/s

4.4 Conclusion

The theoretical analysis of partial condensation processes has led to the following findings:

- Environmental and operating situations, where condensation of *enclosed residual humidity* can occur, are of no minor significance due to the only very thin condensate film that can occupy the inner surface of the compressor and the gas bearing.
- On the other hand, situations, in which *condensate can accumulate* over a certain period, e.g. during the heating process of a fuel cell system, are considered to be critical.
- The minimum allowable cooling water temperature to prevent condensation must be at least 30 °C with an additional safety margin of 5 to 10 °C to cover all land regions on the entire earth. To specify this finding for any land region, the minimum allowable cooling water temperature must be at least the same as the environmental dew point temperature.

The theoretical analysis resulted in a number of questions that will be examined experimentally. It will be investigated:

- to what extend condensation is permitted, so that the gas bearing still operates as designed,
- where the coolest and thus the most critical spots in the sealing gas path are, and
- which of the sealing gas concepts (ISPG, HSPG) is less prone for condensation and therefore the better choice.

5 Condensation Test Rig

For investigating the condensation processes in the turbo compressor under realistic air states a test rig is designed and constructed. A requirements specification serves as the basis for the design of the test rig. These requirements are gathered from standards (see next subchapter 5.1) and from the analysis of critical environmental and operating situations from the previous chapter 4. Moreover, the test rig concepts are evaluated and the realization of the test rig are described. Finally, the commissioning of the test rig is presented.

5.1 Analysis of Test Standards

In order to obtain suitable test conditions for turbo compressors in automotive fuel cell applications, existing test standards are analyzed. During a literature research three test standards could be identified, where climatic loads for technical devices in road vehicles are described. These standards are listed below, with a short description of their purpose:

- *ISO 16750-4: Road vehicles – Environmental conditions and testing for electrical and electronic equipment – Part 4: Climatic loads*. The scope of part 4 of ISO 16750 is restricted to the climatic loads that affect electric and electronic systems and components in respect of their mounting location directly on or in road vehicles and specifies the corresponding tests and requirements.
- *ETSI EN 300 019-2-5: Environmental Engineering (EE); Environmental conditions and environmental tests for telecommunications equipment; Part 2-5: Specification of environmental tests; Ground vehicle installations*. This standard specifies test methods and severities for the verification of the required resistibility of telecommunication

equipment according to the relevant environmental class for ground vehicles.

- *MIL-STD-810G: Environmental engineering considerations and laboratory tests.* This standard contains materiel acquisition program planning and engineering direction for considering the influences that environmental stresses have on materiel throughout all phases of its service life. The addresses different test methods.

The two standards ISO 16750 and ETSI EN 300 019-2-5 give an overview and reference to a dozen of further standards, where detailed information are given on how to perform a test and describe the requirements needed, which are indispensable. Due to the limited access to the referenced standards, it appears to be difficult to define appropriate test conditions. However, the standards note several times to maximum values for temperature and humidity. In summary, these are for the temperature 55–70 °C and for the relative humidity 95–100 %. The minimum temperature is -40 °C.

The standard MIL-STD-810G is a comprehensive document addressing inter alia temperature shock tests (described method 503.5), where a sudden change of air temperature is defined as an air temperature change greater than 10 °C/min. This method applies for example during the transfer of material between climate-controlled environment areas and extreme external ambient conditions or vice versa, e.g., between an air-conditioned enclosure and high temperatures in a desert, or from a heated enclosure in the cold regions to outside cold temperatures. Furthermore, humidity test (described in method 507.5) includes natural and induced temperature/humidity cycles (for guidance purposes) for identified climatic regions. Whenever possible and practical, testing in the natural environment is recommended, which may provide more valuable results. Specifically, this method has limitations and does not address for example condensation resulting from changes of pressure and temperature for airborne or ground material.

5.2 Requirements Specification

In this chapter the requirements specification, which lies the basis for the test rig design, is presented. The requirements are derived from the analysis of the critical situation (chapter 4), the test standards (chapter 5.1) and on the basis of the technical data of the compressor CT-17-700.GB. The requirements are summarized in Table 5-1 and are explained in more detail in the following.

As for the air mass flow range, a minimum option ($\dot{m}_{min} = 3 \dots 13\ g/s$) and a maximum option ($\dot{m}_{max} = 3 \dots 20\ g/s$) have been defined. The minimum option allows the testing of the CT-17-700.GB at its most efficient region with the highest pressure ratio. This operation point is achieved according the compressor map from Figure 2-4 at a speed of 280 krpm and a pressure ratio of 1.6. The maximum version of the air mass flow range enables the testing of the compressor further right in the compressor map at higher mass flows or the testing of larger compressors.

Table 5-1: Requirements specifications for the test rig

Requirement	**Value / Criteria**
Air mass flow range	$\dot{m}_{min} = 3 \dots 13\ g/s$ $\dot{m}_{max} = 3 \dots 20\ g/s$
Min. temperature at inlet of test rig (given by room)	$T_{min} = 15\ °C$
Min. relative humidity at inlet of test rig (given by room)	$\varphi_{min} = 15\ \%$
Max. temperature at outlet of test rig	$T_{max} = 40\ °C$
Max. relative humidity at outlet of test rig (inlet of compressor)	$\varphi_{max} = 95 \dots 100\ \%$
Possible operation time of test rig	> 20 min
Min. cooling water temperature for the turbo compressor	$T_{CW,min} = 0\ °C$
Temperature increase	10 °C/min
Measurement of temperature, pressure and relative humidity	must
Control of temperature and humidity at inlet of compressor with a software/computer	must
Setting of temperature and relative humidity to a value higher than environment (room)	must
Providing a given temperature and humidity profile at the compressor inlet	should
Measurement data acquisition with a software/computer	must

Since the test rig is intended to be placed in a laboratory the environmental conditions, which define the inlet air into the test rig, are given and cannot be influenced. Depending on the air conditioning (heating and ventilation) the room temperature can be within the range of 15–28 °C and the relative humidity between 15–65 %. To cover these air states in the requirements, the minimum inlet temperature of

the test rig T_{min} and the minimum possible inlet relative humidity φ_{min} of the test rig are specified with 15 °C and 15 %, respectively.

According to the analysis of the test standards (chapter 5.1), the maximum relative humidity φ_{max} can reach about 95 % to 100 %, which is why the test rig must also produce a relative humidity of the same value. Although the maximum air temperature can reach values between 55 °C to 70 °C according to the standards, the maximum air temperature T_{max} at the test rig outlet (that is compressor inlet) is limited to 40 °C. This limitation reduces the requirements to achieve a fully saturated air state of 40 °C and reduces the dynamic range of the test rig. With this limitation a reconstruction of e.g. the air state in the Gotthard road tunnel (as mentioned in chapter 4.1) is still possible. Furthermore, the test rig must be able to increase the temperature by 10 °C/min.

Another requirement is the minimum cooling water temperature $T_{CW,min}$. The test rig must be able to pre-cool the compressor to 0 °C in order to reconstruct the initial temperature of the compressor during a transfer from a cold to a warm environment. Although, the minimum temperature of -40 °C is given in the standards, the cooling water temperature is chosen in accordance to reconstruct a higher temperature, e.g. in a temperate winter of 0 °C and due to the reason, that a temperature change in cold air does not cause much condensate.

Further requirements regarding the accuracy of the measurement sensors are listed in Table 5-2. These specifications are required to select accurate sensors. Additional measurement uncertainties, which may occur between the control unit and the sensor should be considered but are not specified in more detail.

Table 5-2: Requirements specification for the measurement sensors

Requirement	Tolerance
Accuracy of temperature measurement	± 0.5 K
Accuracy of relative humidity measurement	± 3 %
Accuracy of pressure measurement	± 0.5 %
Accuracy of mass flow measurement	± 3 %

The test rig must be capable of automatically generating a specific air state (temperature and humidity) of certain accuracy for reproducible tests. This requires further control requirements, which are given in Table 5-3. The accuracy values are chosen according to the MIL-STD-810G standard from chapter 5.1.

Table 5-3: Requirements specification for the control

Requirement	Tolerance
Accuracy of temperature control	± 2 K
Accuracy of relative humidity control	± 5 %

5.3 Concept Development and Selection

In this chapter the concept development process for the test rig is shown. For this process the requirements specification serves as the basis. It is ensured that the function of the test rig meets the requirements specified in chapter 5.2.

5.3.1 Air Conditioning Unit and Humidification Methods

The main subsystem of the condensation test rig is the air conditioning unit that provides the required air state, i.e. temperature and relative humidity. As this is the core function, different humidification methods are discussed first.

In principal, there are two methods to get from the minimum initial air state to the maximum final air. The methods depend on how the water is added to the air: either as water droplets or as steam (as already described in chapter 3.2.4). But for both methods the required energy stays the same.

In the water droplets injection method ($1 \rightarrow 4 \rightarrow 3$, ideally, see Figure 5-1), water is sprayed into the air stream in form of small droplets, which then evaporate and extract the sensitive heat from the air ($4 \rightarrow 3$). To make this humidification method possible the air must be heated up first ($1 \rightarrow 3$) in order to reach the final air state (3).

In the steam injection method ($1 \rightarrow 2 \rightarrow 3$), steam is injected into the air stream ($2 \rightarrow 3$). Since the steam consists of much more specific enthalpy than water, the air needs just a small amount of additional heat ($1 \rightarrow 2$) to reach the final air state (3).

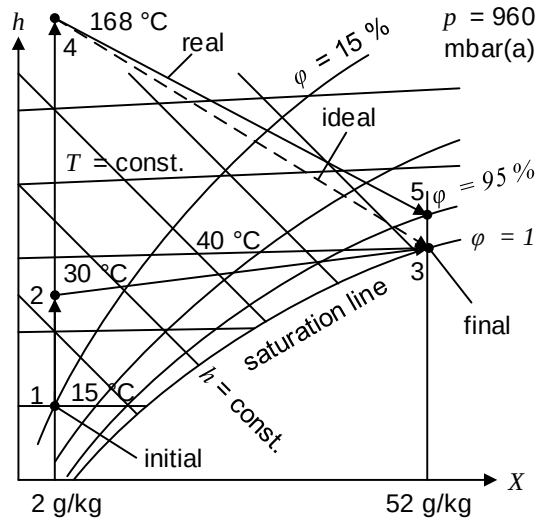

Figure 5-1: Principles of air humidification depicted in the h,X-diagram: with water (1,4,5); with steam (1,2,3)

With the water droplet injection method, the saturation line is not fully reached in reality ($1 \rightarrow 4 \rightarrow 5$) since the efficiency of conventional humidifiers is at best around 95 % [22]. Another reason is to prevent water droplets from being carried along and getting into the compressor. Due to this fact and the fact that a maximum relative humidity of 100 % is required (according to Table 5-1), the steam injection method is preferred.

5.3.2 Commercial Air Humidification Systems

A market research has revealed that there are air humidification systems available from commercial manufacturers. These commercial devices make use of the steam injection method, as described in chapter 5.3.1. The advantage of commercial humidification system is, that it is a developed solution, which shortens the commissioning time of the test rig. However, for a complete test rig, there is still a lot more equipment necessary: e.g. measurement sensors, data acquisition and control unit, power supply. The additional material must be included in budget planning. Prices for the commercial humidifiers (which were inquired with the specifications defined in chapter 5.2) were by itself factors beyond the budget limits for this test rig (approx. CHF 10'000.-). Therefore, a commercial humidification system could not be used, and a self-constructed solution was developed.

5.3.3 Concept Development and Evaluation

To meet the requirements needed several concepts of a possible test rig are analyzed. Both the compressor with the HPSG and the compressor with the IPSG must be able to be tested on the test rig. In principle, the test rig concepts can be divided into closed and open loop concepts. For both open and closed loop type test rig a concept is presented and they are compared with each other.

In Figure 5-2 a closed loop concept of the test rig is depicted, where the air circulates and assumes different air states. At the beginning of the loop the air is filtered and thus freed of particles in order to protect the compressor. In a next step, the air is heated and then humidified with steam, which is injected into the air. This sets the required air state (temperature and relative humidity) upstream of the compressor. The steam is generated by evaporating water. After the humidifier, the pipe needs to be heated with a rope heater if the dew point temperature is higher than the ambient temperature in the laboratory in order to prevent condensation already in the pipe. The turbo compressor works against an adjustable hand valve, which allows to control the pressure ratio. A chiller with a controlled water temperature is connected to the cooling water path of the compressor to cool the compressor. Since the air heats up in a closed loop through the compression process, it must be cooled again afterwards. This is done with a second chiller and a heat exchanger. The chiller can also generate lower temperatures than the ambient temperature. However, the cooling of the air will produce condensate, which must be removed from the closed loop. After the air has passed the heat exchanger the loop starts again.

In contrast, an open loop concept of the test rig is presented in Figure 5-3. The concept essentially consists of the same components and has the same inlet section consisting of a filter, air heater and humidifier. The air is drawn in from the ambient through the air filter and later after the hand valve released back to the ambient.

Further concepts of both closed and open loop test rigs are shown in the appendix A5, where more elaborated versions of test rig concepts can be seen. These include concepts that allow dry air to be mixed with humid air and water droplet injection methods. Also the company internal climate chamber (VCL 4003, Vötsch Industrietechnik) with a chamber volume of approximately 34 liters was also taken into consideration for a closed loop test rig, but it did not fit the requirements due to its inadequate performance for fast air conditioning. In an open loop configuration the climate chamber could not be considered anyway as the highest volume flow of the compressor, the chamber would have been emptied within four seconds.

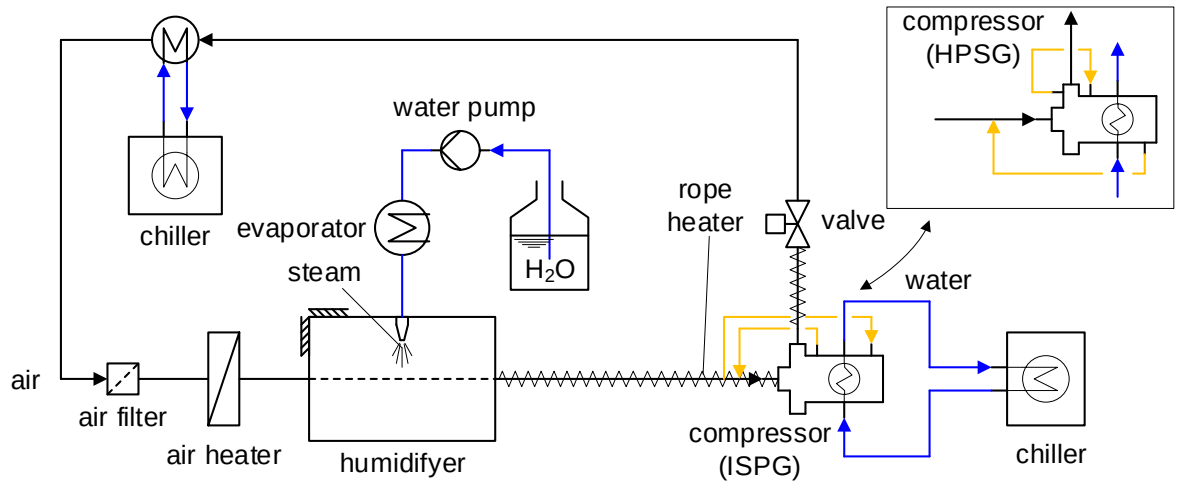

Figure 5-2: Closed loop concept of the test rig

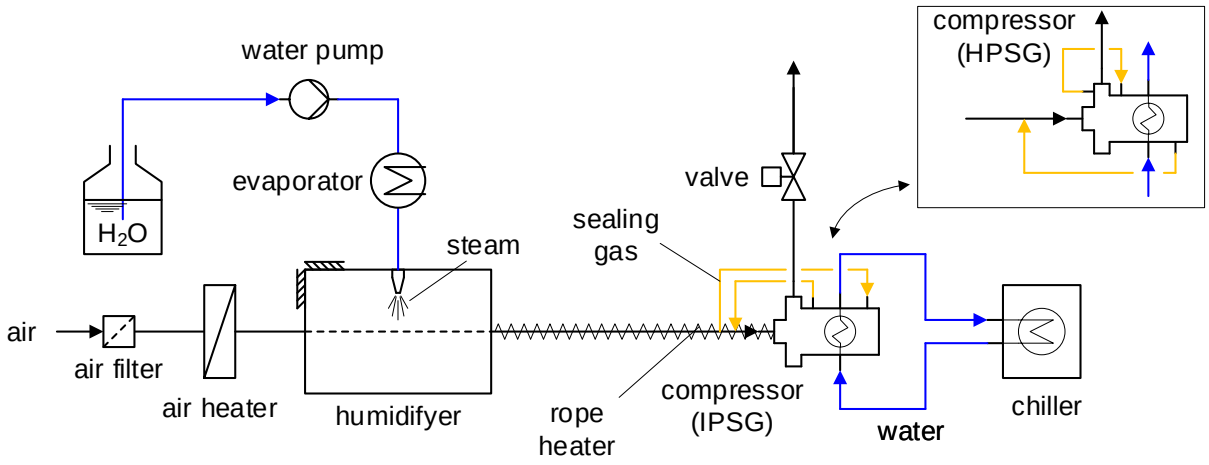

Figure 5-3: Open loop concept of the test rig

Table 5-4 compares and evaluates the two concepts presented above. The comparison was made in the sense of "better" (+) or "worse" (-) based on five criteria.

Table 5-4: Test rig concept comparison

Criteria	Open loop	Closed loop
Number of components / costs	+ (less)	- (additional chiller and heat exchanger)
Complexity of control	+	-
Endurance test (> 20 min)	-	+ (condensate return, thus less water consumption)
Temperature range	-	+ (temp. below room temp. possible)
Condensate in pipe	+	-
Result (No. (+))	3	2

The Table 5-4 shows that the closed loop concept performs slightly better than the closed loop concept. For reasons of simplicity and due to less components needed an open loop test rig is designed.

5.4 Design and Realization

In this chapter, the condensation test rig is presented. It is dealt with the power calculation that is required to select the actuators and parts of the test rig accordingly. Furthermore, the selected actuators, sensors and other parts are presented in more detail.

5.4.1 Calculation of Heat Flow and Water Consumption

Based on the requirements given in Table 5-1 the heat flow of the actuators (air heater, evaporator and rope heater) and the water mass flow of the pump can be calculated. It is assumed, that for the production of humid air water with 20 °C is heated, evaporated, superheated by 50 °C and then injected into an air stream. The calculations are performed with a simulation program (see appendix A4), which is based on the equations described in chapter 2 and the CoolProp C++ library [23] that implements pure and pseudo-pure fluid equations of state and transport properties for 122 components among which is also the humid air. Table 5-5 summarizes the heat flows and water consumption for each of the maximum air mass flow of the minimum and maximum options (as described in chapter 5.2).

Table 5-5: Further requirements

Requirement	Min. option	Max. option
Max. air mass flow $\dot{m}_A$	13 g/s	20 g/s
Max. heat flow air heater $\dot{Q}_{AH}$	182 W	280 W
Max. heat flow evaporator $\dot{Q}_E$	1680 W	2590 W
Max. heat flow rope heater $\dot{Q}_{RP}$	25 W	27 W
Max. water mass flow $\dot{m}_W$	0.62 g/s (37.5 ml/min)	0.96 g/s (57.6 ml/min)

5.4.2 Overview of Test Rig

For planning the test rig a CAD model is created, which is shown in Figure 5-4. Accordingly, the realization of the test rig is depicted in Figure 5-5. These two figures serve as an orientation. More details about the actuators, sensors and compressor modification are given in the following.

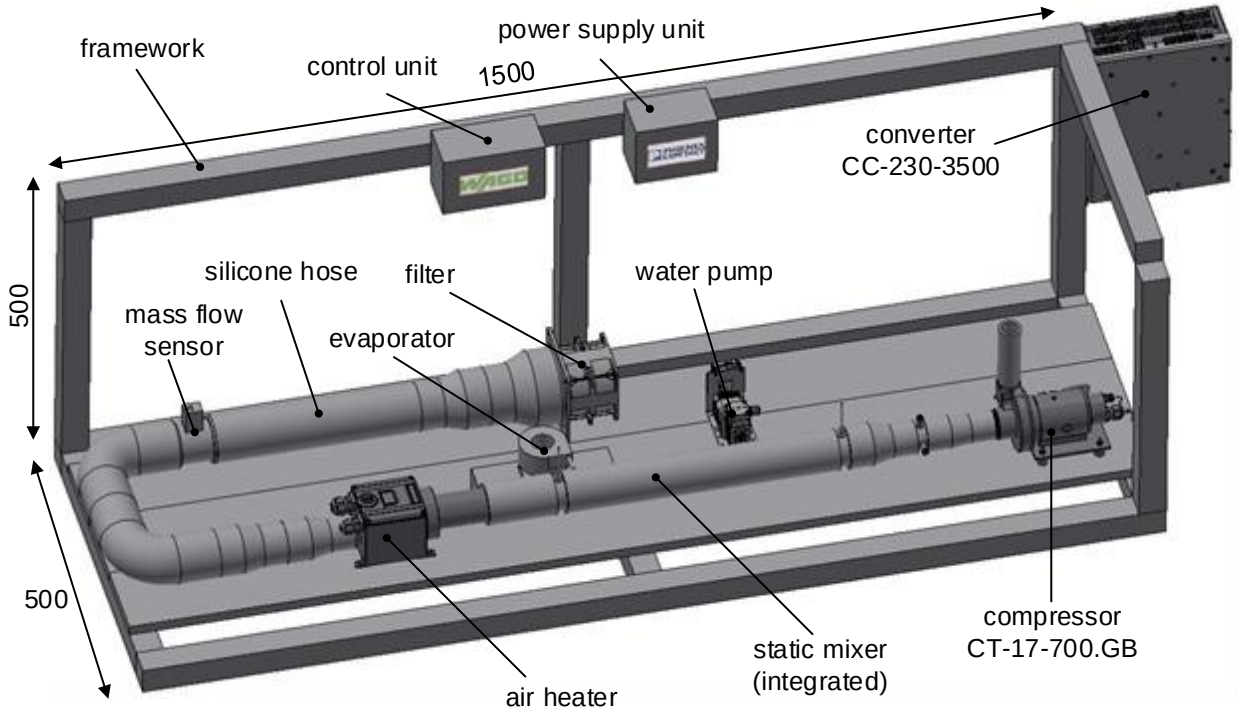

Figure 5-4: CAD model of the condensation test rig (dimensions in mm)

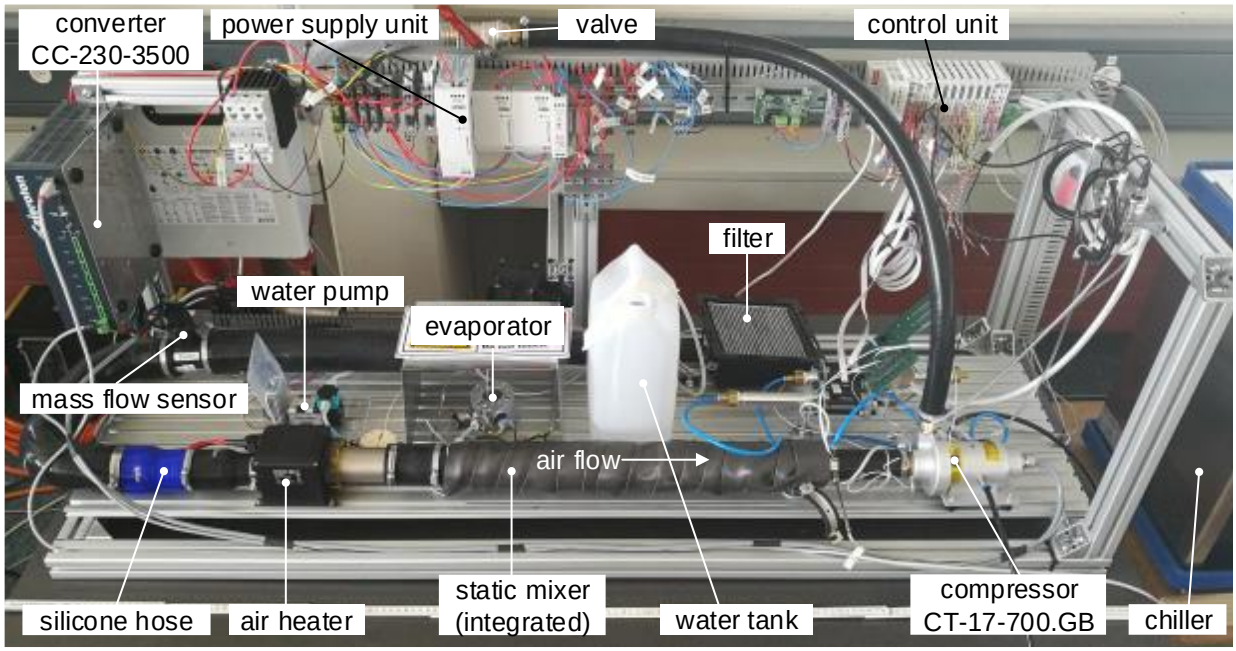

Figure 5-5: Realization of condensation test rig

5.4.3 Actuators

In this chapter all actuators are explained in more detail. The actuators have been chosen according to the calculations in chapter 5.4.1. The Figure 5-6 shows the humidification subsystem of the test rig with all actuators used at a glance.

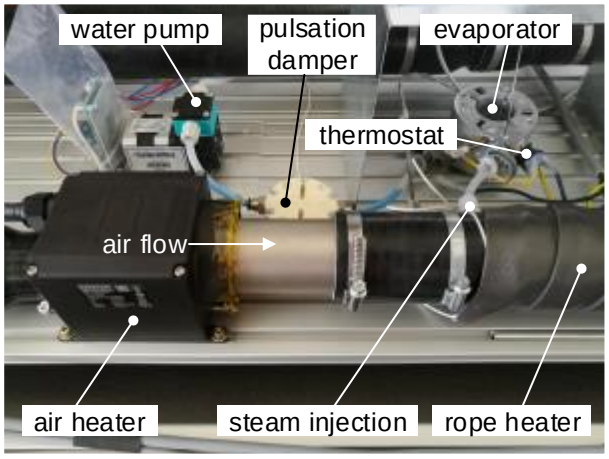

Figure 5-6: Actuators of the test rig

- **Air heater.** The air heater LHS 41S Classic (from Leister Technologies AG) has an input voltage of 230 V and an output heating power of 2.0 kW. Although, the device has an oversized heating power (than calculated in chapter 5.4.1) and the double of the next smaller version (LHS 21S Classic – 230 V / 1.0 kW) it was necessary to use the bigger sized device because of the pressure losses of the air passing through (see appendix A8). With the smaller device the compressor cannot be operated at the maximum mass flow. The air heater has the advantage that it can easily be connected to silicone hoses at the back and front. The device is controlled with a solid state relay (SSR) of type RGC2A (from Carlo Gavazzi Automation SpA), that allows the on/off control of voltages of 230 V with a pulse width modulation (PWM) signal generated by the digital output WAGO module 755-530 (8 channel, digital out, 24 V, 0.5 A).
- **Evaporator.** The evaporator is an instant water heater element of a coffee machine (spare part) with a heating power of 1400 W (230 V). The evaporator with a relay (WAGO module 788-354) and a PWM signal generated by the WAGO module 755-530. In order to protect the heating element from superheating in cases of malfunction of the control, the heating element is equipped with a 175 °C boiler thermostat from a coffee machine. The boiler thermostat is attached to the surface of the heating element with a thermally conductive adhesive (a two-component silicone mixture, DOWSIL 3-6751).
- **Water pump.** As a water pump the diaphragm dosing pump FEM 1.09 (from KNF Flodos AG) was used, which is driven via a stepper motor. The pump has a dispense volume of 0.5 ml per stroke and a maximum dosing rate of 90ml/min at atmospheric pressure. To control the pump

the control module FE Z4 (2-phase stepping motor driver) was used. This control module allows to control the speed of the pump with a 4…20 mA analog signal via the WAGO module 750-555 (4 channel, analog out, 4…20 mA).

- **Pulsation damper.** The KNF diaphragm liquid pulsation damper FPD can reduce pulsations downstream of the pump and has been constructed so that the remaining pulsation will be lower than 200 mbar.
- **Rope heater.** The rope heater has a heating power of 400 W (240 V) and total length of 2.4 m, which was needed to wrap around the silicone hose over the whole length. Additionally, the rope heater is covered with thermal insulation material. The rope heater is controlled in the same way as the evaporator.

5.4.4 Sensors

In the condensation test rig various commercial and sensors built in this work are used. This chapter gives an overview, presents the extra developed sensors and gives a short guideline for placing the sensors correctly into the air flow.

- **Temperature and humidity sensor.** For measuring the relative humidity and temperature of the air combined temperature and humidity sensors of type SHT31-ARP (from Sensirion AG) are used (Figure 5-7). The specified range for the relative humidity is 0…100 % with an accuracy of ±2 % and for the temperature -40…125 °C with an accuracy of ±0.3 °C. These sensors are thanks to their compactness ideally suited for measuring microclimates in the compressor or in hoses. The sensor needs a 5 V supply and is placed on a printed circuit board (PCB), which is additionally equipped with a flexible flat cable (FFC) connector. The PCB is an in-house design based on a sketch and specification by the author (appendix A7).

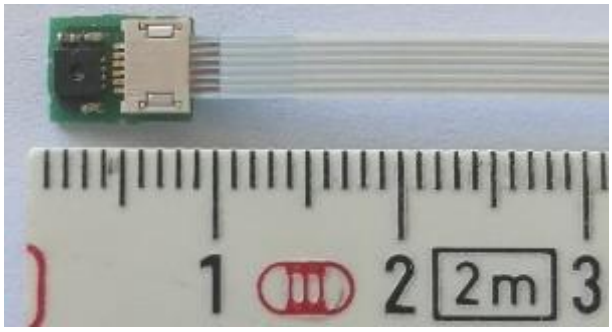

Figure 5-7: Temperature and humidity sensor and the FFC connector on a PCB connected to a FFC

- **Flexible flat cable (FFC) temperature sensor.** This sensor is depicted in Figure 5-8 and is an extra self-developed four-wire temperature sensor consisting of a Pt100 resistor (height 0.45 mm) which is soldered on a flexible flat cable (thickness 0.20 mm). The advantage of the four-wire measurement method is the use of separate pairs of current-carrying and voltage-sensing wires to obtain electrodes to make more accurate measurements than the simpler two-wire measurement method. To protect the resistor from short circuits when mounted, the resistor is covered with a thermally conductive adhesive (the same as is used to attach the boiler thermostat). The total height of the sensor measures about 0.7–0.9 mm. This FFC temperature sensor is used to measure the surface temperature on the compressor and in small gaps within the compressor, which is why they must be very small.

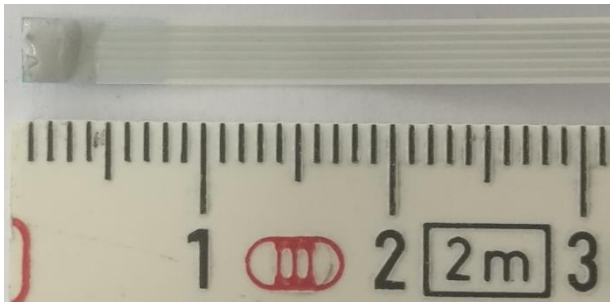

Figure 5-8: Pt100 temperature sensor covered with thermal conductive adhesive

- **Adapter board for sensors.** In order to connect the temperature and humidity sensors as well as the FFC temperature sensors to the data acquisition WAGO module, an adapter board is needed (Figure 5-9). This PCB was developed in-house based on a sketch and specification by the author (appendix A7). On one side of the PCB the FFC can be connected and on the other side four D-sub connectors with cables can be connected. The D-sub cables are connected to the data acquisition WAGO module.

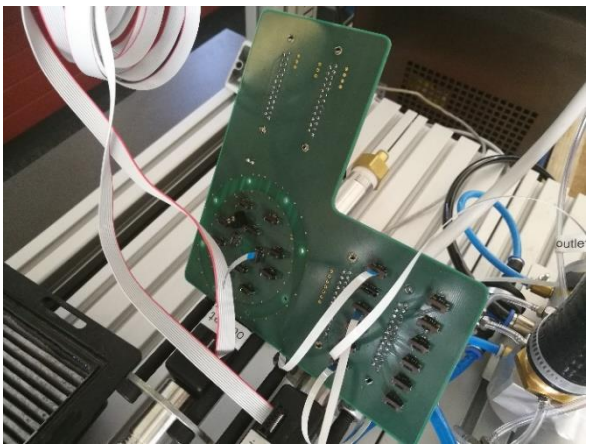

Figure 5-9: Sensor adapter board

- **Mantle resistance thermometer.** For measuring the temperature of the evaporator and the rope heater four-wire Pt100 mantle resistance thermometers are used.
- **Pressure sensor.** Two Huba Control type 528 calibrated absolute pressure transmitters are used in order to measure the inlet and outlet pressure of the compressor. This allows to measure the pressure ratio and to determine the operation point together with the mass flow. The sensors have an analog output signal of 0…10 V, which is analyzed by the WAGO module 750-497 (8 channel, analog input, 0…10 V).
- **Mass flow sensor.** The determination of the mass flow is done with a hot-film air mass meter of type HFM 5 – 3.5 (from Bosch). This sensor is usually used in automotive applications to measure the air flow into gasoline and diesel engines. The sensor needs a voltage supply of 12 V and has an output signal of 0…5 V, which is analyzed by the WAGO module 750-497.

The conversion of the voltage signal of the sensors into the corresponding physical quantity temperature, relative humidity, pressure and mass flow is done by the software. For this, the characteristic curves of the sensors were either implemented as linier functions or polynomials. Some of these functions were available in the data sheets and some had to be determined by a polynomial fit to data points.

The measurement of the temperature and the relative humidity in the air flow of a pipe or hose can be dependent on the heat losses over the wall. If there is a temperature distribution perpendicular to the flow direction at a constant mass loading the relative humidity changes. This risk of stratification and strong changes in humidity can occur near surfaces whose temperature deviates greatly from the air temperature. For this reason, it must be ensured that the temperature and humidity are measured in the middle of the flow.

5.5 Feedback Control of Test Rig and Control Software

For the control of the test rig, a control strategy is developed. A block diagram for the test rig with the feedback control is shown in Figure 5-10. Measurement points are indicated with circles and set points additionally with the symbol (*). The air heater, evaporator and rope heater are temperature controlled with a PWM signal. In order to control the pump, the measured temperature T_2, relative humidity φ_2, and the inlet pressure p_{in} are needed to calculate the mass loading X_2. The corresponding equations for this calculation can be found in chapter 3.1.2. Further, the error in mass loading $(X_2^* - X_2)$ is multiplied with the air mass flow $(\dot{m})$. This yields to an error in water mass flow. This information is processed by the PID controller and a corresponding speed signal is transmitted to the pump.

The PI controllers are implemented in the ideal form given by the transfer function

$$G(s) = K_P\left(1 + \frac{1}{T_I s}\right) \tag{5-1}$$

Where K_P is proportional gain and T_I the integral time constant. The functionalities of these terms are highlighted by the following [24]:

- The proportional term: providing an overall control action proportional to the error signal through the all-pass gain factor.
- The integral term: reducing steady-state errors through low-frequency compensation by an integrator.

For finding appropriate PI parameters, the parameters are manually tuned and increased separately after the same order listed above according to a scheme proposed in [24] until the steady state error is smaller than the requirements listed in Table 5-3.

In order to control the test rig, the LabVIEW program from National Instruments is used. In the LabVIEW program a GUI is written, where the control strategy from Figure 5-11 is implemented. The corresponding GUI is depicted in Figure 5-10. The GUI is separated into three sections: (1) data acquisition, (2) control, (3) monitoring. In the data acquisition section, the measured data can optionally be stored in a frequency of maximum 4 Hz into a csv-file. In the control section, the actuators can be controlled, either in a closed or open-loop feedback control. In the monitoring section, the measurements can be observed.

In the program, the read loop of the sensors and the write loop of the control of the actuators are executed separately. This measure is applied to generate a faster PWM signal. Thus, the write loop is executed seven times faster than the read loop.

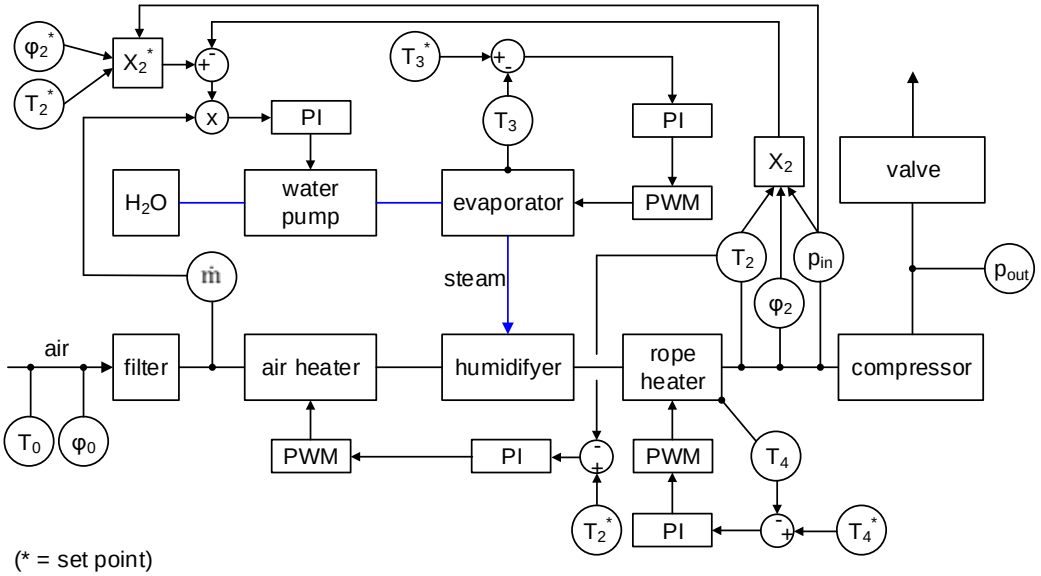

Figure 5-10: Overview of test rig feedback control

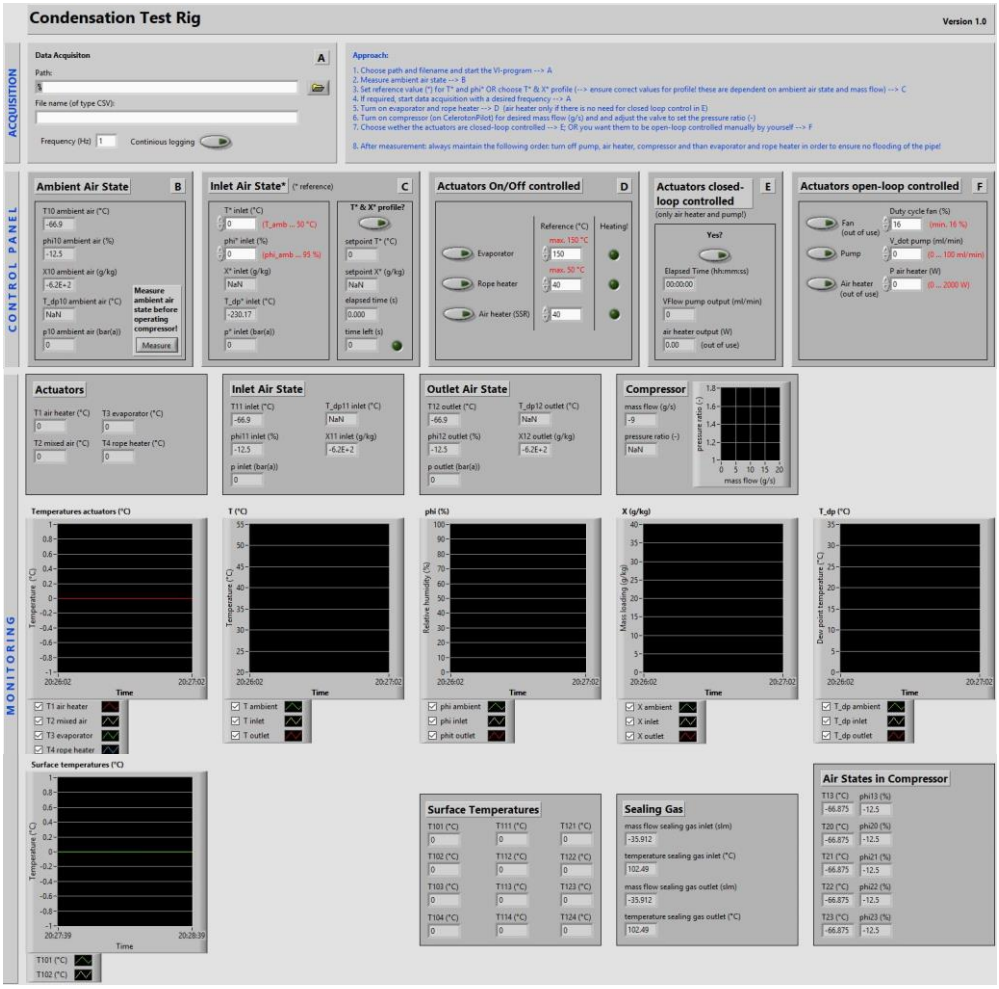

Figure 5-11: Overview of test rig GUI

5.6 Commissioning

In this chapter the commissioning of the test rig is presented. First the pressure losses of the test rig are measured. Afterwards step responses of the test stand are recorded.

5.6.1 Measurement of Test Rig Pressure Losses

In the test rig, there is a static mixer integrated (see Figure 5-5 for location and appendix A6 for photo), that mixes the air and the steam to generate an evenly humidified air. The pressure losses of this static mixer are unknown, because there was no specification in the data sheet available. In addition, the turbo compressor can only be operated to a minimum inlet pressure of 0.9 bar(a). Otherwise the gas bearing would operate unstable at lower pressures. Thus, the total pressure losses of the test rig must be determined to ensure that the compressor can be operated appropriately.

The measurement of the pressure losses is performed at an ambient pressure of 0.97 bar(a) and an ambient temperature of 27 °C. The measured pressure losses are shown in Figure 5-12. It can be seen, that for the maximum mass flow of approximately 14 g/s (corresponding to the maximum speed of 280 krpm of the compressor) the pressure loss is 67 mbar(a). Therefore, the inlet pressure is 0.903 bar(a) and still above the minimum allowable inlet pressure, so that the compressor can be operated on the full speed range.

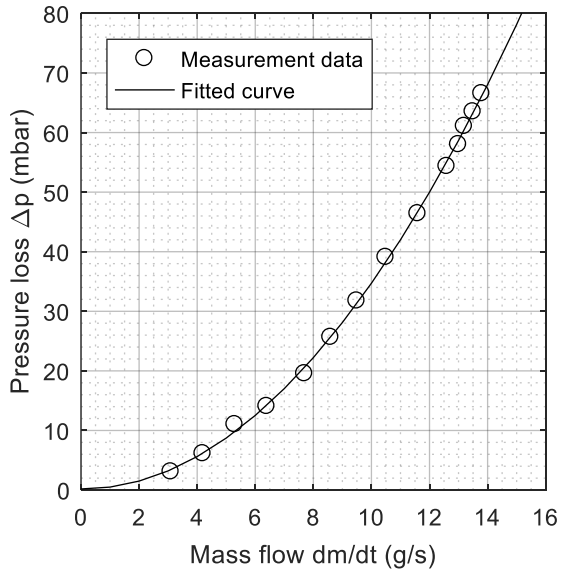

Figure 5-12: Pressure losses in the test rig (measured at an ambient pressure of 0.96 bar(a) and an ambient temperature of 27 °C)

The fitted line to the pressure losses with respect to the mass flow has the following function:

$$\Delta p = \dot{m}^{0.3489} - 0.0366 \cdot \dot{m} + 0.1839 \qquad (5\text{-}2)$$

5.6.2 Step Response of Test Rig for Different Air Mass Flows

In order to proof the functionality of the feedback control loop regarding the inlet temperature and inlet relative humidity two step responses for different mass flows are measured. Figure 5-13 shows the step response for an air mass flow of 10 g/s (280 krpm) and for an air mass flow of 4 g/s (120 krpm). For both measurements, the set points are for the temperature 35 °C and for the relative humidity 95 %.

In both figures the inlet temperature increases fast and reaches a steady state after 40 s close to the set point with an error of maximum 2 K. This confirms that the controller is well adjusted.

On the other hand, the relative humidity takes much longer to reach the set point. This is due to the slow pump control, that had to be selected. A fast control of the pump would lead to strong oscillations, because it is a diaphragm dosing pump that delivers 0.5 ml water per stroke. This makes accurate control difficult. With a slow control, the slightly oscillation in mass loading measurement (respectively calculated from chapter 3.1) is smoothed and not amplified as with a too fast controller.

In steady state, small error of < 5% in the relative humidity is visible with the current PI control parameters. Exact reasons could not be determined in the scope of this work. However, as the error is small it is expected to be of minor significance for the final test results with the compressor.

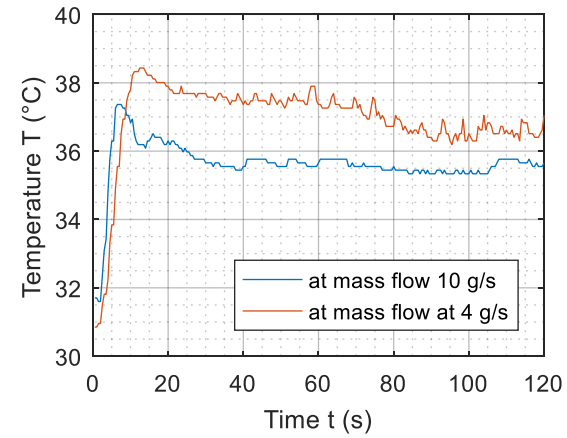

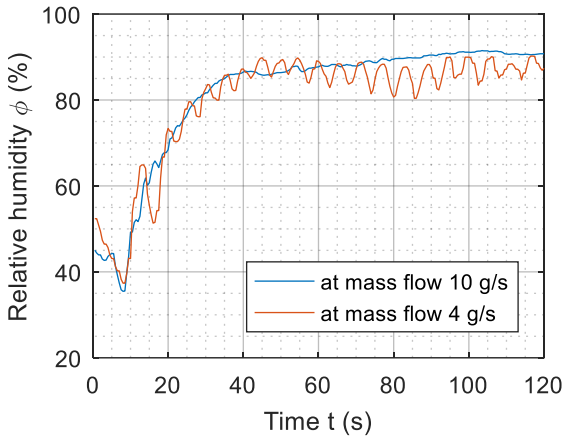

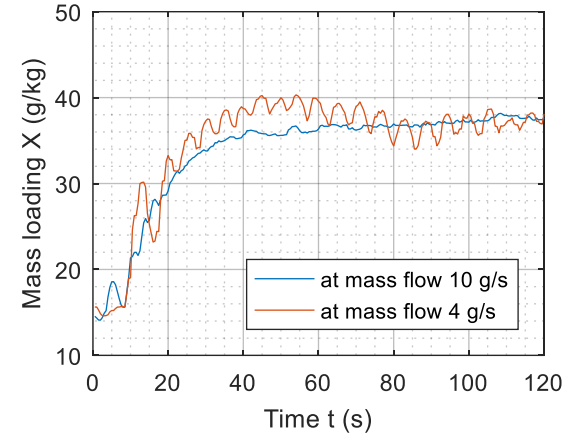

Figure 5-13: Test rig step response for an air mass flow of 10 g/s and 4 g/s

6 Experimental Investigation

By means of experimental tests on the condensation test rig, the condensation behavior of the turbo compressor is investigated. The methodology, the approach as well as the results are described and discussed below.

6.1 Thesis

Through the theoretical analysis of partial condensation processes (in chapter 4) further questions arose which are supposed to be investigated in experiments. It will be investigated:

- to what extend condensation is permitted, so that the gas bearing still operates as designed,
- where the coolest and thus the most critical spots in the sealing gas path are, and
- which of the sealing gas concepts (ISPG, HSPG) is less prone for condensation and therefore the better choice.

In order to answer the above mentioned points, the compressor is equipped with additional temperature sensors. In addition, a systematic procedure and test situations have been developed, which are presented in the next chapters.

6.2 Test Preparation of Compressor

In order to identify the most critical spots for condensation, i.e. the coolest surface temperature, and to quantify these surface temperatures, the compressor is equipped with additional Pt100 temperature sensors as shown in Figure 6-1. One flexible flat cable (FFC) temperature sensors (as presented in chapter 5.4.4) is placed above the sealing gas (SG) inlet and the other one above the sealing gas outlet. They are fixed with an adhesive tape and are additionally covered with a thermal insulation material. The thermal insulation ensures that the sensor does not cool down due to convection and that only the surface temperature is measured. Moreover, there is a temperature sensor mounted on a printed circuit board (PCB) as standard, which is a part of the electric motor (inside the housing, indicated with PTC).

Comparing the surface temperatures with the dew point temperature of the air allows the assessment whether condensation in certain region can occur or not. Since the compressor heats up from the inside to the outside due to the losses, it is further assumed that the outside surface last exceeds the dew point temperature during a cold start.

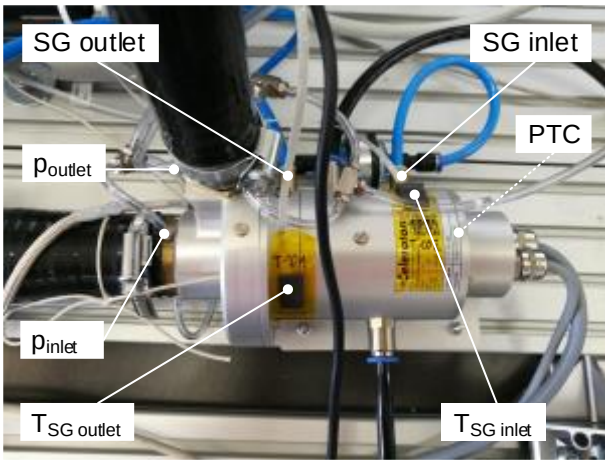

Figure 6-1: Compressor with temperature and pressure sensors

For determination of the pressure ratio (according to equation (3-33)) and thus the operating point of the compressor, the inlet and outlet pressure must be measured. Therefore, the compressor is equipped with pressure sensors (chapter 5.4.4) at the inlet and outlet. These sensors measure the static pressure of the air.

6.3 Approach and Definition of Test Situations

The experimental tests and measurements shall be performed according to a reproducible procedure. For this reason, each test and measurement consist of the following steps, which represent the main procedure. The steps are performed consecutively as follows:

1. **Pre-cooling of compressor**: Before each humidity and temperature test (which is executed as a third step and will be explained later), the compressor is cooled down to 0 °C with a chiller for about 15 min to guarantee an evenly cooled down compressor. At this low temperature, which was colder than the dew point temperature of the ambient air in the laboratory (approximately 9 °C), condensation of the residual humidity within the compressor already occurs. But according to the theoretical analysis (chapter 4.1), the amount of condensate that can occupy the inner surface of the compressor is negligibly small.
2. **Measurement of a rundown**: In this short measurement the turbo compressor is accelerated to a speed of 15 krpm and then turned off. During the rundown the speed n of the rotor can be recorded over time by means of the CelerotonPilot software and the CC-230-3500 converter. With the derivative of the speed $\dot{n}$, the momentum of inertia J of the whole rotor inclusive impeller, which is 5.27E-7 kg/m^2 the friction torque M_{Fr} can be calculated according to the following formulas:

$$M_{Fr} = J \cdot \alpha = J \cdot \dot{\omega} \tag{6-1}$$

with

$$\dot{\omega} = 2\pi \cdot \dot{f} = 2\pi \cdot \frac{\dot{n}}{60} \tag{6-2}$$

whereas f is the frequency and n the speed of the rotor in units (1/min).

This measurement allows to determine the friction torque in the dry state of the gas bearing and must therefore be carried out under ambient air conditions (e.g. room conditions) and with a cooling water temperature higher than the dew point temperature to avoid condensation. As soon as condensate or water droplets would be in the gas bearing, the rundown profile would last shorter (bigger gradient), because the friction moment with water is higher than with air.

The rundown measurement of the CT-17-700.GB is depicted in Figure 6-2. Two consecutive measurements in the dry state were performed to verify the repeatability of the measurement. This measurement defines the state of a dry compressor and is used as a basis for comparison for further measurements. The elbow at about 3 krpm shows the so-called lift-off speed.

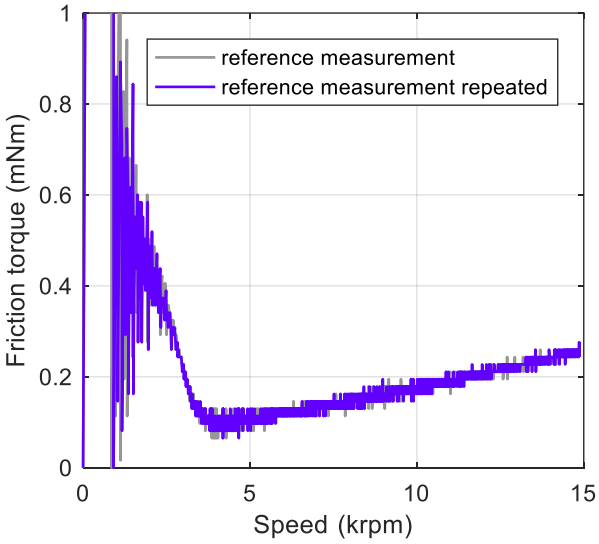

Figure 6-2: Standard rundown profile for a dry compressor

3. **Humidity and temperature test**: In a next step, the turbo compressor is tested under a defined temperature and relative humidity on the condensation test rig with different speeds, cooling water temperature and for a predefined time. Table 6-1 summarizes all parameters. The relative

humidity of 95 % was defined according to the standards, which were described in chapter 5.1. The inlet air temperature is chosen to be slightly higher and defined as 35 °C in accordance with the driving through the Gotthard tunnel scenario from chapter 4.1. The same applies for the cooling water temperature, which is selected lower than the measured ambient temperature from Airolo and Göschenen.

Table 6-1: Parameters for humidity and temperature tests on the test rig

State		**Value / Note**
Temperature at inlet	T_{inlet}	35 °C
R.H. at inlet	φ_{inlet}	95 %
Mass loading at inlet	X_{inlet}	Dependent on inlet pressure $X(T, \varphi, p)$
Pressure at inlet	p_{inlet}	Dependent on ambient pressure and speed $p(p_{amb}, n)$
Dew point at inlet	T_{DP}	$T_{DP}(T, \varphi, p) \approx 34\ °C$
Temperature of evaporator	T_{Evap}	150 °C
Temperature of rope heater	T_{RH}	$T_{DP} + 2\ °C \approx 36\ °C$
Cooling water temperature of chiller	T_{CW}	0 °C
Pressure ratio at 280 krpm	Π	1.6 (valve position kept constant)
Speed	n	120, 160, 200, 240, 280 krpm
Test duration	t	Dependent on test situation

The tests are performed on the most efficient region of the compressor, as indicated with the thick red line in the compressor map in Figure 6-3. It is assumed, that the FC system possess a constant pressure loss and the compressor is only designed for this FC system.

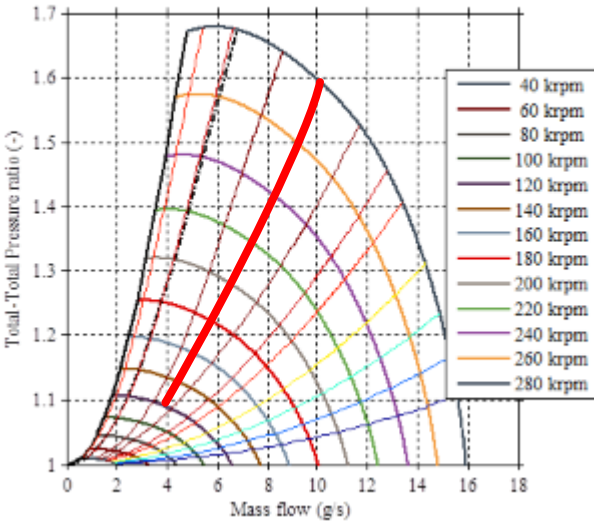

Figure 6-3: Operating region of compressor during tests indicated with the thick red line

4. **Measurement of a rundown**: After the humidity and temperature test is carried out the rundown of the rotor is measured again. With this measurement it can be evaluated if there is condensate or water in the gas bearing. A change in the rundown profile (bigger gradient) would be an indicator for water in the gas bearing.
5. **Inspection**: Since the rundown test only focuses on the gas bearing it cannot be excluded if accumulation of condensate has occurred somewhere else in the compressor. Therefore, the compressor must be disassembled. A complete disassembly was not taken into consideration, because this is time-consuming, and the condensate would already have evaporated again during this time. Since the rear cap is the coolest part of the compressor, only the cap is unscrewed, and the compressor is inspected for condensate.

The definition of suitable and realistic test scenarios turns out to be difficult. No exact test scenarios are known from the standards (chapter 5.1) or from fuel cell vehicle manufacturers. In addition, the system performance of the fuel cell depends on the system integrator. It is therefore possible to use a wide variety of cooling concepts for the fuel cell system and the compressor (a cooling concept is presented in chapter 2.2.3). Nevertheless, the functionality of the compressor must be guaranteed for each cooling concept. To cover most of the cooling concepts the following **test scenarios** are examined:

- **Test with turned off cooling water**: This test assumes that the cooling water initially has a certain temperature

below the dew point temperature of the inlet air of the compressor. However, the cooling water does not circulate, which simulates and represents a FC system with a short time constant of the cooling system. The test makes it possible to determine the heating time of the compressor together with the enclosed cooling water. Because the water is not actively cooled and circulated, this test poses the least risk for condensate accumulation.

- **Test with constant cooling water temperature**: For this test the cooling water temperature is held constant below the dew point temperature of the inlet air with a chiller. This test forces condensation and is supposed to be an overestimation of reality, because the fuel cell system in a vehicle together with the cooling water will heat up over time. Although, the test is an overestimation it has its justification, since it represents fuel cell systems with very long time constant of the cooling system.

It is noted, in reality the cooling system of a FC system is operated somewhere between these two test scenarios.

In this work, tests are performed with the IPSG compressor only, mounted in horizontal orientation as shown in Figure 6-1.

6.4 Tests with Turned off Cooling Water

The focus lies on how fast the compressor can heat up at different speeds such that the amount of accumulated condensate does not represent a risk for the gas bearing.

6.4.1 Methodology

The main procedure for this test is based on chapter 6.3, why only the differences are discussed and specified as well as some more test specific details presented.

A series of tests are performed, each time the compressor is operated at a different speed. During the first test the compressor operates at a speed of 280 krpm. For the subsequent tests the speed is reduced each by 40 krpm down to 120 krpm. In total this result in five tests.

The test is stopped when all temperature sensors measure a value higher than the dew point temperature of the inlet air. With reduced speed, the compressor losses decrease, which increase the heating time as well as the test duration and therefore the accumulation time for condensate.

6.4.2 Results

The measured temperature profiles for five different speeds of the compressor are shown in Figure 6-4. The dew point temperature is not measured directly, but is determined by pressure, temperature and relative humidity according to the formulas in chapter 3.1.

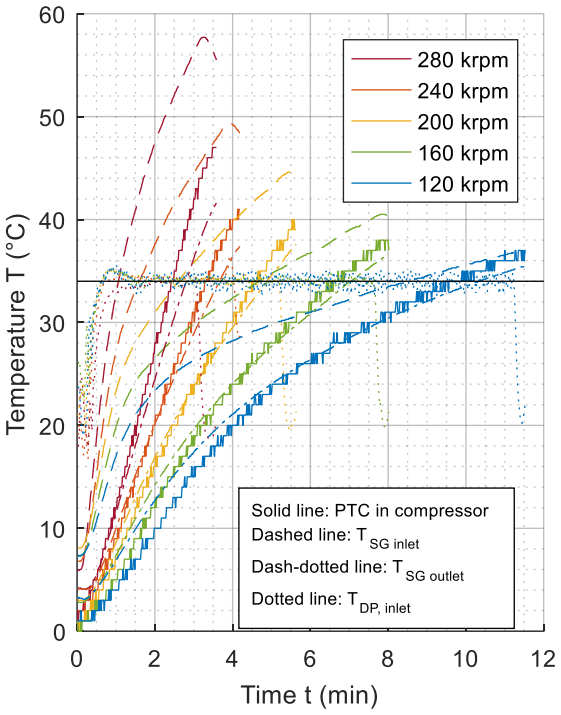

Figure 6-4: Temperature measurement during heating of compressor with turned off cooling water

In the next Figure 6-5 the rundowns after each humidity and temperature test are depicted and compared with the reference measurement of the dry compressor.

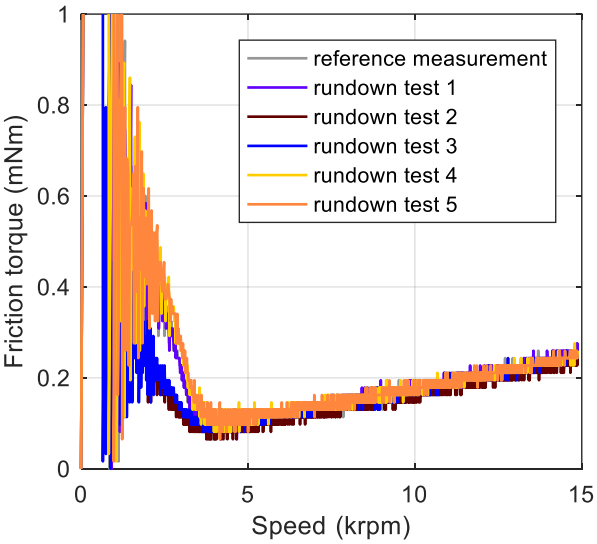

Figure 6-5: Rundown measurements after the tests with turned off cooling water

The Table 6-2 summarizes the evaluation of the inspection with regard to condensate. The criteria for this investigation were: Yes (condensate present after test) and No (condensate not present after test)

Table 6-2: Results of the condensate inspection

Test No.	Compressor speed (krpm)	Test duration time (min)	Condensate present after test? (Yes/No)
1	280	2.8	No
2	240	3.7	No
3	200	4.9	No
4	160	7.0	No
5	120	10.4	No

6.4.3 Discussion

The temperature profiles in Figure 6-4 show the expected behavior that for high speeds the temperature rise faster because of the higher losses, whereas for low speeds the temperature increase is slower due to the lower losses.

Confidential Figure

Figure 6-6: Cross-section of the compressor with indicated losses (in red) and the temperature sensors

In each test the temperature $T_{SG,outlet}$ (surface at SG outlet), whose measuring point is located between the volute and the electric motor, reaches first the temperature level of the dew point temperature. In contrast, the temperature $T_{SG,inlet}$ (surface at SG inlet), whose measuring point is close to the back of the compressor and further away from loss sources, is always the last followed by the PTC. This has to do with the distance of the sensors from the loss sources and where the cooling water is located. This is illustrated in more detail in Figure 6-6. The red lines indicate the loss sources, which are friction losses in the axial and radial gas bearing as well as in the impeller, motor and magnet losses, compression losses and heat transfer from compressed and hot air to the volute housing. The white arrows show the flow direction of the sealing gas.

Before and after each test the rundown was measured. The results are plotted in Figure 6-5 and show no visible change throughout each measurement. This leads to the conclusion that condensation has not occurred in the gas bearings or elsewhere formed water droplets have not reached the bearings. Also, the inspection after disassembling of the rear cap did not reveal any condensate droplets.

6.5 Tests with Constant Cooling Water Temperature

This experimental test is intendent to investigate the impact of FC systems with a long time constant of the cooling system.

6.5.1 Methodology

The main procedure for this test is based on chapter 6.3, therefore only the differences are discussed and specified as well as some more test specific details presented.

For this investigation only one test has been performed. The compressor is operated at a speed of 280 krpm, thus the compressor losses that heat the compressor are the highest.

The test duration is limited and last 30 minutes. Within this time condensation is forced in some regions, which will be identified.

6.5.2 Results

The four measured temperature profiles are shown in Figure 6-7. The dew point temperature of the inlet air (dotted line) has a stationary value of 34 °C and is between the temperatures $T_{SG,inlet}$ and $T_{SG,outlet}$ as well as the PTC temperature.

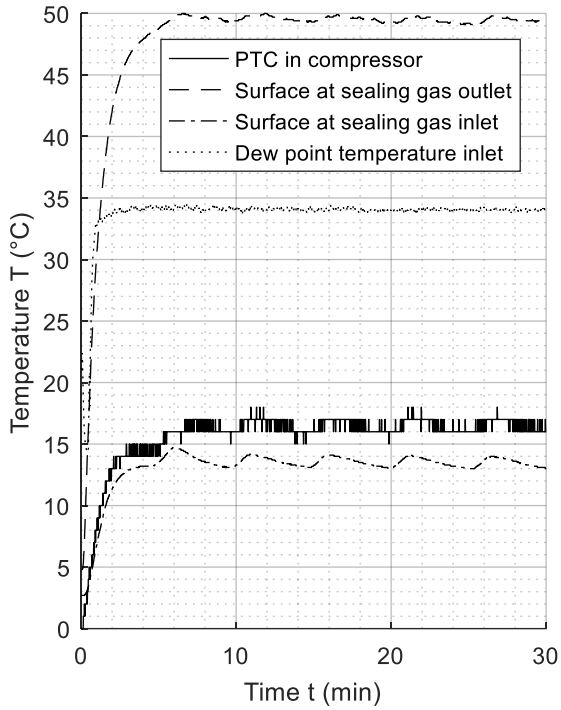

Figure 6-7: Temperature measurement during the 30 minutes endurance test

In the following Figure 6-8 the rundown after the test is depicted and compared with the reference measurement of the dry compressor.

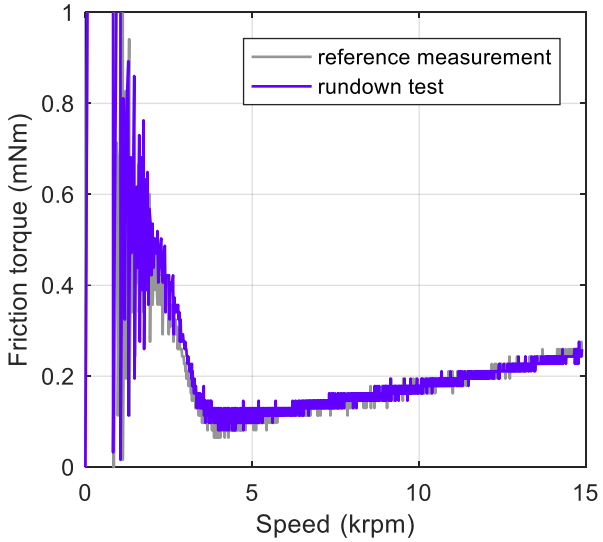

Figure 6-8: Rundown measurement after the test with constant cooling water temperature

The inspection of the compressor revealed an accumulation of condensate (Figure 6-9) and condensate droplets (Figure 6-10).

Confidential Figure

Figure 6-9: Open compressor with accumulation of condensate

Confidential Figure

Figure 6-10: Open compressor with condensate droplets

6.5.3 Discussion

Figure 6-7 clearly shows almost a constant temperature for the measuring point $T_{SG,outlet}$ of 50 °C, which is 16 °C higher than the dew point temperature of 34 °C. This temperature difference possesses the potential for condensation. The small fluctuations in the temperature are due to the chiller that does not cool the water evenly. These fluctuations can also be seen in $T_{SG,inlet}$ and the PTC. The significant higher temperature in $T_{SG,outlet}$ compared to dew point temperature of the inlet air points the fact that condensation is not possible in this region of the compressor.

On the other hand, the temperatures $T_{SG,inlet}$ and PTC are significantly smaller than the dew point temperature. Under

such circumstances condensation inevitably occurs. The evidence that condensate accumulated is shown in Figure 6-9. Some condensate droplets were found close to the electronic plugs and the PCB as Figure 6-10 shows.

Although the condensate was forced by means of a constant cooling water temperature of 0 °C there was no condensate detectable in the gas bearing as the results of the rundown measurements show in Figure 6-8. Both the measurements before and after the test are almost identical compared to the one of the dry compressor.

6.6 Conclusion of the Test Results

The experimental investigations with turned off cooling water, that were supposed to represent a FC system with a short time constant of the cooling system have shown the following findings:

- Condensation does not occur under the given circumstances.
- Higher speeds of the compressor decrease the heating time and thus the risk for accumulation of condensate.

Regarding the test, where the cooling water temperature was hold constant in order to represent a slow time constant of a FC cooling system the following results can be summarized:

- Accumulation of condensate can be forced on parts of the compressor which are close to the cooling water and far enough of loss sources which cannot heat up the parts of the compressor. In addition, the cooling water temperature must be smaller than the dew point temperature of the inlet air.
- With this test the coolest and thus the most critical spot of the compressor for condensate accumulation could be identified, i.e. the rear of the compressor.
- Another reason that favors the accumulation of condensate, is the sealing gas flow, which brings constantly humid air into the compressor.
- It turned out that for a period of 30 minutes a condensate accumulation did not lead to any malfunction of the compressor. However, this statement only applies to the horizontal installation position. Further installation positions should also be investigated. Although, the accumulated condensate did not lead to a malfunction, it possesses still a major risk if it enters the gas bearing via the ventilation ducts due to a change in position and vibration of the compressor.

6.7 Derived Measures from the Tests

Initial constructive optimization measures can be derived from the findings of the experimental investigation and are recommended for implementation. Suggested optimizations are:

In addition, the following measures are conceivable, which need to be examined more closely:

- The application of a thermostatic valve in the cooling water circuit of the fuel cell system in cases of long time constants of the cooling water. The thermostatic valve causes the compressor to heat up faster by turning off the cooling water supply and opens the cooling water supply at a defined temperature, e.g. above the dew point temperature of the ambient air.

7 Conclusion and Future Work

Based on a theoretical analysis of partial condensation processes critical environmental and operating situations of the turbo compressor could be identified. In summary, these are all those situations in which condensate can accumulate over a certain period, e.g. during heating of the compressor from standstill or when the humidity of the ambient air state increases suddenly, e.g. entering a humid and warm tunnel in winter.

With the theoretical analysis and the analysis of standards, the requirements specification for the test rig was defined.

During this work a test rig was developed, constructed and commissioned, which provides temperature and humidity-controlled air to a compressor in order to experimentally investigate the influence of condensation on the functionality and reliability of air lubricated turbo compressors.

For the control of the test rig a specific newly developed LabVIEW GUI and control algorithm was developed. In the same context, the LabVIEW library was expanded with additional sensors, actuators and WAGO modules.

Miniaturized Pt100 temperature sensors as well as combined humidity and temperature sensors were built as a part of the test rig construction and have been successfully tested. These sensors lie the basis for further investigations of the compressor, for example for a system identification in order to better understand the thermal behavior.

Based on the theoretical analysis and the analysis of standards test scenarios for the experimental investigations were defined.

The experimental investigation showed that with turned off cooling water a condensate accumulation was not observable. This could be attributed to the fast time constant of the compressor. On the other hand, for the worst-case scenario with a constant cooling water temperature below the dew point temperature of the ambient air, a significant accumulation of condensate was found in the rear of the compressor.

From the findings of the experimental investigation, measures which are proposed for realization and implementation into the compressor were derived. These are summarized as:

Confidential Text

Although, only the turbo IPSG compressor was tested, the findings with the IPSG compressor can be applied to the HPSG sealing gas concept. In the HPSG concept, the aforementioned measures can be easily implemented and tested.

Concerning the test rig functionality, the following changes can be proposed:

- In order to optimize the steam dozing precision and thus reducing fluctuations in the humidity at the inlet of the compressor a hose pump instead of a diaphragm dosing pump can be used. Such pumps deliver a more uniform mass flow.

Based on the current status of the investigations, it is not yet possible to make a conclusive assessment of the two sealing gas concepts. There are further investigations necessary:

- It should be clarified, which of the sealing gas concepts (IPSG, HSPG) is less prone for condensation and therefore the better choice. Therefore, it is recommended to perform at least the same experimental tests with the HSPG compressor as was done with the ISPG.
- Since the mounting of the compressor is preferably not prescribed in a single orientation, testing of the compressor under other mounting positions is required in order to proof the reliability.

Within the scope of this work, valuable findings were obtained, which can be used to design and built the turbo compressor more robust with regard to condensation and humidity.

List of Symbols and Abbreviations

Latin symbols

c_i	m/s	Velocity at state i
$c_{p,A}$	J/(kg K)	Specific heat capacity at constant pressure of air
$c_{p,V}$	J/(kg K)	Specific heat capacity at constant pressure of water vapor
g	m/s^2	Gravitational acceleration = 9.81 m/s^2
H	J	Enthalpy
$\dot{H}$	W	Enthalpy flow
H_{1+X}	J	Enthalpy of humid air
$\dot{H}_{1+X}$	J	Enthalpy flow of humid air
H_A	J	Enthalpy of air
H_V	J	Enthalpy of water vapor
h_i	J/kg	Specific enthalpy at state i
h_{1+X}	J/kg	Specific enthalpy of humid air per kg dry air
h_A	J/kg	Specific enthalpy of air
h_V	J/kg	Specific enthalpy of water vapor
Δh_v	J/kg	Specific evaporation enthalpy
J	kg/m^2	Moment of inertia
M_A	kg/mol	Molar mass of air = 28.96 g/mol
M_{Fr}	Nm	Friction torque
M_i	kg/mol	Molar mass of component i
M_W	kg/mol	Molar mass of water = 18.02 g/mol
m	kg	Mass
m_A	kg	Mass of air
$\dot{m}_A$	kg/s	Mass flow of air
m_i	kg	Mass of component i
m_V	kg	Mass of water vapor
$\dot{m}_V$	kg/s	Mass flow of water vapor
$\dot{m}_W$	kg/s	Mass flow of water
n	1/min	Speed
$\dot{n}$	1/min^2	Derivative of speed
P	W	Power
P_{comp}	W	Power of compressor
$P_{comp,s}$	W	Isentropic power of compressor
p	Pa	Pressure, total pressure
p_0	Pa	Reference pressure, reference total pressure
p_A	Pa	Partial pressure of air
p_i	Pa	Partial pressure of component i
p_V	Pa	Partial pressure of water vapor
$p_{VS}(\vartheta)$	Pa	Saturation water vapor pressure at a given temperature
$\dot{Q}_{AH}$	W	Heat flow of air heater
$\dot{Q}_C$	W	Heat flow due to cooling
$\dot{Q}_E$	W	Heat flow of evaporator

$\dot{Q}_H$	W	Heat flow due to heating
$\dot{Q}_{RH}$	W	Heat flow of air heater
q	J/kg	Specific heat flow
R	J/(mol·K)	Universal gas constant = 8.314 J/(mol·K)
T	K	Absolute temperature
T_{amb}	K	Absolute temperature of ambient air
T_{DP}	K	Dew point temperature
t	s	Time
V_{gas}	m^3	Volume of gas phase
V_i	m^3	Volume of component i
V_{liquid}	m^3	Volume of liquid phase
w	J/kg	Specific work
X	kg/kg	Mass loading
X_S	kg/kg	Maximum mass loading at saturation state
z_i	m	Height at state i

Greek symbols

α	1/ s^2	Angular acceleration
δ	-	Volume fraction
η_s	-	Isentropic efficiency
Π	-	Pressure ratio
ρ	kg/m^3	Density
ρ_{gas}	kg/m^3	Density of gas phase
ρ_i	kg/m^3	Density of component i
ρ_{liquid}	kg/m^3	Density of liquid phase
ρ_W	kg/m^3	Density of water
ϑ	°C	Temperature in degree Celsius
ϑ_{comp}	°C	Compressor (housing) temperature
ϑ_{CW}	°C	Cooling water temperature
ϑ_{DP}	°C	Dew point temperature
φ	-	Relative humidity
φ_0	-	Reference relative humidity
ψ	-	Degree of saturation
ω	1/s	Angular velocity
$\dot{\omega}$	1/ s^2	Derivative of angular velocity = angular acceleration

Subscripts

0	Reference condition
1,2,3, ...	A state at a specific place
A	Air
amb	Ambient

$comp$	Compressor
DP	Dew point
i	Any component
S	Saturated condition
s	Isentropic
W	Water

Acronyms

CAD	Computer Aided Design
FC	Fuel Cell
FFC	Flexible Flat Cable
HEX	Heat Exchanger
HPSG	High-Pressurized Sealing Gas
IPSG	Impeller-Propelled Sealing Gas
HGJB	Herring Bone Journal Bearing
PCB	Printed Circuit Board
PEM	Proton Exchange Membrane
PEMFC	Proton Exchange Membrane Fuel Cell
PWM	Pulse Width Modulation
SG	Sealing Gas
SSR	Solid State Relay

List of Figures

List of Tables

Bibliography

[1] D. Zhao, *Control of an Ultrahigh Speed Centrifugal Compressor for the Air Managment of Fuel Cell Systems,* University of Technology of Belfort-Montbéliard, 2014.

[2] E. Guenat und J. Schiffmann, *Effects of Humid Air on Aerodynamic Journal Bearings,* Tribology International 127, 2018, p. 333–340.

[3] Celeroton AG, «Datasheet CT-17-700.GB - Rev02,» 09 2017. [Online]. Available: https://www.celeroton.com/fileadmin/user_upload/produkte/kompressor/datasheets/Datasheet-CT-17-700.GB.pdf. [Zugriff am 01 01 2019].

[4] Celeroton AG, «Datasheet CT-17-1000.GB - Rev02,» 09 2017. [Online]. Available: https://www.celeroton.com/fileadmin/user_upload/produkte/kompressor/datasheets/Datasheet-CT-17-1000.GB.pdf. [Zugriff am 01 01 2019].

[5] Celeroton AG, «Gas Bearings,» [Online]. Available: https://www.celeroton.com/en/technology/gas-bearings.html. [Zugriff am 02 01 2019].

[6] F. Dietmann, A. Looser und C. Zwyssig, *Vorteile und Herausforderungen von miniaturisierten, gasgelagerten, ölfreien Turbo Kompressoren für Wärme- & Kälteanlagen,* Kassel, Deutschland: DKV-Tagung, AA II.2.03, 2016.

[7] Celeroton AG, *User Manual CT-17-700.GB, PI-3300-101-Rev03,* 2016.

[8] W. Yu, X. Sichuan und H. Ni, *Air Compressors for Fuel Cell Vehicles: A Systematic Review,* SAE International Journal of Alternative Powertrains, 2015.

[9] B. Blunier und A. Miraoui, *Proton Exchange Membrane Fuel Cell Air Management in Automotive Applications,* Belfort 90000, France: University of Technology of Belfort-Montbéliard, 2010.

[10] S. Pischinger und O. Lang, *Handbook of Fuel Cells: Fundamentals, Technology and Applications,* John Wiley & Sons, 2003, pp. 727-741, (ch. Air-supply components).

[11] B. Blunier und A. Miraoui, *Optimization and Air Supply Management of a Polymer Electrolyte Fuel Cell,* Proceedings of the IEEE Converence an Vehicular Power and Propulsion (VPP), 2005.

[12] G. Zhang und S. G. Kandlikar, *A Critical Review of Cooling Techniques in Proton Exchange Membrane Fuel Cell Stacks,* International Journal of Hydrogen Energy, 37(3):2412-2429, 2012.

[13] Maxwell Technologies, «Ultracapacitors Overview,» [Online]. Available: https://www.maxwell.com/products/ultracapacitors. [Zugriff am 02 02 2019].

[14] P. von Böckh und M. Stripf, *Technische Thermodynamik: Ein beispielorientiertes Einführungsbuch,* Berlin, Heidelberg: Springer-Verlag, 2015.

[15] M. Zeller und U. Busweiler, *Be- und Entfeuchten von Luft,* In: P. Stephan, D. Mewes, S. Kabelac, M. Kind, K. Schaber, T. Wetzel (eds) VDI-Wärmeatlas 12th Hrsg., Springer Vieweg, Berlin, Heidelberg: Springer Reference Technik, 2018.

[16] P. Atkins und J. de Paula, *Atkins' Physical Chemistry,* Oxford, New York: Oxford University Press, 2006.

[17] D. R. Stull, *Vapor Pressure of Pure Substances: Organic and Inorganic Compounds,* Ind. Eng. Chem., 1947, pp. 517-540.

[18] P. Kellerhoff , «Klimatechnische Weltreise,» *VDI nachrichten,* Nr. 51/52, pp. 14-15, 21 12 2018.

[19] U. Steinemann und F. Zumsteg, *Measurements of Air Flow, Temperature Differences and Pressure Differences in Road Tunnels,* Graz, Austria: International Conference „Tunnel Safety and Ventilation“ , 2004.

[20] «World Maps of Köppen-Geiger Climate Classification,» Climate Change & Infectious Diseases Group, 2019. [Online]. Available: http://koeppen-geiger.vu-wien.ac.at/. [Zugriff am 20 04 2019].

[21] «Meteonorm,» Meteotest AG, [Online]. Available: https://meteonorm.com/. [Zugriff am 29 04 2019].

[22] Siemens, «h, x-Diagramm - Aufbau und Anwendung,» 2018. [Online]. Available: https://www.downloads.siemens.com/download-center/Download.aspx?pos=download&fct=getasset&id1=A6V10327345. [Zugriff am 10 06 2019].

[23] I. H. Bell, J. Wronski, S. Quoilin und V. Lemort, *Pure and Pseudo-pure Fluid Thermophysical Property Evaluation and the Open-Source Thermophysical Property Library CoolProp,* Bd. 53, Industrial & Engineering Chemistry Research, 2014, pp. 2498-2508.

[24] K. Ang, G. Chong und Y. Li, *PID control system analyis, design, and technology.,* IEEE Transaction on Control Systems (13(4):, 2005, pp. 559-576.

[25] D. Chen und H. W. Chen, *Using the Köppen Classification to Quantify Climate Variation and Change: An Example for 1901–2010,* Environmental Development, 2013, p. 69–79.

[26] D. Conradie, «Climate Indicators: Köppen-Geiger Climate Classification,» 05 2016. [Online]. Available: http://stepsa.org/climate_koppen_geiger.html. [Zugriff am 19 04 2019].

[27] B. Blunier und A. Miraoui, *Air Management in PEM Fuel Cells: State-of-the-Art and Prospectives,* Belfort 90010 CEDEX, France: University of Technology of Belford-Montbéliard, 2007.

A1 Derivation of Volume Fraction

The volume fraction defines the ratio between the liquid phase and total two-phase volume

$$\delta = \frac{V_{liquid}}{V_{liquid} + V_{gas}}.$$

With the volume given as the ratio of mass and density

$$V_i = \frac{m_i}{\rho_i}$$

the following expression is obtained

$$\delta = \frac{\frac{m_{liquid}}{\rho_{liquid}}}{\frac{m_{liquid}}{\rho_{liquid}} + \frac{m_{gas}}{\rho_{gas}}}.$$

By inserting the mass loading (mass fraction of humid air)

$$X = \frac{m_{liquid}}{m_{gas}} = \left(\frac{m_V}{m_A}\right).$$

the volume fraction becomes to

$$\delta = \frac{\frac{m_{liquid}}{\rho_{liquid}}}{\frac{m_{liquid}}{\rho_{liquid}} + \frac{1}{X} \cdot \frac{m_{liquid}}{\rho_{gas}}}.$$

Simplification yields to

$$\delta = \frac{1}{1 + \frac{1}{X} \cdot \frac{\rho_{liquid}}{\rho_{gas}}}.$$

A2 World Map of Köppen-Geiger Climate Classification

The world map of Köppen-Geiger climate classification is shown in Figure 7-1.

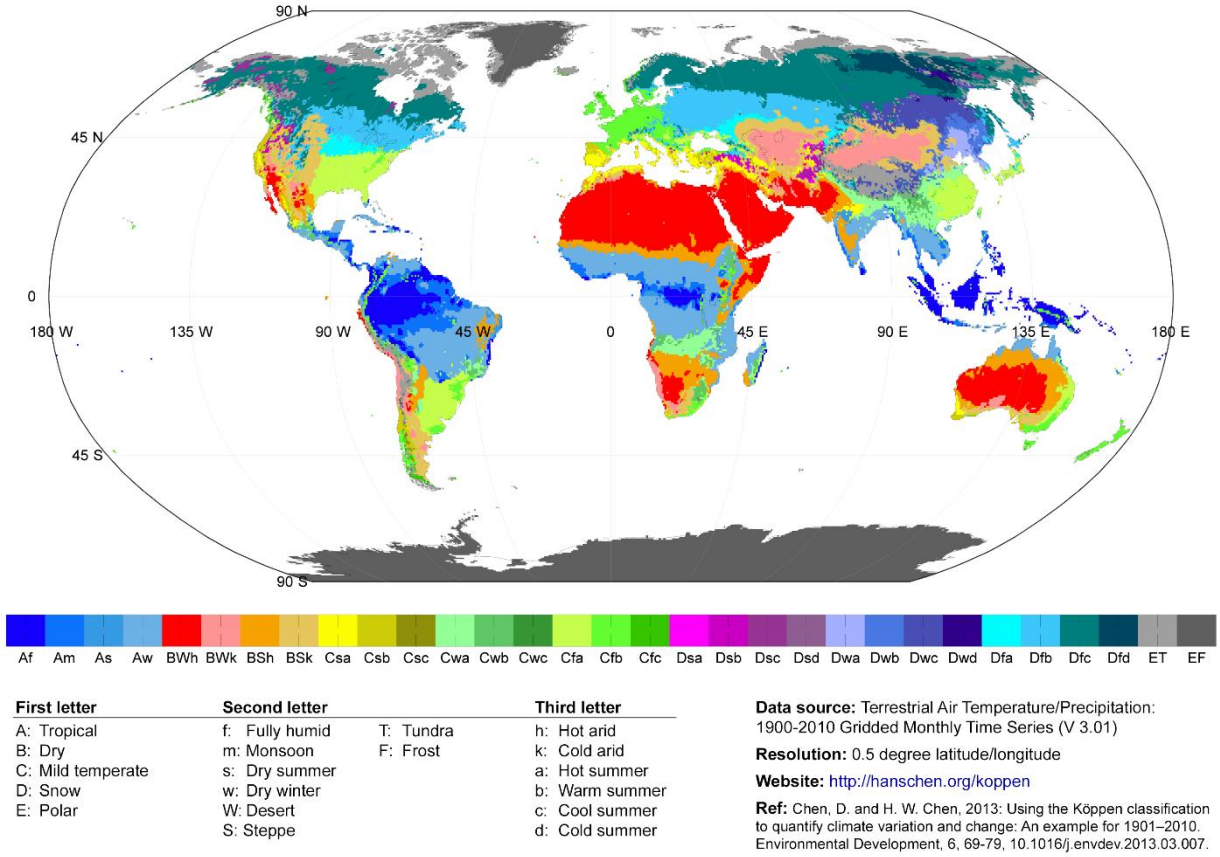

Figure 7-1: World Map of Köppen-Geiger Climate Classification [25]

The Köppen-Geiger classifications consider five primary categories as given in Table 7-1:

Table 7-1: Five primary categories of Köppen-Geiger climate classifications [26]

Type	Description	Criterion
A	**Equatorial climates**	$T_{min} \geq +18$ °C
Af	Equatorial rainforest, fully humid	$P_{min} \geq 60$ mm
Am	Equatorial monsoon	$P_{ann} \geq 25 \cdot (100 - P_{\min})$ mm
As	Equatorial savannah with dry summer	$P_{min} < 60$ mm in summer
Aw	Equatorial savannah with dry winter	$P_{min} < 60$ mm in winter
B	**Arid climates**	$P_{ann} < 10 \cdot P_{th}$
BS	Steppe climate	$P_{ann} > 5 \cdot P_{th}$

BW	Desert climate	$P_{ann} \leq 5 \cdot P_{th}$
C	**Warm temperate climates**	-3 °C < T_{min} < + 18 °C
Cs	Warm temperate climate with dry summer	$P_{smin} < P_{wmin}$, $P_{wmax} > 3 \cdot P_{smin}$ and P_{smin} < 40 mm
Cw	Warm temperate climate with dry winter	$P_{wmin} < P_{smin}$ and $P_{smax} > 10 \cdot P_{wmin}$
Cf	Warm temperate climate, fully humid	Neither Cs nor Cw
D	Snow climates	$T_{min} \leq$ -3 °C
Ds	Snow climate with dry summer	$P_{smin} < P_{wmin}$, $P_{wmax} > 3 \cdot P_{smin}$ and P_{smin} < 40 mm
Dw	Snow climate with dry winter	$P_{wmin} < P_{smin}$ and $P_{smax} > 10 \cdot P_{wmin}$
Df	Snow climate, fully humid	Neither Ds nor Dw
E	**Polar climates**	T_{max} < + 10 °C
ET	Tundra climate	0 °C ≤ T_{max} < + 10 °C
EF	Frost climate	T_{max} < 0 °C

The classifications system further considers six secondary categories as given in Table 7-2:

Table 7-2: Six secondary categories of Köppen-Geiger climate classifications [26]

Type	**Description**	**Criterion**
h	Hot steppe/desert	$T_{ann} \geq$ + 18 °C
k	Cold steppe/desert	T_{ann} < + 18 °C
a	Hot summer	$T_{max} \geq$ + 22 °C
b	Warm winter	not (a) and at least 4 · $T_{mon} \geq$ + 10 °C
c	Cold summer and cold winter	not (b) and
d	Extremely continental	like (c) but

A3 Köppen-Geiger Climate Classification of Cities

Table 7-3: Selection of cities and its climate classification according to Köppen-Geiger

#	City	Country	Climate classification	Climate zone	Latitude (°N)	Longitude (°E)	Weather station (m a.s.l.)	Static pressure (bar(a))	Population (in million)
1	Singapore	Singapore	Af	Tropical	1.28	103.85	30	1.010	5.61
2	Brasilia	Brasil	Aw	Tropical	-15.92	-47.67	960	0.899	4.24
3	Dubai	United Arab Emirates	Bwh	Tropical	25.23	55.28	0	1.014	3.15
4	Lima	Peru	Bwh	Tropical	-12.00	-77.12	10	1.012	8.85
5	Madrid	Spain	Bsk/Csa	Subtropical	40.42	-3.70	662	0.933	3.14
6	Zurich	Switzerland	Cfb	Temperate	47.37	8.54	413	0.963	0.41
7	Bogota	Columbia	Cfb	Tropical	4.63	-74.08	2560	0.737	8.08
8	El Alto	Bolivia	ET	Tropical	-16.51	-68.17	4090	0.609	0.84
9	Moscow	Russia	Dfb	Temperate	55.75	37.62	148	0.995	12.51
10	Yakutsk	Russia	Dfc	Cold	62.17	129.83	106	1.000	0.27

Formula for static pressure with z in meters above sea level:

$$p = p_0 \cdot e^{\frac{-M \cdot g \cdot z}{R \cdot T}}$$

$$p_0 = 1.0135\ bar(a)$$

$$M = 0.02884\ kg/mol$$

$$g = 9.81\ m/s^2$$

$$R = 8.314\ J/(mol \cdot K)$$

$$T = 0\ °C$$

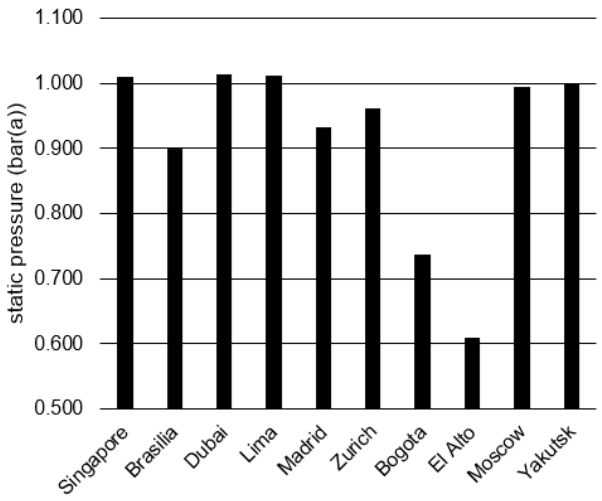

A4 Snapshot of the Excel Tool for the Test Rig Design

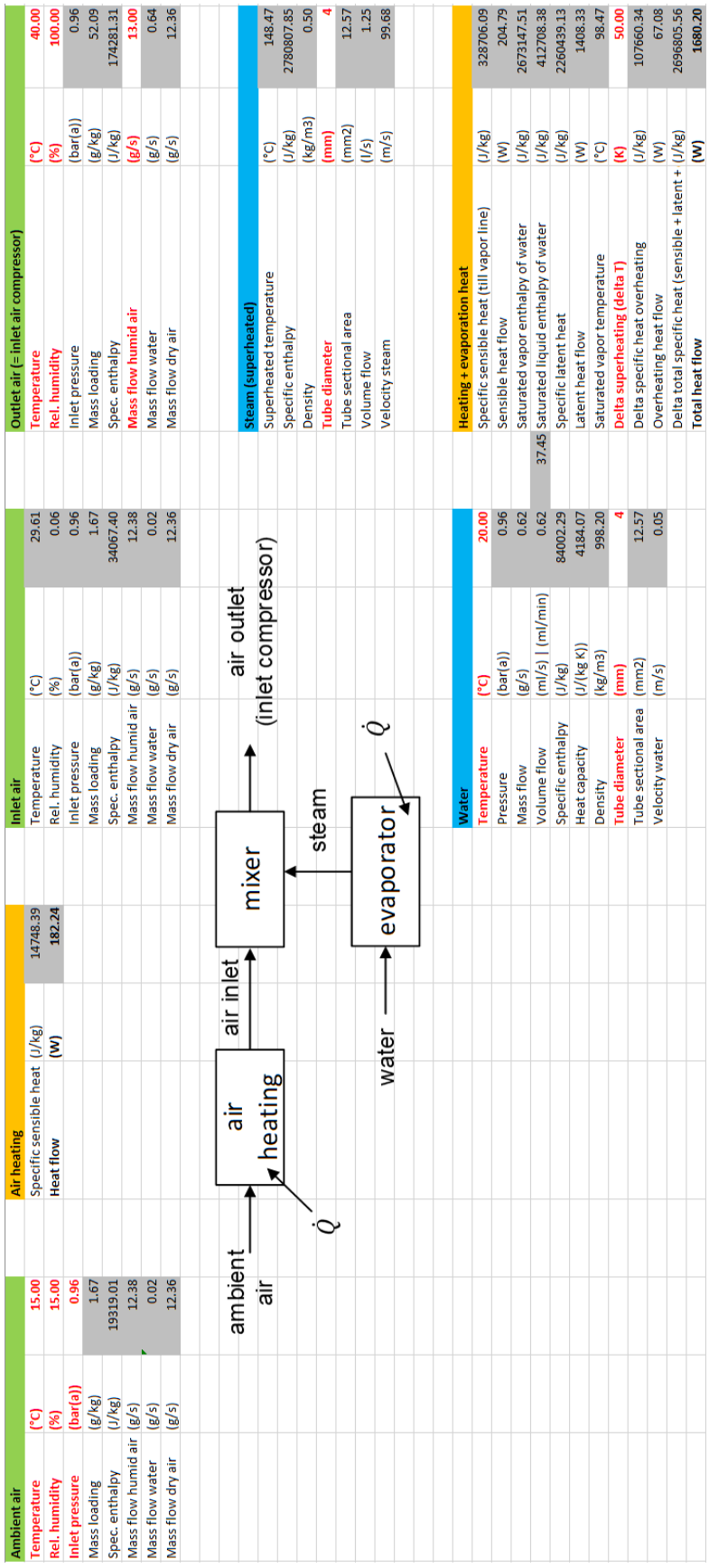

A5 Concepts of the Test Rig

Closed loop concepts

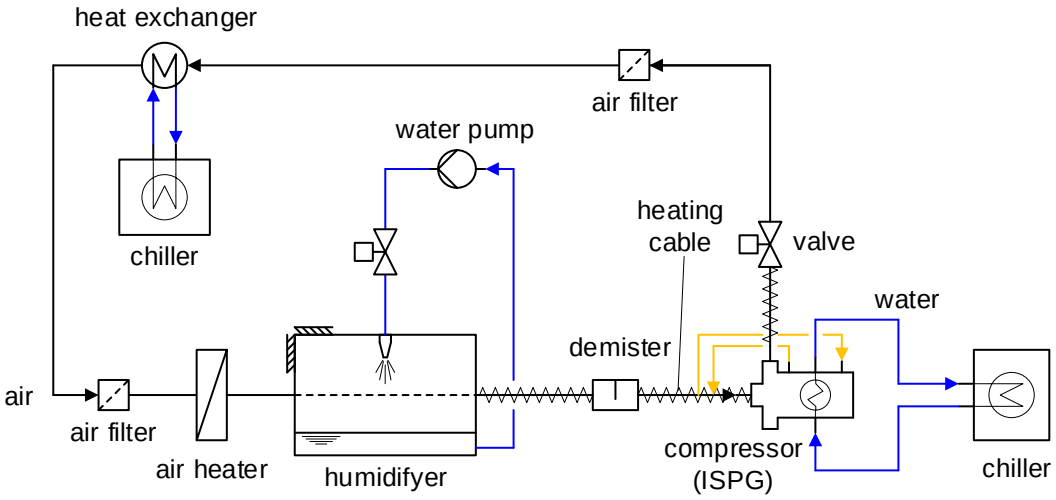

Figure 7-2: A simple closed loop concept of the test rig

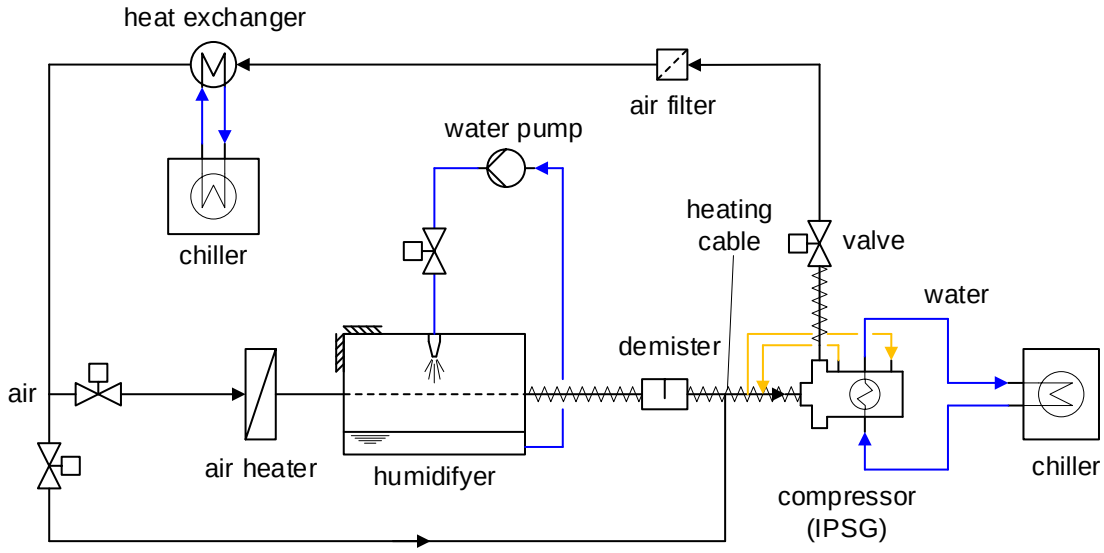

Figure 7-3: Closed loop concept of the test rig with an additional mixing loop (mixing of dry with humid air)

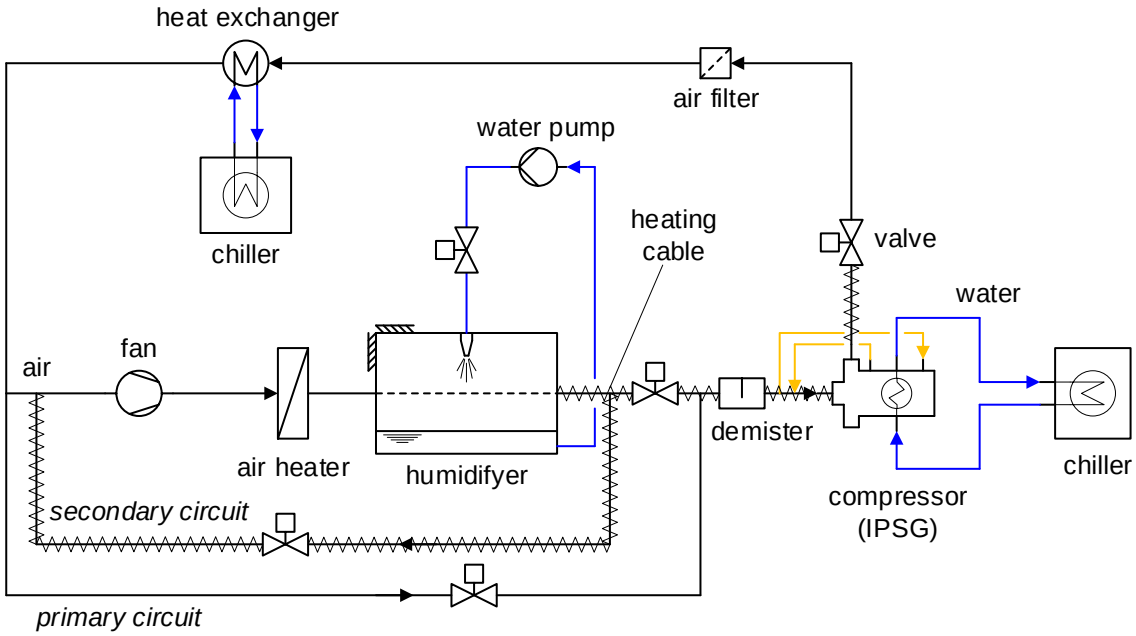

Figure 7-4: Closed loop concept of the test rig with an additional sophisticated mixing loop

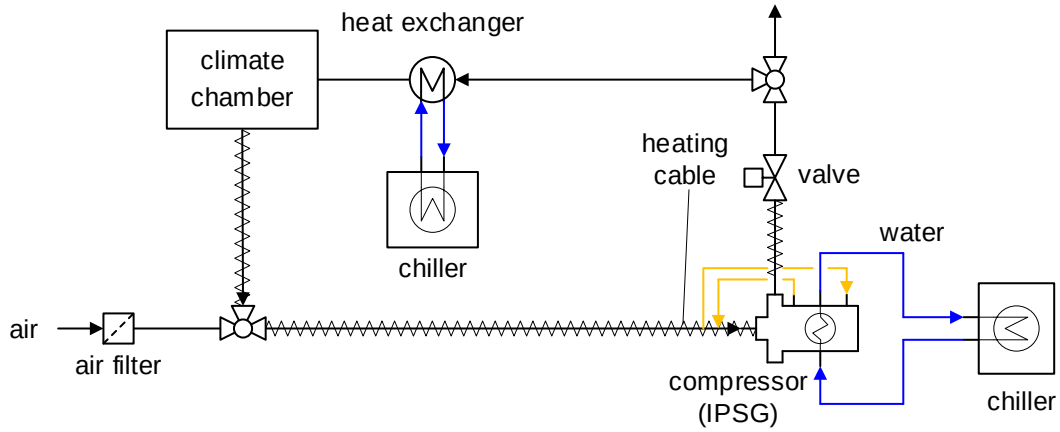

Figure 7-5: Closed loop concept of the test rig with a climate chamber

Open loop concepts

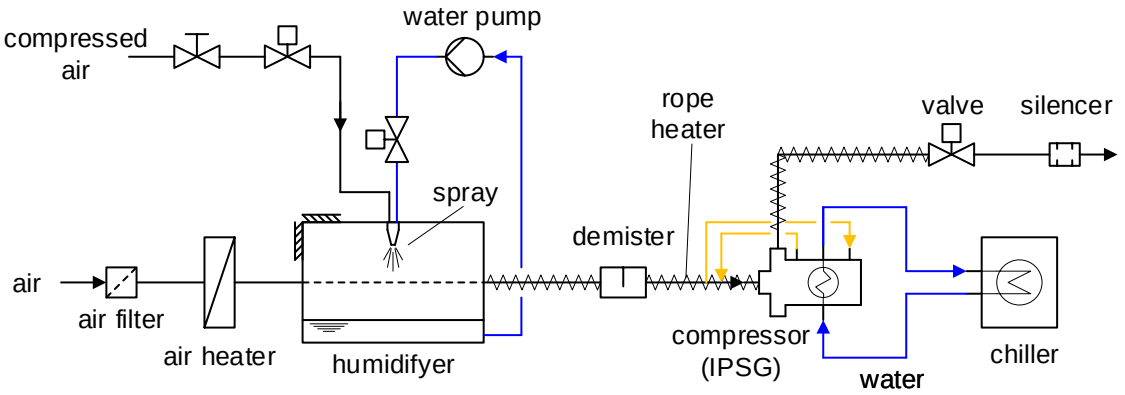

Figure 7-6: Open loop concept of the test rig with compressed air to produce a water spray

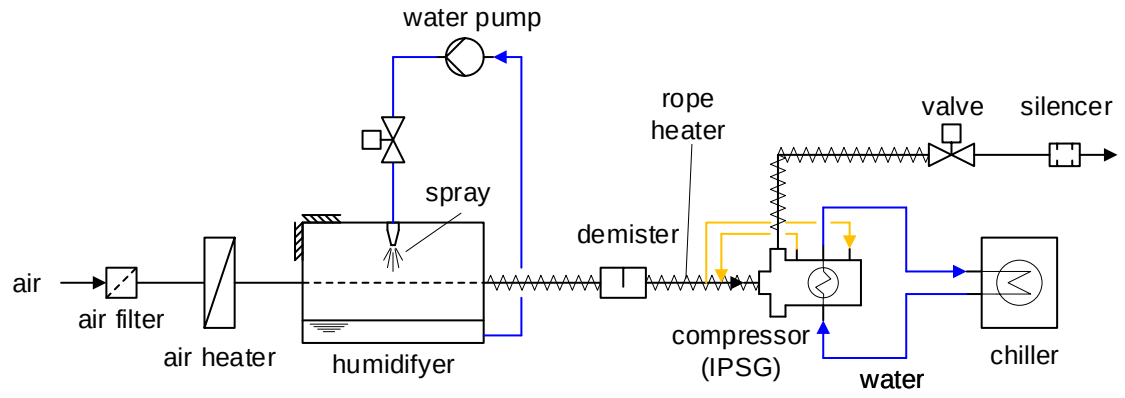

Figure 7-7: Open loop concept of the test rig with spray

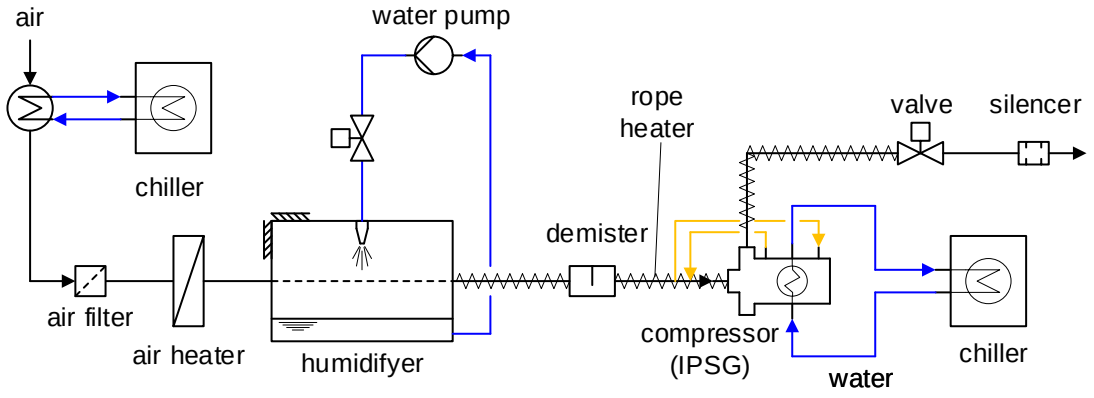

Figure 7-8: Open loop concept of the test rig with an additional chiller to produce an inlet temperature below ambient temperature

A6 Additional Photos of Test Rig

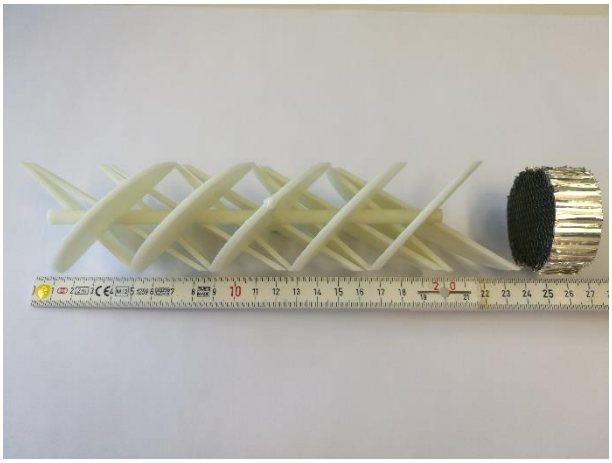

Figure 7-9: Static mixer and an aluminum honeycomb as a flow straigthener

Figure 7-10: Static mixer inserted in the silicone hose

A7 Sketch of Sensor Adapter Board

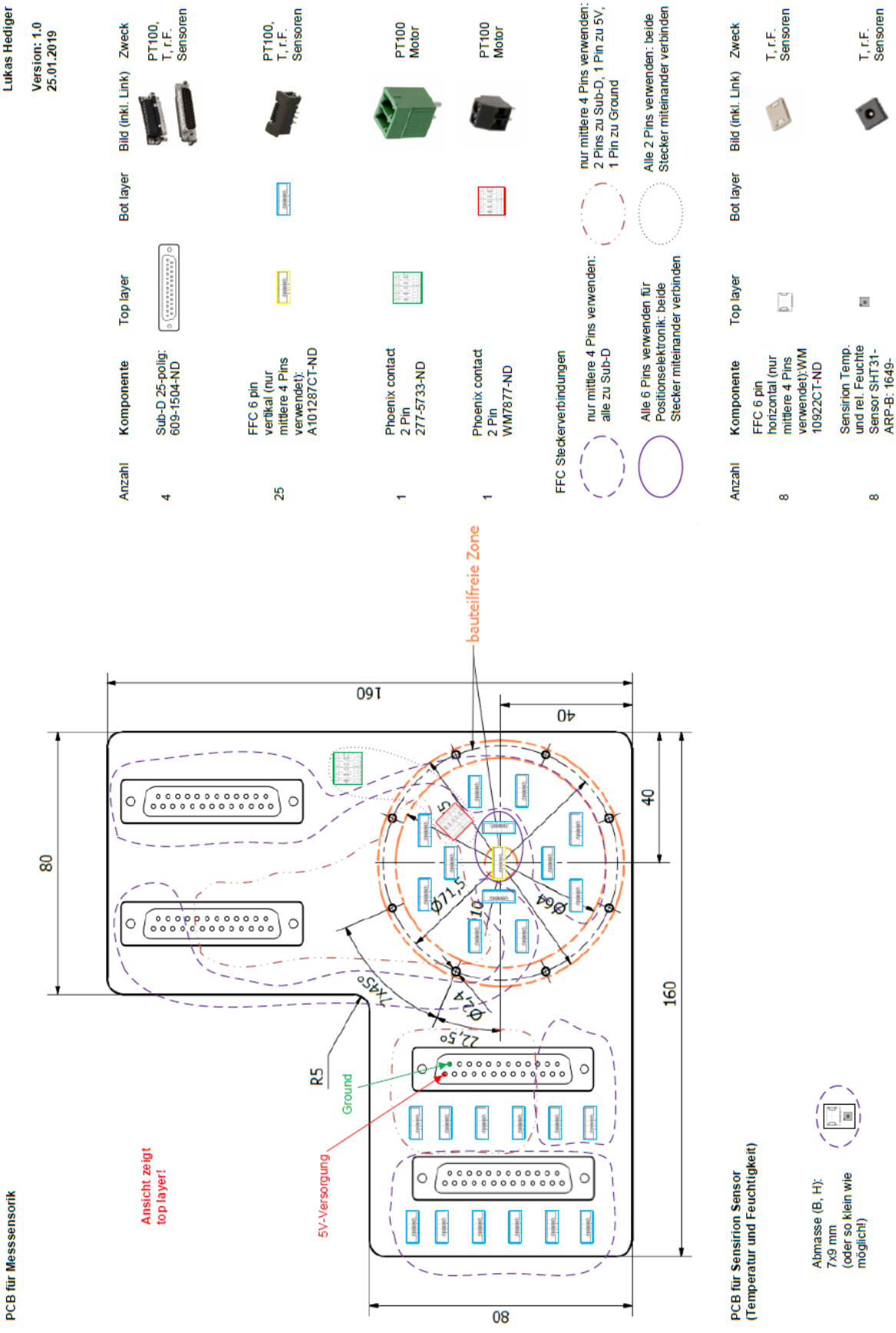

A8 Data Sheets

Standardized Characteristics

Type	sales article / air heater
Component	LHS 41S SYSTEM - 230 V / 2 kW (Art.No. 143.278)
ID	M36 / A0.16 (2016-11-08)